STUDIA

UNIVERSITATIS BABEŞ-BOLYAI

PHYSICA

1

1989

CLUJ-NAPOCA

ANUL XXXIV 1989

STUDIA
UNIVERSITATIS BABEŞ-BOLYAI

PHYSICA

1

Redacţia 3400 CLUJ-NAPOCA, str M Kogălniceanu, 1 ☎ Telefon 1 61 01

SUMAR — CONTENTS

[redacted]

[redacted]

[redacted]

[redacted]

STUDIA UNIV BABEŞ—BOLYAI, PHYSICA, XXXIV, 1 1989

ATOMIC HOMOGENEITY IN THORIA-URANIA ADVANCED FUEL

D. CIURCHEA*

Received: December 14, 1988

ABSTRACT. — The paper deals with the influence of the processing variables on the atomic homogeneity of the (U, Th)O_2 system as studied by X-Ray diffraction The experimental details and the numerical procedures used are presented The physical interpretation of the evolutions observed is discussed. It appears that the grain boundary diffusion is an important factor affecting the homogeneity of the solid solution

Introduction. Thoria-Urania advanced fuel is a promising future for the heavy water moderated reactors The homogeneity of the mixed oxide fuel is of prime importance to prevent local melting during power transients and to allow the reprocessing of the burnt fuel, since pure Thoria is chemically inert [1, 2, 3]

The homogeneity may be studied at different levels of detail . macroscopic, by autoradiography , microscopic, by microprobe and atomic by X-Ray diffraction.

Among the X-Ray diffraction methods presented in the litterature [4, 5, 6, 7], the method of Rudman [4] seems to be the best suited for the Thoria-Urania system, yielding quantitative data relative to the diffusion process. It was successfully applied by Furuya et al. [8] by using the (620) reflexion of the f.c c. structure.

In this paper we present the influence of the processing variables on the atomic homogeneity in the ThO_2—UO_2 system by using the (311) reflexion of the structure and by using our numerical procedure presented previously [9].

Theoretical basis. The study of the diffusion process at an atomic level by X-Ray diffraction is conditioned by some relation between concentration and the lattice parameter. Then the diffracted intensity corresponding to a given lattice parameter is proportional to the number of unit-cells with that concentration. This rationale may be speculated in terms of the diffusion theory to yield the concentration profile versus effective penetration [9].

In quantitative terms, the number of unit cells with the concentration between c and $c + dc$, $N(c)$, is .

$$N(c) = Q \cdot f(\theta) \tag{1}$$

where $f(\theta)$ is the pure diffraction profile and

$$Q = \frac{\frac{\partial d(c)}{\partial c}\,\frac{1}{d(c)}}{KA(0, \mu)[cf_1 + (1 - c)f_2]^2}\,\frac{\sin^3\theta}{1 + \cos^2 2\theta} \tag{2}$$

* *University of Cluj-Napoca, Department of Mathematics and Physics, 3400, Cluj-Napoca, Romania*

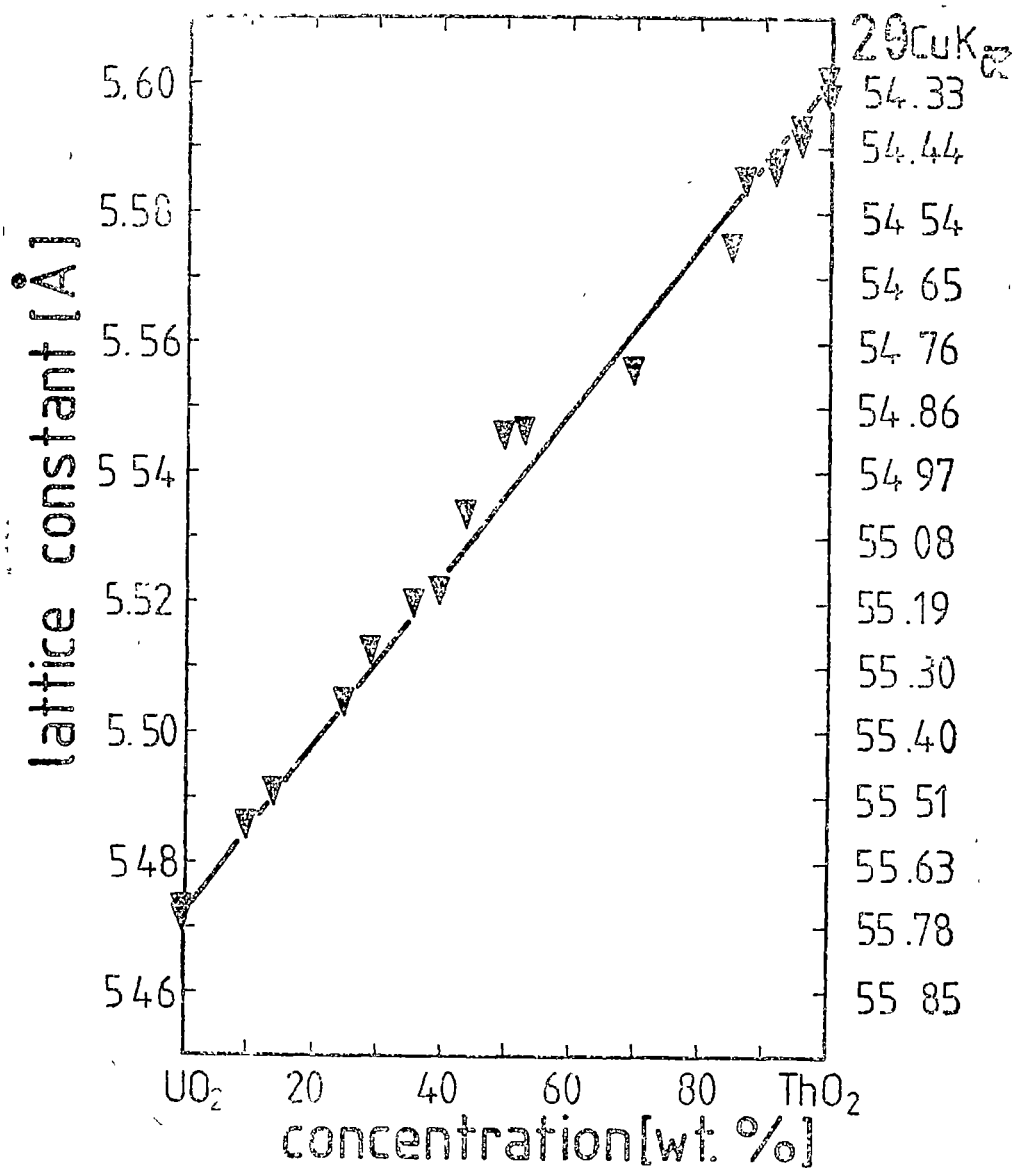

Fig 1 The dependence of the lattice parameter versus concentration in the Thoria-Urania system The specimens were pressed at larger pressures then in the other experiments described

where c is the atomic fraction of UO_2, f_1 and f_2 are the atomic scattering factors for UO_2 and ThO_2 respectively, $A(\theta, \mu)$ is the absorbtion factor, K is a constant.

The pure diffraction profile, $f(\theta)$ should be obtained from the experimentally measured profile, $h(\theta)$ by unfolding with a reference specimen [9].

The effective penetration, y, is obtained as

$$y = \frac{\int_0^c N(c)dc}{\int_0^1 N(c)dc} \qquad (3)$$

Since ThO_2 and UO_2 have isomorphous structures, the Vegard law is expected to apply through the entire range of compositions. This was checked by us by using pellets pressed at large pressures and sintered at 1750°C (see Fig. 1). Since Vegard's law applies to the system, $\partial d(c)/\partial c$ in Eq. (2) may be taken as a constant.

For compliance with other authors [8] the homogeneity parameter H may be defined as the mass of substance migrated through the Matano interface reported to the initial amount, i e. (Fig. 2):

$$H = \frac{H_1 + H_2}{c_0 y_m + (1 - c_0)(1 - y_m)} \qquad (4)$$

However, the Matano interface has a specific definition,

$$\int_0^c (y_m - y)dc = \int_c^1 (y - y_m)\,dc \qquad (5)$$

which is conected to the effective diffusion coefficient Since this feature is not specifically used later in our study, we have taken y_m as the same with c_0, the initial concentration of UO_2.

Moreover, in Eq (4) H results in arbitrary units Therefore, it must be calibrated for 0% and 100% homogeneity, respectively

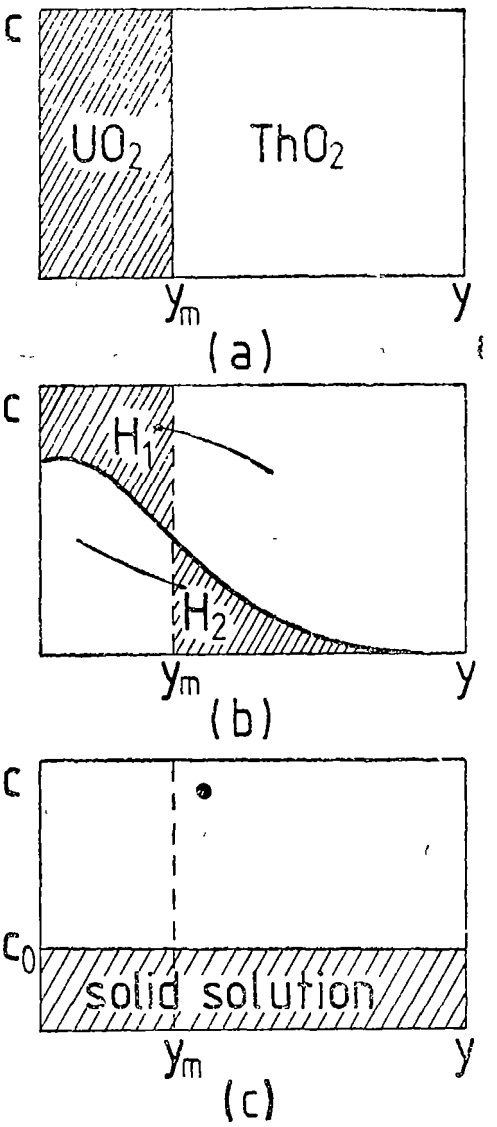

Fig 2 To the definition of the homogeneity parameter, H, in terms if the concentration profile (a) initial, (b) intermediate; (c) final stages of the diffusion process.

Exgerimental. The UO_2 powder was obtained by the ADU process and ThO_2 powder by oxalate calcination UO_2 and ThO_2 powders were mechanically blended in a ball mill for various time intervals The mixed powder was bilaterally pressed in a steel die at 2t/cm² The samples were sintered in the temperature range 1 000—1800°C in reducing atmosphere.

The specimens cover the following processing variables concentration, sintering temperature and milling time.

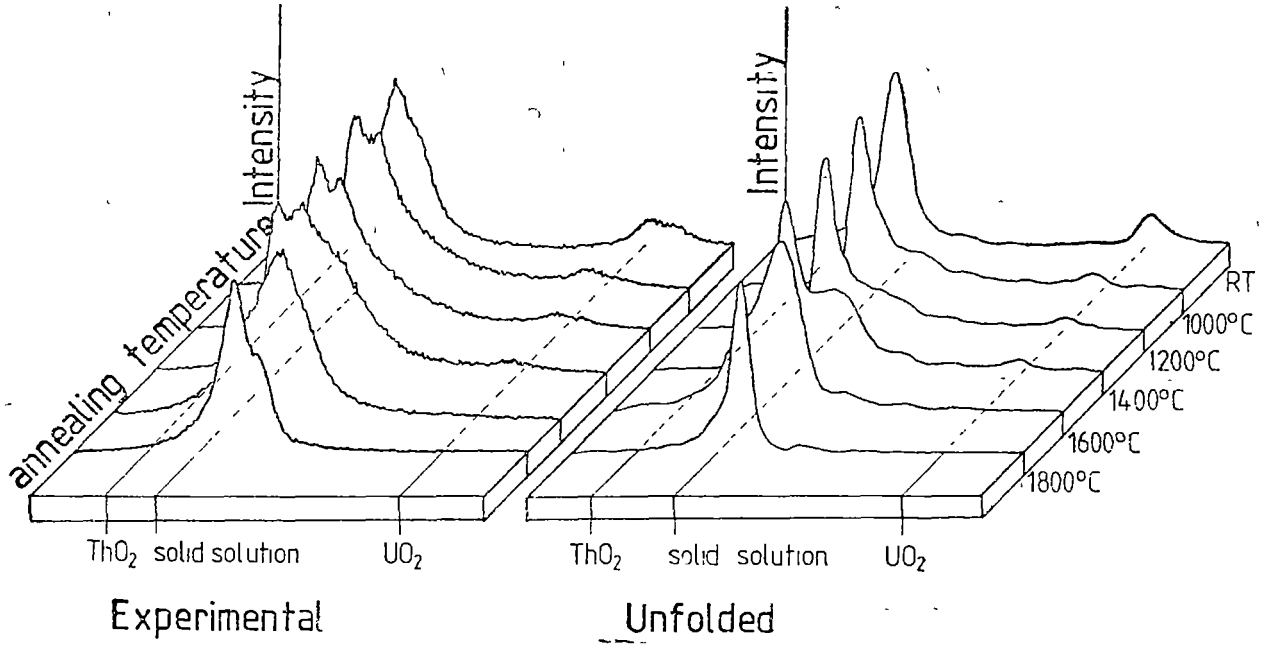

Fig. 3 The evolution of the X-Ray diffraction experimental data with the sintering temperature Since the unfolded profiles are smooth, without riples, the numerical procedure may be reliably validated.

Afte annealing, the specimens were polished to avoid the influence of the surface diffsion.

The X-Ray measurements were performed with a PW 1130/00 Philips powder diffractometer with vertical PW 1150/00 goniometer, a Cu FF tube and AMR graphite monochromator The (311) reflexion of the oxides was chosen for analysis for counting statistics reasons since the numerical procedure is sensitive to this parameter [9] The reference sample was a pure UO_2 sintered pellet. The data were collected at 0 01° 2θ intervals on a HP 9830A computer By using a Tikhonov regularisation procedure the unfolding was perfoimed by the Stokes method The numerical procedure was discussed in detail elsewhere [9] Fig. 3 presents the evolution of the experimental data with the sintering temperature

As mentioned earlier, the homogeneity parameter is defined in relative terms Therefore as 0% homogeneity samples, mechanical blends of powders were chosen Sintered coprecipitated samples provided 100% homogeneity standards

The results of the experiments are presented in Fig. 4—7

Discussions. The decrease of the homogeneity with the UO_2 concentration (Fig 4) may be explained simply by using Fick's first law Along with neutron economy considerations, this suggests that small UO_2 concentrations are preferable in the reactor design. Moreover, the linear decrease is a strong support

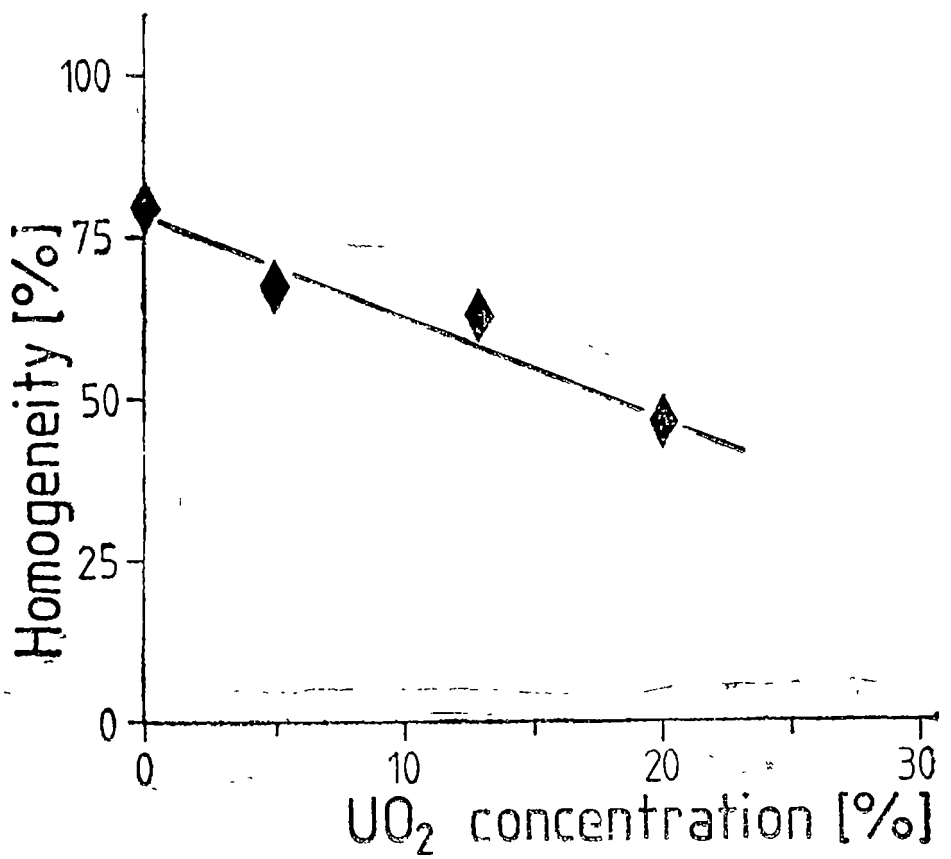

Fig. 4. The homogeneity variation versus UO_2 concentration. The specimens were sintered at 1800 °C.

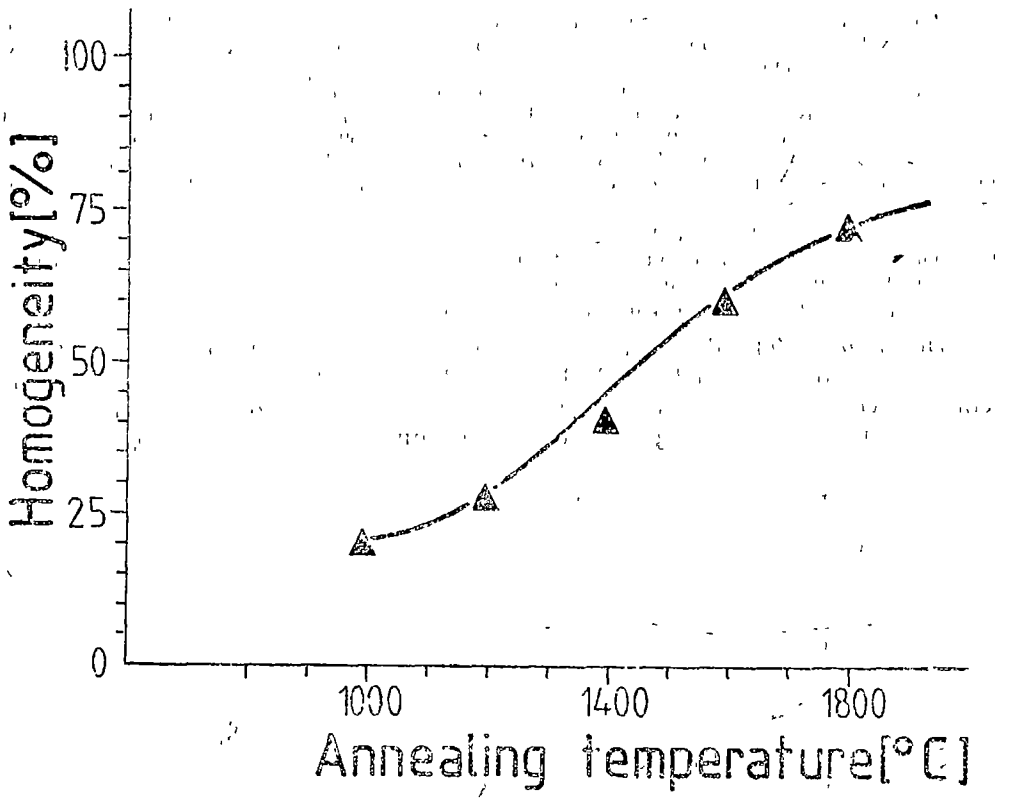

Fig. 5 The homogeneity variation versus sintering temperature

for a simple diffusion model in the formation of the solid solution, e.g. by using Fick's laws.

The increase in homogeneity with the sintering temperature (Fig. 5) is easy to predict. However, due to the small force used during the pressing process, the saturation effect at high temperatures is less pronounced in our data comparatively with Furuya et al [8] Since the results of the study apply at an atomic level this feature stresses the strong influence of the grain boundary diffusion during the sintering process (occuring at a larger distance). Thus, from the point of view of homogeneity only, a pressing force as high as possible would be benefic.

The homogeneity evolution versus milling time (Fig 6) with its saturation effect may be further understood in relationship with the efficience of the mill, i.e the dependence of the grain size (crystallite size) versus milling time The similar hardnesses of the two powders allow this further processing of the data. The results are plotted in Fig. 7. This linear dependence clearly demonstrates the role of the grain boundary diffusion in the formation of the solid solution.

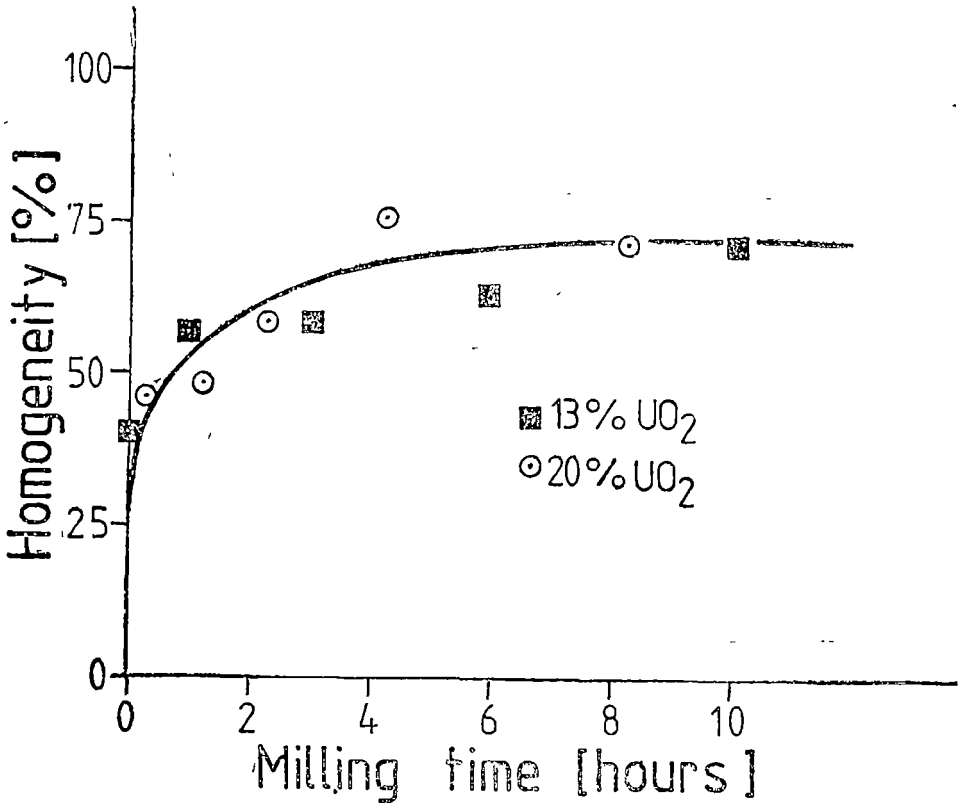

Fig. 6 The homogeneity variation versus milling time The specimens were sintered at 1800 °C.

The obtained evidence that the grain boundary impedes the diffusion may be eventually used to remove the incertitude left in the theory that the effective penetration is given in relative terms, Eq. (3)

An appropriate study by microprobe of the specimens could reveal a correlation between the grain size and the maximum effective penetration, $y = 1$. If such a study will be successfull, the results may be used to the calculation of the effective diffusion coefficients and to the evaluation of the proper role the grain boundary diffusion plays

Conclusions. In this paper we have successfully used X-Ray diffraction data and a performing unfolding procedure to obtain a quantitative estimate of the homogeneity in the system ThO_2—UO_2. This was possible since the two substances are isomorphous and the lattice parameter obeys Vegard's law

Without qualitative alterations in the results some simplifications may be applied comparatively to other authors [8] the use of the (311) reflexion

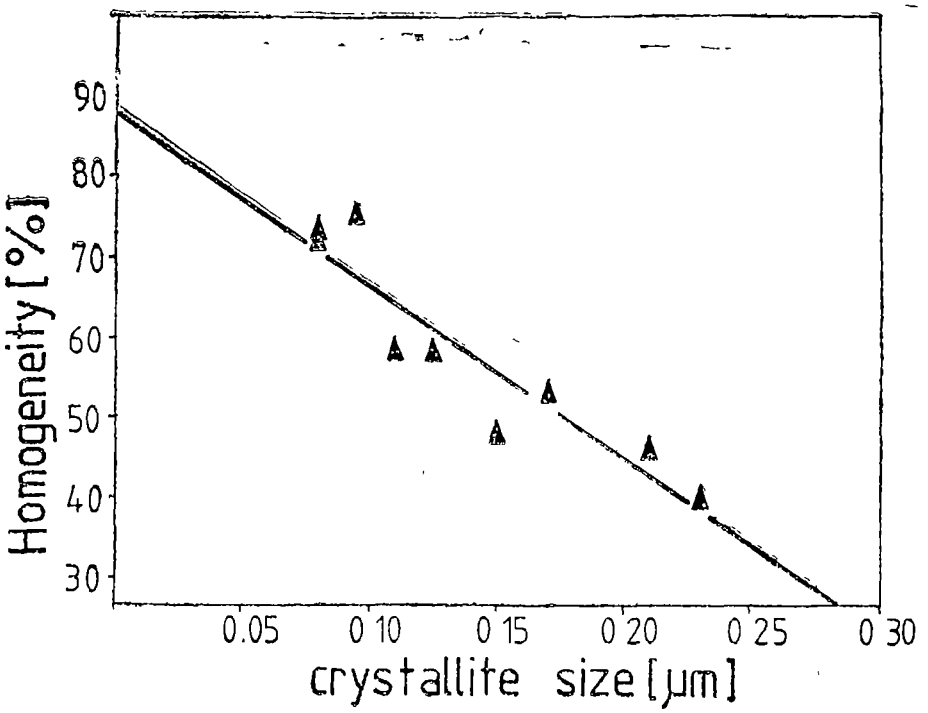

Fig 7 The homogeneity variation versus effective crystallite size The plot was obtained from that in Fig 6 by taking into account the mill efficiene

with better statistics, one can avoid the effective calculation of the Matano interface.

The important role of the grain boundary diffusion is evidenced, suggesting the need for further work by complementary methods to evaluate this contribution.

REFERENCES

1 P E Peterson, *General Electric Company Report*, HW 81259 (1964)
2 P. E Lerch and C. R Cooley, *Hanford Engineering Development Laboratory Report*, HEDL-SA 511 (1973).
3 D Vollath, *J of Nucl Mater*, 81 (1979) 115
4 P S Rudman, *Acta Cryst*, 13 (1960) 905
5 C R Houska, *J Appl Phys*, 41 (1970) 69
6 R Delhez, E J. Mittemeijer, E A van den Beigen, *J Mater Sci*, 13 (1978) 1671
7 D Vollath, C Ganguly, *Microchimica Acta*, suppl 6 (1975) 467
8 H Furuya, H Tajiri, N, Koizumi, *J Nucl Mater*, 106 (1982) 87.
9. D Ciurchea, *Studia Univ "Babeş—Bolyai"*, XXXII(2), (1987) 68.

STUDIA UNIV. BABEŞ—BOLYAI, PHYSICA, XXXIV, 1 1989

THE TESTING OF GRAVITATIONAL EFFECTS USING A LINEAR GYROSCOPE

Z. GÁBOS*

Received: December 10, 1988

ABSTRACT. — The study is focused on the gravitational effect of a rotating mass, distributed on a spherical surface, in the domain near the center of the sphere. Testing of the gravitational effects can be performed using a gyroscope consisting of two material points with equal rest masses and invariant distance.

1. Expression of the Lagrangean. We consider that the rest mass M_0 is uniformly distributed on the spherical surface of radius A, and this sphere has a nonuniform rotating movement around a fixed axis which crosses the center. The quantities of the studied system are given in the laboratory system K which has the origine in the center of the sphere denoted by O, and on the other hand in the system K', associated with the gyroscope, and with the origine O' in its center. The angular velocity $\vec{\Omega}(t)$ of the sphere, the position vector $\vec{X}$ of a point from the surface of the sphere, the position vector $\vec{x}$, and the translation velocity $\vec{v}$ of the center of the gyroscope are quantities defined in K, and the angular velocity $\vec{\omega}$ of the gyroscope as well as the position vectors $\vec{x}_0$, respectively $-\vec{x}_0$ of the materials points of the gyroscope (each of them with the rest mass $m_0/2$) are given in the system K'.

We will be satisfied with a second order approximation, in the domain near O we can write

$$|\vec{X} - \vec{x} - \vec{x}_0|^{-n} = A^{-n}\left[1 + \frac{2n}{A^2}(\vec{X}, \vec{x} + \vec{x}_0) - \frac{n}{A^2}(\vec{x} + \vec{x}_0)^2 + \right.$$

$$\left. + \frac{2n(n+1)}{A^4}(\vec{X}, \vec{x} + \vec{x}_0)^2 + \ldots\right] \tag{1}$$

If we consider that due to the relativistic combination of the velocity $\vec{v}$ given in K and of the velocities $(\vec{\omega}\ x\ \vec{x}_0)$ and $-(\vec{\omega}\ x\ \vec{x}_0)$ respectively given in K', we obtain the square of the velocity of the material points of the gyroscope in K as

$$V_{\pm}^2 = \frac{1}{\left[1 \pm \frac{1}{c^2}(\vec{v}, \vec{\omega}, \vec{x}_0)\right]^2}\left\{[\vec{v} \pm (\vec{\omega}\ x\ \vec{x}_0)]^2 - \frac{1}{c^2}(\vec{v}\ x(\vec{\omega}\ x\ \vec{x}_0))^2\right\}, \tag{2}$$

* *University of Cluj-Napoca, Faculty of Matematics and Physics, 3400 Cluj-Napoca Romania*

and using the Fock-Fichtenholtz Lagrangean, in the framework of the considered approximation, we can write

$$L = \frac{m_0}{2}\left(1 + \frac{3\lambda}{A} + \frac{v^2}{4c^2}\right)v^2 + \frac{1}{2}\left(1 + \frac{3\lambda}{A} - \frac{v^2}{2c^2} + \frac{1}{4m_0c^2} I_{km}\omega_k\omega_m\right) \times$$

$$\times I_{ij}\omega_i\omega_j - \frac{m_0}{c^2}(\vec{\omega}, \vec{x}_0, \vec{v})^2 + \frac{m_0c^2\lambda}{A}\left(1 - \frac{\lambda}{2A}\right) + m_0\lambda A\Omega^2 +$$

$$+ \frac{m_0\lambda}{10A}[\vec{x}^2\Omega^2 - 3(\vec{x}, \vec{\Omega})^2] + \frac{m_0\lambda}{10A}[\vec{x}^2\vec{\Omega}^2 - 3(\vec{x}_0, \vec{\Omega})^2] - \tag{3}$$

$$- \frac{4m_0\lambda}{3A}(\vec{\Omega}, \vec{x}, \vec{v}) - \frac{4\lambda}{3A} I_{ij}\Omega_i\omega_j,$$

where

$$\lambda = \frac{kM_0}{c^2}, \quad I_{ij} = m_0(\vec{x}_0^2\delta_{ij} - x_{0i}x_{0j}). \tag{4}$$

2. **The Equation of Motion.** Let us consider the third axis of the system K in the direction of $\vec{\Omega}$ (thus $\vec{\Omega}$ has the components $0, 0, \Omega$). The third axis of the system K' will have the orientation of $\vec{x}_0$. If the position of the system K' to K is given by the Euler angles ϑ, φ, Ψ, the components of $\vec{\omega}$ and $\vec{x}_0$ are

$$\vec{\omega}(\dot{\vartheta}\cos\Psi + \dot{\varphi}\sin\vartheta\sin\Psi,\ \dot{\vartheta}\sin\Psi - \dot{\varphi}\sin\vartheta\cos\Psi,\ \dot{\Psi} + \dot{\varphi}\cos\vartheta), \tag{5}$$

$$\vec{x}_0(x_0\sin\vartheta\ \sin\Psi,\ -x_0\sin\vartheta\ \cos\Psi,\ x_0\cos\vartheta).$$

Using (3) from the Euler-Lagrange equation

$$\frac{\partial L}{\partial x_i} - \frac{d}{dt}\left(\frac{\partial L}{\partial \dot{x}_i}\right) = 0, \tag{6}$$

we obtain the equation of motion wich describes the translation of the gyroscope

$$\frac{d\vec{v}}{dt} = \frac{\lambda\Omega^2}{10A}\operatorname{grad}\Phi + \frac{8\lambda}{3A}(\vec{\Omega}\,x\,\vec{v}) + \frac{4\lambda}{3A}(\dot{\vec{\Omega}}\,x\,\vec{x}), \tag{7}$$

where

$$\Phi = x_1^2 + x_2^2 - 2x_3^2 \tag{8}$$

Taking into consideration the equation (5), the Euler-Lagrange equation which describe the rotation of the gyroscope can be written as

$$\frac{d}{dt}\left(\frac{\partial L}{\partial \omega_i}\right) = \varepsilon_{ijk}\left(\omega_j\frac{\partial L}{\partial \omega_k} + x_{0j}\frac{\partial L}{\partial x_{0k}}\right). \tag{9}$$

Using (3), (9) and the equation

$$\frac{dI_{ij}}{dt} = \varepsilon_{ikm}\omega_k I_{mj} + \varepsilon_{jkm}\omega_k I_{mi}, \tag{10}$$

we get the equation of motion which describes the rotation of the gyroscope as

$$I_{ij}\dot{\omega}_j = \frac{4\lambda}{3A}\varepsilon_{jkm}\omega_k I_{mi}\Omega_j + \frac{4\lambda}{3A} I_{ij}\dot{\Omega}_j + \frac{m_0\lambda}{10A}\Omega^2\varepsilon_{ikp}x_{0k}\frac{\partial\Phi_0}{\partial x_{0p}} -$$

$$- \frac{4\lambda}{3A}\varepsilon_{ikp}\frac{\partial I_{rm}}{\partial x_{0p}}\Omega_r\omega_m, \tag{11}$$

where

$$\Phi_0 = x_{01}^2 + x_{02}^2 - 2x_{03}^2 \tag{12}$$

The obtained results can be generalized for the case when the gyroscope presents symmetry to a point

3 **Conclusions.** The calculations [1], [5], [6] performed up to present have been performed for a punctiform gyroscope, or for a spherical homogeneous gyroscope

For the linear gyroscope we reach the above conclusions concerning the translation and rotation motion

The equation of motion (7) valid for the translation of the center of gyroscope is identical with the motion equation obtained for a spherical and punctiform gyroscope

The equation (11) obtained for the rotation motion is more complicated, because, this equation contains components of the tensor of inertial momentum Between the contributions wich gives rise to a change in the rotation motion of the gyroscope are the coupling of the rotation moments due to the rotating sphere and the gyroscope, the quadratic training effect given by the rotation of the sphere as well as the training effect given by the nonuniform rotation of the sphere.

From the equation (11) we can eliminate the rest mass of the gyroscope, thus the equivalence principle concerning the translation motion (the insensibility concerning value of m_0) can be generalized also at the rotation motion.

The magnitude of the relativistic effects is given by λ/A, Ω, $\dot{\Omega}$ and $|\vec{x}_0|$.

REFERENCES

1 H Thirring, *Phys Z*, 19, 33 (1918), 22, 29 (1921)
2 I G Fichtenholtz, *JETF*, 20, 233 (1950).
3 Z Gábos, *Analele Univ "Al I. Cuza" Iaşi*, 5, 101 (1959)
4 L D Landau, E M Lifşiţ, *"Teoria cîmpului"*, Bucureşti, 1963, p 363
5 S Weinberg, *"Gravitaţia i kosmologia"*, Moskva, 1975, p. 251—257
6 B Mashhoon, F. W Hehl, D S Theiss, *Gen Rel. and Grav*, 16, 711 (1984).

STUDIA UNIV. BABEŞ—BOLYAI, PHYSICA, XXXIV, 1 1989

RECTANGULAR WAVEGUIDE IMPATT OSCILLATOR DESIGN

LINDENMAIER J*. and D. STĂNILĂ*

Received: January 12, 1989

ABSTRACT. — The paper presents a complete analysis of a microwave oscillator in rectangular waveguide, using an IMPATT device The IMPATT diode is fixed in the wavequide by means of a metallical rod The diameter of this rod influence the frequency of the oscillator. We have performed both a theoretical and experimental analysis of the oscillation frequency as a function of the rod diameter The results show a good concordance between the theory and the experiment A computer program is also presented.

Theory. The frequence of the oscillator may be determined knowing the parameters of the wavequide mounture. The driving point impedance of the mount has been determined by the extention of the induced EMF method of Carter [1], developed by Eisenhart [2] Such a monture in a general case is shown in Fig. 1

The post mount equivalent circuit, for the H_{10} mode is shown in Fig. 2. The components X_L and Y_{RP} have the following expressions:

$$jX_L = \sum_{m=2}^{\infty} Z_{m0} \left(\frac{K_{pm}}{K_{p1}}\right)^2 \left(1 - \frac{\omega}{a}\right) \tag{1}$$

$$Y_{RP} = (K_{p1}^2) \sum_{m=1}^{\infty} \left[\frac{1}{\sum_{m=1}^{\infty} Z_{mn} \left(\frac{K_{pm}}{K_{gn}}\right)^2}\right] \tag{2}$$

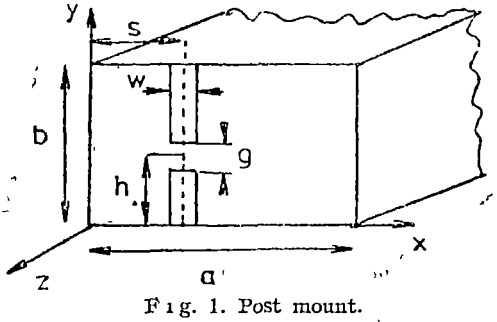

Fig. 1. Post mount.

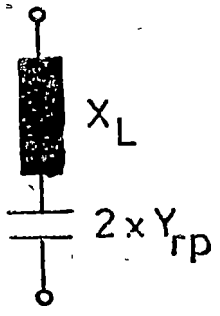

Fig 2. Post mount circuit for incident H_{10} mode.

* *University of Cluj-Napoca, Faculty of Mathematics and Physics, 3400 Cluj-Napoca, Romania*

where

$$Z_{mn} = \frac{j\eta b}{ak} \cdot \frac{K^2 - K_y^2}{(2 - \delta_0)(K_x^2 + K_y^2 - K^2)^{1/2}} \tag{3}$$

is the impedance of the H_{mn} mode,

$$K_{pm} = \sin K_x S \left(\frac{\sin \theta_m}{\theta_m}\right)$$

is the post cupling factor,

$$K_{gn} = \cos K_y h \left(\frac{\sin \Phi_n}{\Phi_n}\right)$$

is the gape coupling factor,

$$K = \frac{2\pi}{\lambda} \quad K_x = \frac{m\pi}{a} \quad K_y = \frac{n\pi}{b}$$

$$\delta_0 = \begin{cases} 1 & \text{for} \quad n = 0 \\ 0 & \text{for} \quad n \neq 0 \end{cases}$$

$$\theta_m = \frac{m\pi\omega}{2a}, \quad \Phi_m = \frac{n\pi g}{2b}$$

and η is the wave impedance.

In this way the equivalent circuit for the oscillator reprezented in Fig. 3 becomes as shown in Fig. 4.

In Fig. 4 Z_{sc} represents the equivalent impedance of the waveguide with the shortcircuit in the right side of the IMPATT device. Z_{sc} is expressed as:

$$Z_{sc} = jZ_0 \operatorname{tg} \beta L \tag{4}$$

where

$$Z_0 = \frac{2b}{a} \frac{377}{\left[1 - \left(\frac{\lambda_g}{\lambda_c}\right)^2\right]^{1/2}}$$

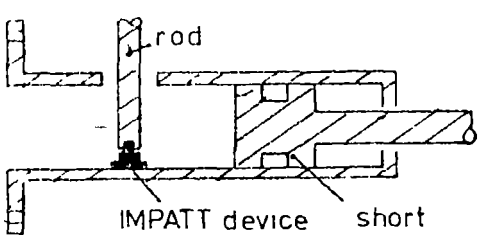

Fig 3. Scheme of the waveguide oscillator.

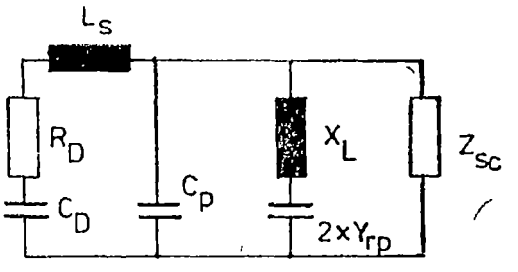

Fig. 4. General reprezentation of the equivalent cicuit.

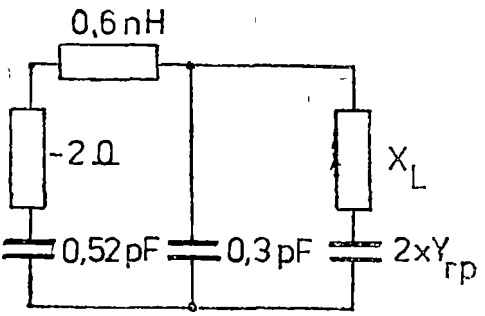

Fig. 5. Practical equivalent circuit

is the characteristic impedance of the waveguide; R_D is the negative resistance of the junction; C_D junction capacitance; L_S wire inductance; C_P case capacitance.

At $L = \frac{\lambda_g}{2}$, Z_{sc} becomes ∞ so that, knowing the diode parameters, the new equivalent circuit becomes as shown in Fig 5.

The impedance of the active device $\dot{Z}_D$ has the following expression:

$$\dot{Z}_D = \frac{-X_p[R_D + j(X_s - X_p)]}{R_D + j(X_s - X_D - X_p)}$$

From the resonance condition [3] $I_m \dot{Z}_D = X_L + Y$ we obtain the frequence of the oscillator

Exgeriments. Such an oscillator may be seen in photographs 1 and 2

The theoretic calculus of the oscillation frequencis has been obtained by means of a computer program, given in Appendix, for different diametervalues of the rod.

The oscillator has also been experimented with seven rod diameters, The theoretical and experimental results are given in Tab 1

Tab I

D (10^{-3}m)	ω (10^{-3}m)	s (10^{-3}m)	g (10^{-3}m)	h (10^{-3}m)	F_{theor} (GHz)	F_{exp} (GHz)
2,7	5	11,35	2,4	1,2	9,48	9,12
3	5,4	11,35	2,4	1,2	9,7	9,35
3,3	6	11,35	2	1	9,9	9,26
3,5	6,3	11,35	2,4	1,2	10,3	9,8
4	7,2	11,35	2,4	1,2	10,9	10,45
4,2	7,56	11,35	2,4	1,2	—	—
4,5	8,1	11,35	2,4	1,2	11,46	11,1
5	9	11,35	2,4	1,2	12,4	12,2

A = 22,7 10^{-3}m, B = 10,2 10^{-3} m

Conclusion. From Table 1 it can be seen that the theory previously described is in agreement with the experiment. The small differences between the theoretical and experimental values occur because of the following facts.

Photo 1, 2

1. The parameters of the IMPATT diode strongly depend of the bias current
2. The equivalent circuit of the IMPATT diode is a simplified one.
3. The resistive loss of the metallical rod has been neglected.

APPENDIX

```
      REAL L KP1  KPM KGN
      DATA A/0 02277.B/0 0102/ S/0 01135/
      NR=0
    1 READ(105,3)W G.H
    3 FORMAT(3F7 5)
      PC=3 0OE+08/2/A
      WR TE(108 10)A B S W G M
   10 FORMAT(5X A= F7 5 5X B= .r7 5 5X. S= Fr 5//
     *5X .W=. F7 5 5X G= F7 5 5X H= F7 5/ //)
      WP=W/A
      PT=3.14159
      KP1=SIN(PI*S/A)*(SIN(PI*W/2/A)(PI*W/2/A))
      F=8 OE+09
   20 CONTINUE
      XL=0
      YR=0
      DO 30 M=2 30
      N=0
      ZMN=FZMN(A B PI M N P)
      KPM=FKPM(M A S W PI)
      XL=XL+ZMN*  (KPM/KP1**2*(1-WP)
   30 CONTINUE
      DO 40 N=1.30
      Z=O
      DO 41 M=1 30
      ZMN=FZMN(A B PI.M N )
      KPM=FKPM(M A S W PI)
      KGN=FKGN(N.B G.PI H)
```

```
29      Z=Z+ZMN*(KPM/KGN)**2
30   41 CONTINUE
31      YR=YR+1/Z
32   40 CONTINUE
33      YRP=KP1**2*YR
34      DIF=XL+1/YRP/2
35      WRITE(108.50)F AL YRP DIF
36   50 FORMAT(8X F 18X XL 15X TRP UIF.//
37      *1X E14.7 4X.E14 7.4X.E14 7 4XE14(//)
38      IF(F GE 12 OE+09)GO TO 70
39      F=F+0 1E+09
40      GO TO 20
41   70 CONTINUE
42      NR=NR+1
43      IF(NR LE 6)GO TO 7
44      STOP
45      END
 1      FUNCTION FZMN(A B.PI.M N F)
 2      REAL L
 3      L=3 0E+08/F
 4      ETA=377 0
 5.     IF(N EQ O) GO TO 700
 6      DO = 0
 7      GO TO 110
 8  100 DO=1
 9      GO TO 110
10  110 CONTINUE
11      FZMN=(ETA*B*((2*P+/L)**2-(N*PI/B)**2))/((A*2*P)
12      *(SORT((M*PI/A)**2+(N*PI/B)**2-(2*PI/L)**2))
13      RETURN
14      END
 1      FUNCTION FKPM(M A W PI)
 2      FKPM=SIN(M*PI*S/A)*(SIN(M*PI*W/2)/(M*PI*W/2/A
 3      RETURN
 4      END
 1      FUNCTION FKGN(N.B G PI M)
 2      FKGN=COS(N*PI*H/B)*(SIN(N*PI*G/2/B))/(N*PI*G/2/
 3.     RETURN
 4      END
  MODULE    F MUATA     TYPE    P    LONGUEUR    0558
  MODULE    FZMN        TYPE    P    LONGUEUR    0180
  MODULE    FKPM        TYPE    P    LONGUEUR    00D0
  MODULE    FKGN        TYPE    P    LONGUEUR    00D0
```

REFERENCES

1. P S Carter, *Proc IRE*, vol 20, June 1932, pp 1004—1041.
2. R. L Eisenhart, P. J. Khan, *IEEE—MTT*, vol MTT—19, No. 8, Aug 1971, pp. 706—719.
3. R Baican, *"Oscilatoare şi amplificatori de microunde cu dispozitive semiconductoare"*, Ed Acad. R.S R., Bucureşti, 1979

STUDIA UNIV BABEŞ—BOLYAI, PHYSICA, XXXIV, 1. 1989

ON THE EVALUATION OF HIGHER ORDER ACCELERATIONS IN A MOVING SYSTEM OF REFERENCE

CONSTANTIN TUDOSIE*

Received: January 12, 1989

ABSTRACT. — The object of the present paper is to evaluate moduli for higher order accelerations in a moving system of reference in a moving point trajectory in E_3. For rectilinear trajectoris, Taylor formula expressible in terms of integrals is deduced and used

1. **Introduction.** The very rapid evolution of the phenomena, where higher order accelerations occur, and, consequently, at the same time very high velocity, has oriented the scientific researches towards a higher analysis, both from the theoretical as well as from practical point of view. In a previous paper [5], I have investigated these accelerations by considering them as vectorial quantities.

In the present paper 1 resume their study with the purpose of discussing their behaviour with respect to a moving reference system.

2. **The intrinsic kinematical aspect.** Let be $\bar{\tau}$, $\bar{\nu}$, $\bar{\beta}$ the unit vectors of an intrinsic orthogonal reference system in the moving point P of a trajectory in E_3. The derivatives relatively to the time of these unit vectors are

$$\dot{\bar{\tau}} = \dot{s}\, C\, \bar{\nu},\ \dot{\bar{\nu}} = \dot{s}(-C\bar{\tau} + T\bar{\beta}),\qquad \dot{\bar{\beta}} = -\dot{s}\, T\, \bar{\nu}, \tag{1}$$

where $s = s(t)$ is the equation of motion of the considered point, C the trajectory curvature in P, and T the torsion of the trajectory in this point.

It is well known that the vector velocity of the moving point may be written in the following way

$$\bar{v} = v(t) \cdot \bar{\tau}(t). \tag{2}$$

Further, in order to set out a correspondence between the order of the accelerations and the order of the derivatives, we shall call the vector velocity $\bar{v}$ zero-order acceleration, its time-derivative $\dot{\bar{v}}$ first-order acceleration and the vector $\overset{(i)}{\bar{v}}$ for $i > 1$ higher order accelerations.

By taking in (2) the first two successive derivatives, we obtain the expressions

$$\dot{\bar{v}} = v\dot{\bar{\tau}} + v^2 C\, \bar{\nu}, \tag{3}$$

$$\ddot{\bar{v}} = \ddot{v}\bar{\tau} + 2v\dot{\bar{\tau}} + v\,\ddot{\bar{\tau}}. \tag{4}$$

* *Polytechnic Institute of Cluj-Napoca, 3400 Cluj-Napoca, Romania*

Or, the second order derivative of the unit vector $\bar{\tau}$ is

$$\dot{\bar{\tau}} = \varphi_2(t)\bar{\tau} + \omega_2(t)\bar{\nu} + \varepsilon_2(t)\bar{\beta}, \tag{5}$$

where

$$\varphi_2(t) = -(v\,C)^2,\ \omega_2(t) = (v\,C)^{\cdot},\ \varepsilon_2(t) = v^2CT$$

By virtue of (1) and on substituting (5) into (4), we get

$$\ddot{\bar{v}} = f_2(t)\bar{\tau} + g_2(t)\bar{\nu} + h_2(t)\bar{\beta}, \tag{6}$$

where

$$f_2(t) = \ddot{v} - v^3C^2,\ g_2(t) = 3v\,\dot{v}\,C + v^2\dot{C},\ h_2(t) = v^3CT$$

With regard to the notations from (6), it follows, immediatly, that the vector acceleration of i-order is

$$\overset{(i)}{\bar{v}} = f_i(t)\bar{\tau} + g_i(t)\bar{\nu} + h_i(t)\bar{\beta}, \tag{7}$$
$$(i = 1,\ 2,\ 3,\quad .).$$

In accordance with the previous expressions (2), (3) and (6), the zero-order acceleration is directed parallel to the tangent of the trajectory, the first-order acceleration lies in the osculating plane of the trajectory, whilst the accelerations corresponding to $i > 1$ constitute a system of concurrent vectors in space in the moving point on the trajectory, each of these vectors possessing certain position with respect to the reference frame of Frenet

With the same relations as in (5), the time derivative of order $i + 1$ of the unit vector $\bar{\tau}$ may be written under the form

$$\overset{(i+1)}{\bar{\tau}} = \varphi_{i+1}(t)\bar{\tau} + \omega_{i+1}(t)\bar{\nu} + \varepsilon_{i+1}(t)\bar{\beta}. \tag{8}$$

3. **The method.** According to the Leibnitz formula, the vector acceleration of order i has the expression

$$\overset{(i)}{\bar{v}} = \sum_{k=0}^{i}\binom{i}{k} v^{(i-k)}\overset{(k)}{\bar{\tau}}, \qquad (i = 1,\ 2,\ 3,\quad .). \tag{9}$$

where

$$\overset{(k)}{\bar{\tau}} = \sum_{\sigma=0}^{i-k}\bar{\tau}_{k+\sigma}(0)\,\frac{t^\sigma}{\sigma!} + \int_0^t Q(t,\,s)\,\bar{\tau}_{i+1}(s)\,ds, \tag{10}$$

with the notations

$$\overset{(k+\sigma)}{\bar{\tau}}(0) = \bar{\tau}_{k+\sigma}(0), \qquad \overset{(i+1)}{\bar{\tau}} = \bar{\tau}_{i+1}, \qquad Q(t,\,s) = \frac{(t-s)^{i-k}}{(i-k)!}, \quad (k = 0,\ 1,\ 2,\quad ,\ i).$$

For $k = 0$, the expression (10) becomes

$$\bar{\tau} = \sum_{\sigma=0}^{i}\bar{\tau}_\sigma(0)\,\frac{t^\sigma}{\sigma!} + \int_0^t N(t,\ s)\bar{\tau}_{i+1}(s)\ ds, \tag{11}$$

where

$$N(t,\ s) = \frac{(t-s)^t}{t\,!}.$$

Now, by substituting (10) into (9), we get

$$\overset{(i)}{\bar{v}} = \sum_{k=0}^{i} \binom{i}{k} \overset{(i-k)}{v} \left[\sum_{\sigma=0}^{i-k} \bar{\tau}_{k+\sigma}(0)\ \frac{t^\sigma}{\sigma\,!} + \int_0^t Q(t,\ s)\ \bar{\tau}_{i+1}(s)\ ds \right]. \tag{12}$$

On account of the initial conditions

$\overset{(j)}{v}(0) = v_j(0)$, $\overset{(j)}{\varphi}(0) = \varphi_j(0)$, $\overset{(j)}{\omega}(0) = \omega_j(0)$, $\overset{(j)}{\varepsilon}(0) = \varepsilon_j(0)$, $(j = 0,\ 1,\ 2,\ \ldots,\ i)$,

the expressions of the vectors $\bar{\tau}_\sigma(0)$ and $\bar{\tau}_{k+\sigma}(0)$, in the reference system $\bar{\tau}$, $\bar{\nu}$, $\bar{\beta}$ are the following

$$\bar{\tau}_\sigma(0) = \varphi_\sigma(0)\bar{\tau} + \omega_\sigma(0)\bar{\nu} + \varepsilon_\sigma(0)\bar{\beta}, \tag{13}$$

$$\bar{\tau}_{k+\sigma}(0) = \varphi_{k+\sigma}(0)\bar{\tau} + \omega_{k+\sigma}(0)\bar{\nu} + \varepsilon_{k+\sigma}(0)\bar{\beta} \tag{14}$$

If $v(t)$ is a given function, we may write down the equation

$$\int_0^t K(t,\ s)\ v_{i-k}(s)\ ds = F(t), \qquad \overset{(i-k)}{v} = v_{i-k}, \quad (i-k = 1,\ 2,\ 3,\ \ldots), \tag{15}$$

where

$$K(t,\ s) = \frac{(t-s)^{i-k-1}}{(i-k-1)\,!}, \qquad F(t) = v(t) - \sum_{\sigma=0}^{i-k-1} v_\sigma(0)\ \frac{t^\sigma}{\sigma\,!}$$

The above equation (15) is a Volterra linear integral equation of first kind [4]

Recalling (8) and (13), we see that by scalar multiplication of the vector equation (11) separately with $\bar{\tau}$, $\bar{\nu}$ and $\bar{\beta}$ it results the following three scalar integral equations

$$\sum_{\sigma=0}^{i} \varphi_\sigma(0)\ \frac{t^\sigma}{\sigma\,!} + \int_0^t N(t,\ s)\ \ \varphi_{i+1}(s)\ ds = 1, \tag{16}$$

$$\sum_{\sigma=0}^{i} \omega_\sigma(0)\ \frac{t^\sigma}{\sigma\,!} + \int_0^t N(t,\ s)\ \ \omega_{i+1}(s) ds = 0, \tag{17}$$

$$\sum_{\sigma=0}^{i} \varepsilon_\sigma(0)\ \frac{t^\sigma}{\sigma\,!} + \int_0^t N(t,\ s)\ \ \varepsilon_{i+1}(s) ds = 0. \tag{18}$$

By introducing the notations

$$\Psi_1(t) = 1 - \sum_{\sigma=0}^{i} \varphi_\sigma(0)\ \frac{t^\sigma}{\sigma\,!}, \qquad \Psi_2(t) = \sum_{\sigma=0}^{i} \omega_\sigma(0)\ \frac{t^\sigma}{\sigma\,!}, \qquad \Psi_3(t) = \sum_{\sigma=0}^{i} \varepsilon_\sigma(0)\ \frac{t^\sigma}{\sigma\,!},$$

equations (16), (17) and (18) become

$$\int_0^t N(t, s)\varphi_{i+1}(s)ds = \Psi_1(t), \tag{19}$$

$$\int_0^t N(t, s)\omega_{i+1}(s)ds = \Psi_2(t), \tag{20}$$

$$\int_0^t N(t, s)\varepsilon_{i+1}(s)ds = \Psi_3(t). \tag{12}$$

On the other hand, by resorting to the relations (7), (8) and (14), after separate scalar multiplication of equation (12) with $\bar{\tau}$, $\bar{\nu}$ and $\bar{\beta}$, we obtain

$$f_i(t) = \sum_{k=0}^{i} \binom{i}{k} \overset{(i-k)}{v} \left[\sum_{\sigma=0}^{i-k} \varphi_{k+\sigma}(0) \frac{t^\sigma}{\sigma!} + \int_0^t Q(t, s)\varphi_{i+1}(s)\, ds \right], \tag{22}$$

$$g_i(t) = \sum_{k=0}^{i} \binom{i}{k} \overset{(i-k)}{v} \left[\sum_{\sigma=0}^{i-k} \omega_{k+\sigma}(0) \frac{t^\sigma}{\sigma!} + \int_0^t Q(t, s)\omega_{i+1}(s)\, ds \right], \tag{23}$$

$$h_i(t) = \sum_{k=0}^{i} \binom{i}{k} \overset{(i-k)}{v} \left[\sum_{\sigma=0}^{i-k} \varepsilon_{k+\sigma}(0) \frac{t^\sigma}{\sigma!} + \int_0^t Q(t, s)\varepsilon_{i+1}(s)\, ds \right], \quad (i=1, 2, 3, \ldots). \tag{24}$$

The functions f_i, g_i and h_i permit us to determine the modulus of the higher acceleration of order i

$$\left| \overset{(i)}{\bar{v}}(t) \right| = [f_i^2(t) + g_i^2(t) + h_i^2(t)]^{\frac{1}{2}}, \quad (i = 1, 2, 3, \ldots). \tag{25}$$

The equations (15), (19) and (22) together constitute a system (S_1) of $3i$ equations with $3i$ unknown quantities

$$f_i(t),\ \varphi_{i+1}(t),\ v_{i-k}(t),\ (i = 1, 2, 3, \ldots),\ (i - k = 1, 2, 3, \ldots).$$

The equations (20) and (23) together represent a system (S_2) of $2i$ equations containing $2i$ unknown quantities

$$g_i(t),\ \omega_{i+1}(t),\ (i = 1, 2, 3, \ldots).$$

The equations (21) and (24) constitute a system (S_3) of $2i$ equations with $2i$ unknown quantities

$$h_i(t),\ \varepsilon_{i+1}(t),\ (i = 1, 2, 3, \ldots).$$

4 **The solution of the system (S_1).** An approximate solution of the system of equations (S_1) may be determined by a method of numerical integration [2] If we apply in the interval $[0,\ t_1)$, $t_1 > 0$, the quadrature formula

$$\int_0^{t_\beta} f(s)ds \approx \delta \sum_{\nu=1}^{\beta} f(\nu\delta), \quad (\beta = 1,\ 2,\ 3,\ \ldots,\ m),$$

where $t_\beta = \beta\delta$, $\delta = \frac{t_1}{m}$, the system (S_1) becomes a system of $3mi$ algebraic equations with $3mi$ unknown quantities

$$\begin{cases} F(t_\beta) - \delta \sum_{\nu=1}^{\beta} K(t_\beta,\ \nu\delta)v_{i-k}(\nu\delta) = 0, \\ \Psi_1(t_\beta) - \delta \sum_{\nu=1}^{\beta} N(t_\beta,\ \nu\delta)\varphi_{i+1}(\nu\delta) = 0, \\ f_i(t_\beta) - \sum_{k=0}^{i} \binom{i}{k} v^{(i-k)}(t_\beta)\left[\sum_{\sigma=0}^{i-k} \varphi_{k+\sigma}(0)\frac{(t_\beta)^\sigma}{\sigma!} - \delta \sum_{\nu=1}^{\beta} Q(t_\beta,\ \nu\delta)\varphi_{i+1}(\nu\delta)\right] = 0, \\ (i = 1,\ 2,\ 3, \ldots),\ \beta = \overline{1,\ m}. \end{cases} \tag{26}$$

These unknown quantities are the following

$$f_i(\delta),\ f_i(2\delta),\ \ldots,f_i(t_1),\ \varphi_{i+1}(\delta),\ \varphi_{i+1}(2\delta),\ \ldots,\ \varphi_{i+1}(t_1),\ v_{i-k}(\delta),$$

$$v_{i-k}(2\delta),\ \ldots,\ v_{i-k}(t_1).$$

The modulus of the acceleration $\overset{(i)}{\bar{v}}$ in the points t_β is

$$\left|\overset{(i)}{\bar{v}}(t_\beta)\right| = [f_i^2(t_\beta) + g_i^2(t_\beta) + h_i^2(t_\beta)]^{\frac{1}{2}}, \quad (i = 1,\ 2,\ 3, \ldots).$$

The solutions of the system of equations (S_2) and (S_3) can be determined in a similar way.

a. The case of rectilinear trajectory. If the trajectory is rectilinear, we have

$$\bar{\tau} = \text{const}\ ,\ g_i(t) = 0,\ h_i(t) = 0,\ f_i(t) = v_i(t),$$

and (7) becomes

$$\overset{(i)}{\bar{v}} = v_i(t)\bar{\tau}. \tag{27}$$

The zero-order acceleration is given by the Taylor formula expressible in terms of the derivatives

$$v(t)=\sum_{i=0}^{n-1}\frac{v_i(t_1)}{i!}(t-t_1)^i+v_n(\xi)\frac{(t-t_1)^n}{n!}, \tag{28}$$

where

$$\xi=t_1+\theta(t-t_1),\quad \theta\in(0,1).$$

As we see, the Taylor formula contains all the derivatives with respect to the time of the function $v(t)$ in a certain point t_1, and namely from the derivative of zero-order till that of order n, this means that the Taylor formula (28) contains all the accelerations at the time t_1, corresponding to $i=0,\ldots,n-1$ as well as the last acceleration v_n at the time

Our aim is to establish in what follows for the Taylor formula an expression in terms of integrals.

Let be the Taylor formula expressible in terms of derivatives [1]

$$u(t)=\sum_{i=0}^{n-1}\frac{u_i(t_1)}{i!}(t-t_1)^i+u_n(\xi)\frac{(t-t_1)^n}{n!}, \tag{29}$$

where we have set $\overset{(i)}{u}(t)=u_i(t)$.

Taking into account the initial conditions

$$\overset{(j)}{u}(0)=u_j(0),\ (j=0,\ 1,\ 2,\ 3,\quad ,\ n+1),$$

we have

$$u_i(t_1)=F_{n-i}(t_1)+\int_0^{t_1}S_{n-i}(t_1,\ s)u_{n+1}(s)ds, \tag{30}$$

with the notations

$$F_{n-i}(t_1)=\sum_{\sigma=0}^{n-i}u_{i+\sigma}(0)\frac{t_1^\sigma}{\sigma!},$$

$$S_{n-i}(t_1,\ s)=\frac{(t_1-s)^{n-i}}{(n-i)!}.$$

We also have

$$u_n(\xi)=u_n(0)+\int_0^{\xi}u_{n+1}(s)ds. \tag{31}$$

Now, on substituting (30) and (31) into (29) it results Taylor formula in terms of integrals

$$u(t) = \sum_{i=0}^{n-1} \frac{(t-t_1)^i}{i!}\left[F_{n-i}(t_1) + \int_0^{t_1} S_{n-i}(t_1, s)u_{n+1}(s)\,ds\right] + \\ + \frac{(t-t_1)^n}{n!}\left[u_n(0) + \int_0^{\xi} u_{n+1}(s)\,ds\right], \tag{32}$$

$$\xi = t_1 + \theta(t-t_1), \quad \theta \in (0, 1).$$

In contrast to the formula (28), which involves the $n+1$ accelerations of all orders from zero to n, the last formula (32) contains only two accelerations, that is the acceleration of zero-order and the acceleration of order $n+1$ With the purpose of determining their expressions, we introduce the socalled "function of direct connection" $\omega_{n+1,0}(t)$, by writing down the equation [6], [7]

$$u_{n+1}(t) = \omega_{n+1,0}(t)\; u(t) \tag{33}$$

By substitution of (33) into (32), it gives

$$u(t) = \sum_{i=0}^{n-1} \frac{(t-t_1)^i}{i!}\left[F_{n-i}(t_1) + \int_0^{t_1} S_{n-i}(t_1, s)\omega_{n+1,0}(s)\cdot u(s)ds\right] + \\ + \frac{(t-t_1)^n}{n!}\left[u_n(0) + \int_0^{\xi} \omega_{n+1,0}(s)\cdot u(s)ds\right]. \tag{34}$$

The equations (32), (33) and (34) together represent a system (A) of 3 equations with the 3 unknown quantities

$$u(t),\; u_{n+1}(t),\; \omega_{n+1,0}(t).$$

The constant $\omega_{n+1,0}(0)$ is determined from (33) by putting there $t = 0$, that is

$$\omega_{n+1,0}(0) = u_{n+1}(0)\quad [u(0)]^{-1}.$$

One obtains the approximate solution of the system (A) by applying the known method of numerical integration [2].

REFERENCES

1. Ciorănescu, N, *Curs de algebră si analiză matematică*, Editura tehnică, Bucureşti, 1955
2. Démidovitch, B, Maron, I, *Éléments de calcul numérique*, Éditions Mir, Moscou, 1973
3. Iacob, C, *Mecanică teoretică*, Editura didactică şi pedagogică, Bucureşti, 1971
4. Lalescu, T, *Introducere la teoria ecuaţiilor integrale*, Editura Academiei Republicii Populare Române, Bucureşti, 1956
5. Tudosie, C, "On higher order accelerations", *Bulletin Mathématique de la Soc Sci Math de la R. S. de Roumanie*, Tome 19 (67), **3—4**, p 383—390, 1975
6. Tudosie, C, "Determination of higher order accelerations by a functional method", *Acta Technica ČSAV*, 2, p 218—224, 1983
7. Tudosie, C, "Determination of higher order accelerations by means of direct and inverse connexion functions", *Strojnícky Časopis*, **35**, p. 613—619, 1984, č. 5.

STUDIA UNIV. BABEŞ—BOLYAI, PHYSICA, XXXIV, 1 1989

ON HIGHER ORDER ACCELERATIONS IN THE NONLINEAR DOMAIN

CONSTANTIN TUDOSIE*

Received: January 12, 1989

ABSTRACT. — In this paper a method of deduction of the accelerations of any order is given when the differential equation describes a very fast phenomenon, with a high degree of nonlinearity. The method was named by the author "a division method".

1. **Introduction.** The natural phenomena, in their complexity, manifest a nonlinear behaviour. Consequently, a linearization procedure is adopted in order to reduce as far as possible the mathematical difficulties of the nonlinear problem under investigation.

However, as a result of the linearization procedure the structure of the differential equations itself undergoes a modification, that leads to the loss of certain qualitative features in the mathematical description of the evolution of the considered phenomena. Or, if the evolution of these phenomena is a very fast one, the order od the differential equations is higher, so that the solving of the problem becomes still more difficult.

In the present paper we give a method to determine the accelerations of any order in the case when the considered differential equations describe a very fast phenomenon having a higher degree of nonlinearity.

2. **The method.** Let be the following nonlinear differential equations from the domain of phenomena with very fast evolution

$$\sum_{i=0}^{n} a_i(t) \cdot \overset{(i)}{x}_{2p+1} = A(t), \tag{1}$$

together with the following initial conditions

$$\overset{(i)}{x}(0) = \overset{(i)}{x}_0, \quad (i = 0, 1, \ldots, n-1),$$

where

$$\overset{(i)}{x}_{2p+1} = [\overset{(i)}{x}]^{2p+1}, \qquad (p \in N, \text{ fixed}).$$

With the view to determine all the accelerations appearing in (1), we will apply a method, that we have named "the division method". Further, in order to introduce a consistent notation, we have called x the zero-order acceleration, $\dot{x}$ the first-order acceleration, $\ddot{x}$ the second-order acceleration and we have named the accelerations for $i > 2$ the higher-order accelerations [2], [3], [4], [5], so that the order of accelerations corresponds to the order of derivatives.

* *Polytechnic Institute of Cluj-Napoca, 3400 Cluj-Napoca, Romania*

Next, we introduce the functions

$$\omega_{i,2p+1}(t) = [\omega_i(t)]^{2p+1}, \quad (i = 0, 1, 2, \ldots, n),$$

called "division functions", we can write down the following equations

$$a_i(t) \cdot \overset{(i)}{x}_{2p+1}(t) = \omega_{i,2p+1}(t) \cdot A(t), \quad (i = 0, 1, 2, \ldots, n). \tag{2}$$

By substituting (2) into (1) we obtain

$$\sum_{i=0}^{n} \omega_{i,2p+1}(t) = 1. \tag{3}$$

Or, from (2) it follows

$$\overset{(i)}{x}(t) = \omega_i(t)\,[a_i^{-1}(t) \cdot A(t)]^{(2p+1)^{-1}}, \qquad (i = 0, 1, 2, \ldots, n). \tag{4}$$

Then replacing here i by $i - 1$, we get

$$\overset{(i-1)}{x}(t) = \omega_{i-1}(t)\,[a_{i-1}^{-1}(t) \cdot A(t)]^{(2p+1)^{-1}}. \tag{5}$$

Taking the ratio of (4) and (5) and integrating afterwards, we get

$$\overset{(i-1)}{x}(t) = \overset{(i-1)}{x_0} \exp\left\{\int_0^t \omega_{i-1}^{-1}(s)\,\omega_i(s)[a_{i-1}(s)\,a_i^{-1}(s)]^{(2p+1)^{-1}} ds\right\}, \quad (i=1, 2, 3, \ldots, n) \tag{6}$$

The equalities (3), (4) and (6) together represent a system (S) of $2(n+1)$ equations with $2(n+1)$ unknowns.

These unknown quantities are

$$\overset{(i)}{x}, \ \omega_i, \ (i = 0, 1, 2, \ldots, n).$$

α). *The case* $A(t) = 0$

If $A(t) = 0$, the equation (1) takes the form

$$\sum_{i=0}^{n} a_i(t) \cdot \overset{(i)}{x}_{2p+1} = 0. \tag{7}$$

By introducing here the following "division functions"

$$\varepsilon_{i,2p+1}(t) = [\varepsilon_i(t)]^{2p+1}, \quad (i = 1, 2, 3, \ldots, n),$$

we obtain the equations

$$a_i(t) \cdot \overset{(i)}{x}_{2p+1}(t) = \varepsilon_{i,2p+1}(t) \cdot x(t), \quad (i = 1, 2, 3, \ldots, n) \tag{8}$$

For $i = 0$, this last equation becomes

$$a_0(t) \cdot x_{2p}(t) = \varepsilon_{0,2p+1}(t) \tag{9}$$

Now, substituting (8) into (7), it results

$$\sum_{i=0}^{n} \varepsilon_{i,2p+1}(t) = 0. \tag{10}$$

On the other hand, one obtains from (8)

$$\overset{(i)}{x}(t) = \varepsilon_i(t)\,[a_i^{-1}(t)\cdot x(t)]^{(2p+1)^{-1}}, \qquad (i = 1,\ 2,\ 3,\ \ldots,\ n), \tag{11}$$

and replacing here i by $i-1$, we get

$$\overset{(i-1)}{x}(t) = \varepsilon_{i-1}(t)[a_{i-1}^{-1}(t)\cdot x(t)]^{(2p+1)^{-1}}. \tag{12}$$

By taking the ratio of (11) and (12), then performing an integration, we obtain

$$\overset{(i-1)}{x}(t) = \overset{(i-1)}{x_0}\exp\left\{\int_0^t \varepsilon_{i-1}^{-1}(s)\ \varepsilon_i(s)\,[a_{i-1}(s)\ a_i^{-1}(s)]^{(2p+1)^{-1}}\right\},\ (i=1,2,3,\quad,n) \tag{13}$$

The equalities (9), (10), (11) and (13) together represent a system (Q) of $2(n+1)$ equations with $2(n+1)$ unknown quantities The unknown quantities of this system are

$$\overset{(i)}{x},\ \varepsilon_i,\ (i = 0,\ 1,\ 2,\quad,\ n).$$

3. **The solution of the system (S).** An approximate solution of the system (S) of the $2(n+1)$ equations (3), (4), and (6) may be derived by a numerical integration method as follows We will namely apply on the interval $[0,\ a]$, $a > 0$, a numerical method similar to that of the polygonal lines method, that is to say we will divide this interval by the points $t_k = k\delta$, $\delta = \frac{a}{m}$, $k = \overline{1,m}$ and we will take into account the quadrature formula

$$\int_0^{k\delta} f(s)ds \approx \delta\sum_{\nu=1}^{k} f(\nu\delta),\ (k = 1,\ 2,\ .\ \ ,\ m) \tag{14}$$

Now, if we write down that the system (S) is verified for $t_k = k\delta$, and use (14) for the approximate evaluation of the integrals, we obtain the following system of $2m(n+1)$ algebraic equations with $2m(n+1)$ unknown quantities,

$$\begin{cases} \sum_{i=0}^{n} \omega_{i,2p+1}\ (k\delta) - 1 = 0, \\ \overset{(i)}{x}(k\delta) - \omega_i(k\delta)[a_i^{-1}(k\delta)\cdot A\,(k\delta)]^{(2p+1)^{-1}} = 0, \quad (i = 0,\ 1,\ 2,\quad .\ ,\ n), \\ \overset{(i-1)}{x}\ (k\delta) - \overset{(i-1)}{x_0}\exp\left\{\delta\sum_{\nu=1}^{k}\omega_{i-1}^{-1}\ (\nu\delta)\,\omega_i(\nu\delta)\cdot[a_{i-1}\,(\nu\delta)\ a_i^{-1}(\nu\delta)]^{(2p+1)^{-1}}\right\} = 0, \\ \qquad (i = 1,\ 2,\ 3,\ \ldots,\ n),\ (k = 1,\ 2,\ \ldots,\ m). \end{cases} \tag{15}$$

The unknown quantities in this system are

$$\overset{(i)}{x}(\delta),\ \overset{(i)}{x}(2\delta),\ \ldots,\ \overset{(i)}{x}(a),$$
$$\omega_i(\delta),\ \omega_i(2\delta),\ \ldots,\ \omega_i(a), \qquad (i = 0,\ 1,\ 2,\ \ldots,\ n).$$

The values of the constant $\overset{(n)}{x}_0$ result from (1) if we set there $t = 0$

$$\overset{(n)}{x}_0 = \left\{ a_n^{-1}(0) \left[A(0) - \sum_{i=0}^{n-1} a_i(0) \cdot \overset{(i)}{x}_{2p+1}(0) \right] \right\}^{(2p+1)^{-1}}$$

The constants $\omega_i(0)$ are obtained from (4), for $t = 0$, $(i = 0,\ 1,\ 2,\ \ldots,\ n)$.

$$\omega_i(0) = \overset{(i)}{x}_0 [a_i^{-1}(0) \cdot A(0)]^{-(2p+1)^{-1}}$$

The diagrams representing the variation of the functions $\overset{(i)}{x}$ and ω_i, built up through the points t_k, give the approximate evaluation of the solution of the system (S) on the interval $[0, a]$, $a > 0$

The numerical values of the solution of the system (15) may be obtained by using a known method [1]

REFERENCES

1 Démidovitch, B., Maron, I., *Éléments de calcul numérique*, Éditions Mir, Moscou, 1973

2 Tudosie, C., "Deduction of higher order accelerations by the method of associated angular velocity", *Strojnicky Časopis*, **34**, č. 3, pp 337–341, 1983

3 Tudosie, C., "Determination of higher order accelerations by a functional method", *Acta Technica, ČSAV*, 2, pp 218–224, 1983.

4 Tudosie, C., "A method for calculating the higher order accelerations", *Mathematica*, Tome 25 (48), **1**, pp 69–74, 1983

5 Tudosie, C., "On a product-type differential equation" "Babeş–Bolyai" University, Faculty of Mathematics and Physics, *Research seminars, Seminar on Differential Equations, Preprint* **8**, pp 37–42, 1988

STUDIA UNIV. BABEŞ—BOLYAI, PHYSICA, XXXIV, 1 1989

ON THE INVESTIGATION OF FREE CARRIER CONCENTRATION OF LEAD CHALCOGENIDES SEMICONDUCTORS BY $1/f$ NOISE MEASUREMENTS

D. DĂDĂRLAT* and RODICA TURCU*

Received January 18, 1989

ABSTRACT. — The free carrier concentration of $PbS_{0\,73}$ $Se_{0\,27}$ monocrystalline semiconductors is determined by $1/f$ noise measurement method and the result is compared with that obtained by Hall effect investigations The method was also applied to PbSe polycrystalline films that obey the Hooge—Vandamme relation. In order to obtain the free carrier concentration for polycrystalline materials, additional electrical resistivity vs temperature measurements are necesary. The method is very useful in the case of semiconductor with high electrical resistivity and low Hall mobility.

1. **Introduction.** In an infrared detection system, as in any information-transmitting system, spontaneous fluctuations, that are called noise, impose the ultimate limit on the transmission of information This is why the electrical noise is largely studied and now a rather well understood phenomenon.

In the particular case of infrared detectors based on lead chalcogenides semiconductors, we can list as typical noises: the Johnson noise, the shot noise, the generation-recombination noise, the photon noise and the $1/f$ noise, the last type of noise being dominant at usual temperatures and low enough frequencies ($f < 1 - 10$ kHz) [1, 2].

The $1/f$ noise manifests itself as fluctuations in electrical conductance and it is named $1/f$ after its spectrum

$$S(f) \sim \frac{1}{f^k}; \qquad K \approx 1 \tag{1}$$

The conductance fluctuations of an ohmic sample can be measured as voltage fluctuations when a constant current is passed through the sample or as current fluctuations when the voltage drop across the sample is kept constant, so that one can write (3):

$$\frac{S_I(f)}{I^2} = \frac{S_V(f)}{V^2} = \frac{S_R(f)}{R^2} = \frac{S_G(f)}{G^2} = \frac{C_{1/f}}{f} \tag{2}$$

where I, V, R and G represent the current through the sample, the voltage drop across the sample, the resistance and the conductance of the sample, respectively, and $S_a(f)$ $(a = I, V, R, G)$ is the corresponding fluctuation spectrum $C_{1/f}$ is a number which is a measure of the relative noise of the sample. It was empiricaly found by Hooge [4] to be

$$C_{1/f} = \frac{\alpha_H}{N} \tag{3}$$

* *Institute of Isotopic and Molecular Technology, Cluj-Napoca 5, P.O. Box 700, 3400 Cluj-Napoca, Romania*

where α_H is a dimensionless constant with a value of about $2 \cdot 10^{-3}$ and N is the total number of charge carriers in the sample

Combining (2) and (3) one obtains the Hooge—Vandamme relation [5].

$$\frac{S_v(f)}{V^2} = \frac{\alpha_H}{n \cdot V_{eff}} \cdot \frac{1}{f} \tag{4}$$

where n is the free carrier concentration and V_{eff} is the effective volume depending on the sample geometry.

For the infrared devices (detectors or diode lasers) based on lead chalcogenide materials the carrier concentration is a very sensitive parameter to the method of preparation and to the thermal annealing processes On the other hand it determines the final performances of the device

Unfortunately, for the polycrystalline semiconductor films used as IR dectectors (PbSe, PbS, PbTe) the usual Hall effect measurement is very difficult to be performed in any d c or a c setup because of the high electrical resistivities ($1 - 10^4 k\Omega$), low Hall mobilities and large asymmetry voltages (orders of magnitude larger then the Hall voltage).

In these conditions a method using Hooge—Vandamme formula that does not involve experimental difficulties is to be prefered.

In this paper we extend the application of Hooge—Vandamme relation to polycrystalline films (section 2) and, based on this relation, we determined the carrier concentration for PbSSe monocrystals and PbSe polycrystals from $1/f$ noise measurements (section 3). Some concluding remarks are presented in section 4

2 **Theory.** Starting from the relation (4) one can obtain

$$S_V(f) = \frac{\alpha_H \cdot I^2 R^2}{n \cdot V_{eff} \ f} \tag{5}$$

with

$$R = \frac{\beta}{en\mu} \tag{6}$$

where $\beta = 1/S$ is a geometrical factor and μ is the actual mobility of the sample

Using (5) and (6) we obtain.

$$n = \left[\frac{\alpha_H I^2 \beta^2}{f \ S_v(f) \cdot V_{eff} \cdot e^2 \cdot \mu^2}\right]^{\frac{1}{3}} \tag{7}$$

If we put in (7) $V_{eff} = V_s$ and $\mu = \mu_L$, where V_s is the volume of the sample and μ_L is the mobility due to pure lattice scattering, we can apply the relation (7) to determine the carrier concentration for semiconducting monocrystals

For polycrystalline films the relation (7) presents two different features: (*i*) μ is reduced by an exponential factor due to the intercrystalline barriers [6, 7], so that:

$$\mu = \mu_L \cdot e^{-\frac{E_b}{kT}} \tag{8}$$

where E_b represents the energy of the intercrystalline barriers and V_{eff} can be different from the geometrical volume of the sample V_s. Using Bube's method [8] we determined

$$V_{eff} = \frac{\left(\int_V j^2 dV\right)^2}{\int_V j^4 dV} = \frac{1}{1+\gamma} V_s \tag{9}$$

where j is the total current density through the polycrystalline film and γ is a dimensionless parameter equal to the width of the intercrystalline region to the width of the crystallite ratio

$$\gamma = \frac{l_t}{l_c} \tag{10}$$

Usually [6] $l_t \ll l_c$ and $V_{eff} \approx V_s$.

Using (8), (9) and (10) in (7) we obtain for the carrier concentration of a polycrystalline semiconducting film.

$$n = \left[\frac{\alpha_H I^2 \cdot \beta^2}{f \cdot S_V(f) V_s e^2 \mu_L^2}\right]^{\frac{1}{3}} e^{\frac{2E_b}{3kT}} \tag{11}$$

The relation (11) points out the fact that only the measurement of the spectrum of the voltage fluctuation, $S_V(f)$ is not enough for determining n, additional electrical resistivity vs temperature measurements being necessary in order to find E_b.

3. **Experimental.** The noise measurements are performed on two lead chalcogenide types of material (i) a $PbS_{0.73}$ $Se_{0.23}$ monocrystal of $6 \times 2.5 \times 0.7$ mm³ and 3Ω electrical resistance and (ii) a PbSe polycrystalline film obtained by chemical organic deposition [9]] of $1.5 \times 1 \times 10^{-3}$ mm^{+3} and 45 kΩ electrical resistance The electrical contacts were evaporated gold and the wires were soldered with silver paste

The samples were placed in an electrical circuit represented in Fig. 1, where the load resistance R_L is almost one order of magnitude higher then the sample resistance in order to ensure a constant current through the sample:

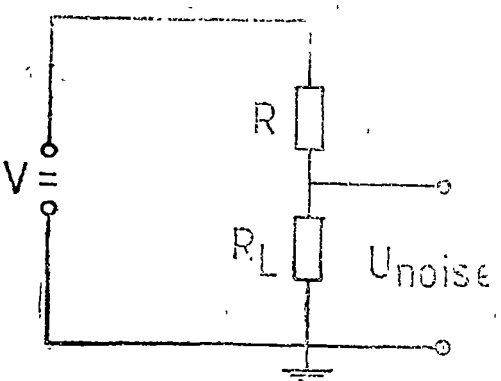

Fig. 1. The electrical circuit used for $1/f$ noise measurements.

The spectrum of voltage fluctuations, $S_V(f) = U^2$ noise/Δf, was measured with a Unipan 233 selective nanovoltmeter with a selectivity of 36 dB, in the 10—10 000 Hz frequency range.

The results are plotted in Fig. 2 and 3.

As one can see from figs. 2 and 3 the samples present, in this fre-

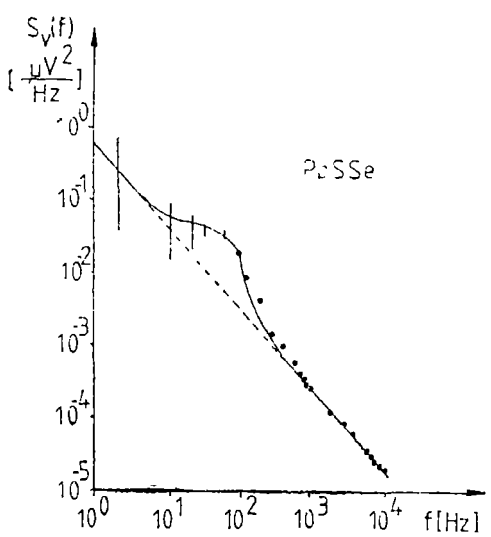

Fig 2 The voltage noise spectrum vs frequency for $PbS_{0.73}Se_{0.27}$.

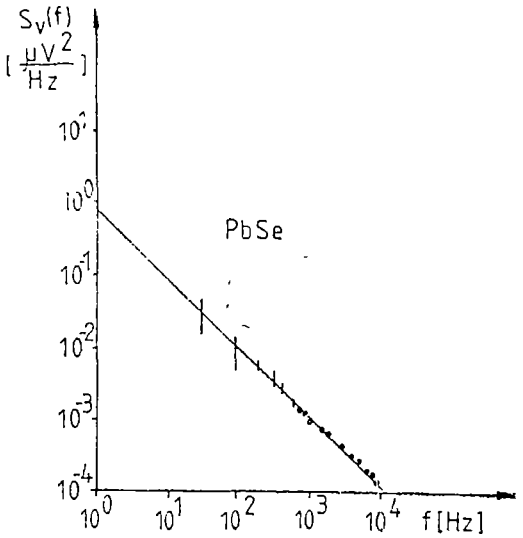

Fig 3 The voltage noise spectrum vs frequency for polycrystalline PbSe film.

quncies range, a conductivity noise spectrum of $1/f$ type, the anomaly observed at around 100 Hz for PbSSe being probably due to generation-recombination noise [2]

Using the results from Fig. 2 in the relation (7) we obtain $n = 1{,}4 \cdot 10^{17}$ cm^{-3} for the monocrystalline $PbS_{0.73}$ $Se_{0.27}$.

For this sample the result is easy to be verified by Hall effect measurements Passing through the sample a current of 1A at 0,69 T magnetic field we obtained a 1,3 mV Hall voltage which means $n = 5{,}2 \cdot 10^{17}$ cm^{-3}. This result is in rather good agreement with that obtained from $1/f$ noise measurements

In order to determine E_b, and to use the relation (11) for obtaining the carrier concentration for polycrystalline PbSe films, electrical resistivity vs. temperature measurements were performed in a standard configuration [10], using a cold finger refrigerator system, in the 120—320 K temperature range. The results are presented in Fig. 4.

Using the results from Fig. 4, and substracting the $T^{-5/2}$ dependence of μ_L [11], we obtain $E_b = 0{,}13$ eV Introducing in (11) this value, together with the value for the spectrum of the voltage fluctuations (Fig 3), we obtain $n = 5 \cdot 10^{17}$ cm^{-3} for the PbSe films

4 **Conclusions.** The method presented in this paper, that uses $1/f$ noise measurements in order to determine the free carrier concentration, is simple and does not involve experimental difficulties The method can be applied both for monocrystalline and for polycrystalline nondegenerate semiconductors, provided that the spectrum of the sample resistance fluctuations obeys the

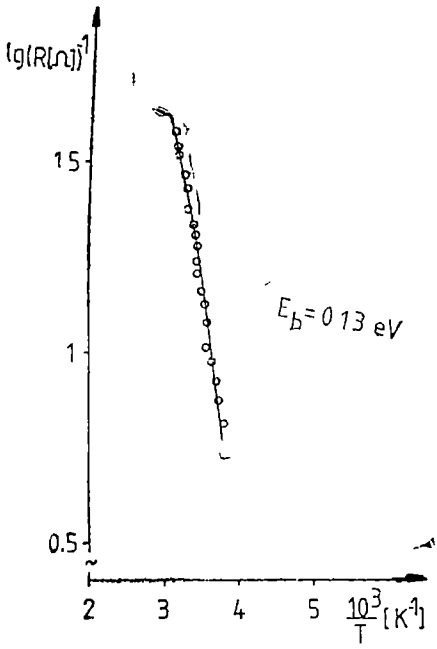

Fig 4. lg R^{-1}vs $10^3/T$, plot in the high temperature region, for PbSe semiconducting film

Hooge—Vandamme relation For degenerate semiconductors the effective number of carriers N_{eff} available for the $1/f$ fluctuations is smaller than the total number of carriers N in the band [12], the two carrier concentrations being related by the formula :

$$\frac{n_{eff}}{n} = \frac{1}{1 + \frac{E_F}{3KT}} \tag{12}$$

where E_F is measured from the bottom of the conduction band.

The method does not give the exact values for the carrier concentration especially because the value of α_H can be different from $2 \cdot 10^{-3}$ for different types of samples [13] On the other hand the relations (7) and (11) are very insensitive to the inaccuracies of measured and calculated geometrical parameters β^2 and V_{eff} that are reduced by the power 1/3 However, relation (11) is very sensitive to the value of E_b, accurate electrical resistivity vs. temperature measurements being necessary

In conclusion, even if this method gives only the order of magnitude of the carrier concentration it is very useful in the cases when Hall effect measurements can not be performed : samples with high electrical resistivity and low mobility

REFERENCES

1. K. M van Vliet, *Appl Optics*, 6, 1145 (1967)
2 R D Hudson, Jr, "Infrared System Engineering", Wiley-Interscience, p. 304, 1969.
3 F. N Hooge, T G M Kleinpenning, L.K J Vandamme, *Rep. Prog Phys*, **44**, 479 (1981)
4 F. N Hooge, *Phys Lett*, **29A**, 139 (1969)
5 F. N. Hooge, L K J. Vandamme, *Phys Lett*, **66A**, 315 (1978).
6 R L Petritz, *Phys Rev*, **104**, 1508 (1956).
7 D Dădârlat, R Turcu, M Chirtoc, R M Candea, C. Fulea, *Studia Univ. Babes—Bolyai, Physica*, **XXXII**, 74 (1987)
8 R. H Bube, *Appl. Phys Lett*, **13**, 136 (1968).
9 See for example D. Dădârlat, R M Candea, R Turcu, L P Biro, I. I. Zasavitskii, M V. Valeiko, A P Shotov, *Phys Stat Sol*, (a) **108**, 637 (1988) and references.
10 R M Candea, R Turcu, P Mărgineanu, D Dădârlat, *Phys. Stat Sol*, (a) **96**, 337 (1986)
11. U. Schlichting, K H Gobrecht, *J Phys Chem Solids*, **34**, 753, (1973)
12. T. G M Kleinpenning J Bisschop, *Physica*, **128B**, 84 (1985)
13. L B Kiss, M I Torok, I Kevesi, *Solid State Commun*, **61**, 731 (1987)

STUDIA UNIV BABEŞ—BOLYAI, PHYSICA, XXXIV, 1 1989

QUASI-LINEAR EQUATIONS FOR AN ELECTROMAGNETIC INSTABILITY

I. ARDELEAN* and J. KARÁCSONY*

Received: February 10, 1989

ABSTRACT. — The quasi-linear theory is developed to derive a kinetic energy change equation for a relativistic electron beam by taking a Weibel-type electromagnetic instability into account in a collisionless magnetized plasma.

1. **Introduction.** The progress in the production of relativistic electron-beams (R.E.B.) gives ground for hoping that the relativistic electron beams can be used to heat a plasma to the thermonuclear temperature. Coupling of the energy of a R.E.B into a plasma the rough collective processes can occur by several mechanisms In the microscopic collective mechanism, the beam excites an instability, and the individual electrons interact directly with large amplitude waves Thus, the beam transfers its energy to waves, which in turn pass it to the plasma The instability which has received the most attention in this regard is the electron-electron two-stream instability [1, 2].

In the beam-plasma system, it is found that an electromagnetic instability can be excited independently of the electrostatic two-stream instability [3]. This is a Weibel-type instability. A linear theory for this instability in the R.E.B.-magnetized plasma system has been elaborated [4]. Using the quasi-linear equations and some nonlinear results, Okada and Niu [5] have investigated the stopping power of the plasma for R.E.B. by the Weibel-type electromagnetic instability. However, the above authors consider the interaction of R.E.B. with an unmagnetized plasma.

The purpose of this paper is to deduce the quasi-linear equations for Weibel instability in R.E.B -magnetized plasma system.

2. **Deduction of the quasi-linear equations.** In our model a warm R.E.B. with density n_{ob} and a velocity $\vec{v}_0$ streams through a cold magnetized plasma of density n_{op} along a magnetic field $\vec{B}_0$. Due to relativistic electron beam induced return current the plasma electrons have a drift velocity $\vec{v}_{eo}$ with respect to plasma ions [6] To derive the quasi-linear kinetic equations for R.E.B. distribution function we will consider the following configuration:

$$\vec{k} = (k,\ 0,\ 0);\ \vec{B}_0 = (0,\ 0,\ B_0);\ \vec{E}_1 = (0,\ 0,\ E_1);\ \vec{B}_1 = (0,\ B_1,\ 0) \quad (2.1)$$

where $\vec{E}_1$ and $\vec{B}_1$ are the perturbed electric and magnetic fields which satisfy the following Maxwell's equations:

$$\text{rot}\ \vec{E}_1 = -\ \partial \vec{B}_1/\partial t \quad (2.2)$$

* *University of Cluj-Napoca, Faculty of Mathematics and Physics, 3400 Cluj-Napoca, Romania.*

and

$$\frac{1}{\mu_0} \operatorname{rot} \vec{B}_1 = \vec{j} + \varepsilon_0 \frac{\partial \vec{E}_1}{\partial t} \tag{2.3}$$

The beam electron dynamics are described by the distribution function $f(\vec{r}, \vec{p}, \vec{t})$ which satisfies the relativistic Vlasov equation

$$\frac{\partial f}{\partial t} + \vec{v} \cdot \nabla f - e\,[\vec{E}_1 + \vec{v} \times (\vec{B}_0 + \vec{B}_1)] \cdot \nabla_{\vec{p}} f = 0 \tag{2.4}$$

For the derivation of the quasi-linear kinetic equations we follow the procedure used in [5]. According to this, we consider the distribution function of the form

$$f(\vec{r}, \vec{p}, t) = f_0(\vec{p}, t) + f_1(\vec{r}, \vec{p}, \vec{t}) \tag{2.5}$$

where

$$f_0(\vec{p}, t) = \langle f(\vec{r}, \vec{p}, t) \rangle = \frac{1}{V} \int f(\vec{r}, \vec{p}, t) d\vec{p} \tag{2.6}$$

is the spatial average of the actual distribution function We also assume that $f_0(\vec{p}, t)$ is a slowly varying function of time, while $f_1(\vec{r}, \vec{p}, t)$ is the perturbed, rapidly oscillating part of the distribution function, which satisfies the condition $f_1 \ll f_0$.

Using a Fourier analysis for the perturbed cantities

$$\vec{E}_1(\vec{r}, t) = \sum_{k=-\infty}^{\infty} \vec{E}_k \exp[i(\vec{k} \cdot \vec{r} - \omega t)] \tag{2.7}$$

$$\vec{B}_1(\vec{r}, t) = \sum_{k=-\infty}^{\infty} \vec{B}_k \exp[i(\vec{k} \cdot \vec{r} - \omega t)] \tag{2.8}$$

$$f_1(\vec{r}, \vec{p}, t) = \sum_{k=-\infty}^{\infty} f_{1k} \exp[i(\vec{k} \cdot \vec{r} - \omega t)] \tag{2.9}$$

the equation for $f_0(\vec{p}, t)$ is obtained by averaging the equation (2.4), with the result

$$\frac{f_0(\vec{p}, t)}{\partial t} = e \left\langle (\vec{E}_1 + \vec{v} \times \vec{B}_1) \downarrow \cdot \frac{\partial f_1}{\partial \vec{p}} \right\rangle \tag{2.10}$$

Using (2.2) and (2.7)—(2.9) the equation (2.10) can be written in the form

$$\frac{\partial f_0}{\partial t} + e \sum_{k=-\infty}^{\infty} \frac{B_{-k}}{k} \left(k v_z \frac{\partial}{p \partial_x} - \omega_{-k} \frac{\partial}{\partial p_y} - k v_r \frac{\partial}{\partial p_z} \right) f_{1k} = 0 \tag{2.11}$$

where $\langle f_1 \rangle = 0$ and $(\vec{v} \times \vec{B}_0) \cdot \partial f_0 / \partial \vec{p} = 0$ have been used

The equation for $f_1(\vec{r}, \vec{p}, t)$ is obtained by substituting $f = f_0 + f_1$ into the Vlasov equation (2.4) and using (2.10) for $\partial f_0/\partial t$, with the result

$$\frac{\partial f_1}{\partial t} + \vec{v} \cdot \frac{\partial f_1}{\partial \vec{r}} - e(\vec{E}_1 + \vec{v} \times \vec{B}_1) \cdot \frac{\partial f_0}{\partial \vec{p}} - e(\vec{v} \times \vec{B}_0) \cdot \frac{\partial f_1}{\partial \vec{p}} -$$

$$- e(\vec{E}_1 + \vec{v} \times \vec{B}_1) \cdot \frac{\partial f_1}{\partial \vec{p}} + e\left\langle (\vec{E}_1 + \vec{v} \times \vec{B}_1) \cdot \frac{\partial f_1}{\partial \vec{p}} \right\rangle = 0 \qquad (2.12)$$

To find $\partial f_0/\partial t$ to lowest order in perturbed quantities, the perturbed distribution function f_1 is calculated as in linear theory. The linear solution to (2.12) is obtained by neglecting the two last terms in this equation. In adition the time dependence of f_0 is neglected because $\partial f_0/\partial t$ is second-order in perturbed quantities. This results from the equation (2.10).

To find the linear result for f_1 we write the equation (2.12) under the form

$$\frac{\partial f_1}{\partial t} + \gamma\vec{u} \cdot \frac{\partial f_1}{\partial \vec{r}} - \frac{e}{m}(\vec{E}_1 + \gamma\vec{u} \times \vec{B}_1) \cdot \frac{\partial f_0}{\partial \vec{u}} - \frac{e}{m}(\gamma\vec{u} \times \vec{B}_0) \cdot \frac{\partial f_1}{\partial u} = 0 \qquad (2.13)$$

where $\vec{u}$ is the relativistic reduced velocity, defined by [7]

$$\vec{v} = \gamma\vec{u} \qquad (2.14)$$

$$\text{with } \gamma = (1 - v^2/c^2)^{1/2} = (1 + u^2/c^2)^{-1/2} \qquad (2.15)$$

and m is the rest-mass of the electron.

Since we are interested with the relativistic beam, one can use the approximation introduced in [8]

$$\vec{v} = \gamma\vec{u} \simeq \gamma_0\vec{u}_0 + \gamma_0\vec{\mu} - \gamma_0^3 \frac{u_0^2}{c^2} \vec{\mu}_{||} \qquad (2.16)$$

where

$$\vec{u}_0 = \vec{v}_0/\gamma_0 = \vec{v}_0(1 - v_0^2/c^2)^{-1/2} \qquad (2.17)$$

is the mean reduced velocity of the relativistic beam particles oriented along the Oz-axis and

$$\vec{\mu} = \vec{u} - \vec{u}_0 \qquad (2.18)$$

while $\vec{\mu}_{||}$ is the component of $\vec{\mu}$ parallel to the beam direction.

Using the above expressions and taking in the reduced velocity space a suitable chosen cylindrical coordinate system having its Oz-axis oriented along the direction of external magnetic field $\vec{B}_0 = B_0\vec{e}_z$, we obtain for the Fourier component f_{1k} of the perturbed distribution function f_1 the expression

$$f_{1k}(\theta) = \frac{ie}{m\omega_{ce}\gamma_0} \cdot \frac{\omega_k B_k}{k} \sum_{n=-\infty}^{\infty} J_n(\alpha) \left\{ \frac{a_2}{2} \left[\frac{\exp[-i\alpha \sin\theta + i(n+1)\theta]}{n + \beta + 1} + \right. \right.$$

$$\left. \left. + \frac{\exp[-i\alpha \sin\theta + i(n-1)\theta]}{n + \beta - 1} \right] + \frac{a_1}{n + \beta} \exp[-i\alpha \sin\theta + in\theta] \right\} \qquad (2.19)$$

where

$$\alpha = \frac{k_0\mu_\perp}{\omega_{ce}}; \qquad \beta = -\frac{\omega_k}{\omega_{ce}\gamma_0}; \qquad a_1 = \frac{\partial f_0}{\partial \mu_{||}}$$

$$a_2 = \frac{\gamma_0 k}{\omega}\left[(u_0 + \gamma_0^3\mu_{||})\frac{\partial f_0}{\partial \mu_\perp} - \mu_\perp \frac{\partial f_0}{\partial \mu_{||}}\right], \qquad \omega_{ce} = \frac{eB_0}{m} \tag{2 20}$$

and $\mu_\perp^2 = \mu_x^2 + \mu_y^2$

Substituting (2.19) into (2.11) and taking into account that the steady-state velocity distribution function is given by the expression [8]

$$f_0(\mu_\perp, \mu_{||}) = \frac{n_{b0}}{(2\pi)^{3/2}\bar{\mu}_\perp^2\bar{\mu}_{||}}\exp\left[-\frac{1}{2}\left(\frac{\mu_\perp^2}{\bar{\mu}_\perp^2} + \frac{\mu_{||}^2}{\bar{\mu}_{||}^2}\right)\right] \tag{2.21}$$

after the straightforward but tedious calculations we obtain the quasi-linear kinetic equation for f_0 under the following form

$$\frac{\partial f_0}{\partial t} = \frac{e}{m}\sum_{k=-\infty}^{\infty}\frac{B_{-k}}{k}\left\{[\omega_{-k}\sin\theta - k(\gamma_0 u_0 + \gamma_0^3 u_{||})\cos\theta]\frac{\partial f_{1k}}{\partial \mu_\perp} + \right.$$

$$\left. + \frac{1}{\mu_\perp}[k(\gamma_0 u_0 + \gamma_0^3\mu_{||})\sin\theta - \omega_{-k}\cos\theta]\frac{\partial f_{1k}}{\partial \theta} + k\gamma_0\mu_\perp\cos\theta\frac{\partial f_{1k}}{\partial \mu_{||}}\right\} \tag{2.22}$$

3. Equation for the change in the R.E.B. kinetic energy. Using the quasi-linear kinetic equation (2.22) the change in the kinetic energy of the relativistic electron beam can be determined For this we define the average R E B. kinetic energy as:

$$W_b = \int d\vec{\mu}\, mc^2\left(\frac{1}{\gamma} - 1\right)f_0(\vec{\mu}, t) \tag{3 1}$$

Taking into account that for R E.B.

$$\frac{1}{\gamma} - 1 = (1 - u^2/c^2)^{-1/2} - 1 \simeq \frac{1}{\gamma_0} - 1 + \gamma_0 u_0\mu_{||}/c^2 \tag{3 2}$$

the change in the beam kinetic energy can be written as

$$\frac{dW_b}{dt} = mc^2\int\left(\frac{1-\gamma_0}{\gamma_0} + \frac{\gamma_0 u_0}{c^2}\mu_{||}\right)\mu_\perp\frac{\partial f_0}{\partial t}\,d\mu_{||}\,d\mu_\perp\,d\theta \tag{3 3}$$

To arrive at the equation for the change in the kinetic energy of the relativistic electron beam, we take the appropriate velocity moments of (2 22) Thus, we obtain.

$$\frac{dW_b}{dt} = ec^2\sum_{k=-\infty}^{\infty}\frac{B_{-k}}{k}\int\int\left(\frac{1-\gamma_0}{\gamma_0} + \frac{\gamma_0 u_0}{c^2}\mu_{||}\right)\left\{[\omega_{-k}\sin\theta - k(\gamma_0 u_0 + \gamma_0^3\mu_{||})\cos\theta]\frac{\partial f_{1k}}{\partial \mu_\perp} + \right.$$

$$\left. + \frac{1}{\mu_\perp}[k(\gamma_0 u_0 + \gamma_0^3\mu_{||})\sin\theta + \omega_{-k}\cos\theta]\frac{\partial f_{1k}}{\partial \theta} + k\gamma_0\mu_\perp\cos\theta\frac{\partial f_{1k}}{\partial \mu_{||}}\right\}\mu_\perp d\mu_\perp d\mu_{||}\,d\theta \tag{3 4}$$

Finally, after the algebraic calculations, we obtain the change in the R.E.B. kinetic energy under the form:

$$\frac{dW_b}{dt} = -\frac{e^2\gamma_0^3 u_0 n_{b0}}{m} \sum_{k=-\infty}^{\infty} \sum_{n=-\infty}^{\infty} |B_k|^2 e^{-\frac{k^2\bar{\mu}_\perp^2}{\omega_{ce}^2}} \frac{(n+1)\delta_k}{(n+1)^2\omega_{ce}^2\gamma_0^2 + \delta_k^2} \times$$

$$\times \left[I_n\left(\frac{k^2\bar{\mu}_\perp^2}{\omega_{ce}^2}\right) - I_{n+1}\left(\frac{k^2\bar{\mu}_\perp^2}{\omega_{ce}^2}\right)\right] \tag{3.5}$$

where δ_k is the linear growth rate of the excited wave and I_n is the Bessel function of the first kind of imaginary argument.

For the following applications it is more convenient to write the equation (3.5) in terms of the usual velocity rather than the reduced velocity. To do this we remember the following relations [8]:

$$\vec{v}_0 = \gamma_0 \vec{u}_0 \tag{3.6}$$

and

$$v_\perp^2 = (\gamma_0 \bar{\mu}_\perp)^2 \tag{3.7}$$

where $\bar{v}_\perp^2$ is the Watson's and coworkers mean square velocity differences from the average velocity [9]. So we obtain the final form of the R.E.B. energy change equation as:

$$\frac{dW_b}{dt} = -\frac{e^2\gamma_0 n_{b0} v_0}{m} \sum_{k=-\infty}^{\infty} \sum_{n=-\infty}^{\infty} |B_k|^2 e^{-\frac{k^2\bar{v}_\perp^2}{\omega_{ce}^2\gamma_0^2}} \frac{(n+1)\delta_k}{(n+1)^2\omega_{ce}^2\gamma_0^2 + \delta_k^2} \times$$

$$\times \left[I_n\left(\frac{k^2\bar{v}_\perp^2}{\omega_{ce}^2\gamma_0^2}\right) - I_{n+1}\left(\frac{k^2\bar{v}_\perp^2}{\omega_{ce}^2\gamma_0^2}\right)\right] \tag{3.8}$$

4 **Conclusion.** When an intense relativistic electron beam is injected into a plasma, a part of the kinetic energy of the beam is transferred to the field energy and to the kinetic energy of the background plasma electrons. To determine the effective stopping length due to the electromagnetic instability the equation (3.8) may be used For this purpose must be calculated the right-hand side of the equation (3.8). To do this it is necessary to construct a non-linear theory of the interaction with a view to determining the nonlinear saturation level of the excited waves. This will be elaborated in a forthcoming paper.

REFERENCES

1 L I Rudakov, *Zh Eksp Teor Fiz*, **59.** 2091 (1970).
2 T Tajima, *J. Plasma Phys.*, **19.** 63 (1978).
3. M Bornatici, K F. Lee, *Phys. Fluids*, **13.** 3007 (1970)
4 J. Karacsony, S. Coldea, C Băleanu, to be published.
5. T Okada, K Niu, *J Plasma Phys.*, **23.** 423 (1980)
6 R Lee, R N Sudan, *Phys. Fluids*, **14.** 1213 (1971)
7 M Drăganu, *Mathematica*, **7** (30), 211 (1965)
8. J Karacsony, *Bull Math Soc Sci. Math R.S.R*, **19** (67), 71 (1975)
9. K. M. Watson, S. A. Bludman, M N Rosenbluth, *Phys. Fluids*, **3.** 741 (1960).

STUDIA UNIV BABEŞ—BOLYAI, PHYSICA, XXXIV, 1 1989

COHERENT-POTENTIAL APPROXIMATION METHOD IN HIGH-T_c SUPERCONDUCTIVITY

D. VĂCARU*

Received February 18, 1989

ABSTRACT. — We give a method to calculate the critical temperature of a high-T_c superconductor using the coherent-potential-approximation The general formula obtained has been applied for three-dimensional, two-dimensional and one-dimensional models of high-T_c superconductors

I **Introduction.** The general method used in conventional theory of superconductivity is that of Green function which is appropriate for the case of the itinerant-electron systems The main approximation in this method is a generalized mean-field approximation which gives us the possibility to treat the weakly correlated fermionic systems. However, the discovery of the high-T_c superconductors showed that this materials have a particular structure where the three-dimensional (3d) character is the result of a combination between the twodimensional (2d) planes and onedimensional (1d) chains containing electrons strongly correlated.

In this case we prefer to the free electrons picture the tightbinding picture, and the most appropriate method to study the superconducting phase transition in this model is the Coherent-Potential-Approximation (CPA) used in the theory of binary alloys. We will present the general method and we will show how we can calculate the critical temperature T_c for a high-T_c superconductor using this method.

We have to mention that the method is more general than the standard Green function method and can be generalized at the study of the superconducting alloys with high T_c

II **Coherent potential approximation.** 1 *The general method* The electronic structure of disordered binary alloys has been developed within the framework of the multiple scattering approach of a disordered system which has the form A_xB_y, where x is the concentration of the A atoms and $y = 1 - x$ is the concentration of the B atoms In order to describe the physical properties of this system Soven [1] and Velicky et al [2] developed the so-called Coherent-Potential-Approximation (CPA) using the multiple scattering approximation. In this approach the propagation of an electron or lattice wave in an alloy is regarded as a succession of elementary scattering on the random atomic scatteres, which are averaged over all configurations of atoms.

The system consisting from electrons which are scattering on the atoms will be described by an effective one-electron Hamiltonian H of the system in a given configuration.

* *University of Cluj-Napoca, Faculty of Mathematics and Physics, 3400 Cluj-Napoca, Romania*

The single-particle properties can be obtained from the Green function

$$G(z) = (z - H)^{-1} \tag{1 II}$$

If we consider that the average on the configuration can be performed, we will define the averaged (denoted by $\langle .. \rangle$) Green function

$$\langle G(z) \rangle = (z - H_{eff})^{-1} \tag{2 II}$$

where H_{eff} has the full crystal symmetry, but is non-Hermitian and energy dependent.

We assume now that the exact effective Hamiltonian can be well approximated by $K = K(z)$ and in this case we have the identity

$$\langle G \rangle = R + R(H_{eff} - K)\langle G \rangle \tag{3 II}$$

where

$$R = (z - K)^{-1} \tag{4 II}$$

is in fact an equation for $\langle G \rangle$ given by the unperturbed Green function R.

At this stage of the investigation we will consider a result from the multiple scattering theory, where a similar equation for the T-matrix can be written as

$$G = R + RTR \tag{5.II}$$

If we perform the average of (5 II), we get

$$\langle G \rangle = R + R\langle T \rangle R \tag{6 II}$$

and H_{eff} can be expressed as

$$H_{eff} = K + \langle T \rangle \cdot \frac{1}{1 + R\langle T \rangle} \tag{7.II}$$

where we used (2.II) and (6 II)
This result can be used in two ways The first one is to insert $T(K)$ (the T-matrix for a given K) in (7 II) and to obtain a better approximation for the Hamiltonian (7 II) The second way is to use the condition .

$$\langle T(K) \rangle = 0 \tag{8 II}$$

to determine K

In fact we can apply the multiple scattering method if we can descompose the random-perturbating potential $H-K$ into a sum of contributions of single scatters associated with each site i.e

$$H - K = \sum_n V_n \tag{9.II}$$

From the equation (5 II) and using the identity

$$G = R + R(H - K)G \tag{10 II}$$

yields

$$T = (H - K)(I + RT) \tag{11.II}$$

or using (9.II) we get

$$T = \sum_n V_n(1 + RT) = \sum_n Q_n \tag{12 II}$$

This equation gives T-matrix as a sum of contributions arising from the individual scatteres Introducing

$$T_n = (1 - V_n R)^{-1} V_n \tag{13.II}$$

which is the T-matrix for the site n we obtain

$$Q_n = T_n(1 + R \sum_{m \neq n} Q_m) \tag{14.II}$$

and from (12 II) and (14.II) we obtain the equation of the T — matrix as

$$T = \sum_n T_n + \sum_n T_n R \sum_{m \neq n} T_m + \ldots \tag{15.II}$$

The equations (10.II) and (14.II) are exact, and lead to the exact averaged equations

$$\langle T \rangle = \sum_n \langle Q_n \rangle \tag{16 II}$$

$$\langle Q_n \rangle = \langle T_n(1 + R \sum_{m \neq n} Q_m) \rangle \tag{17.II}$$

equation which can be written as

$$\langle Q_n \rangle = \langle T_n \rangle (1 + R \sum_{m \neq n} \langle Q_m \rangle) + \langle T_m R \sum_{m \neq n} (Q_m - \langle Q_m \rangle) \rangle \tag{18.II}$$

The first term of this equation describes the effects of the averaged effective wave seen by n-th atom, and the second term correspond to fluctuations of the effective wave term which corresponds to the fluctuations of the effective wave, term that will be neglected, which is in fact a basic approximation of CPA Then (18 II) becomes

$$\langle Q_n \rangle = \langle T_n \rangle (1 + R \sum_{m \neq n} \langle Q_m \rangle) \tag{19 II}$$

From (7 II) and (16.II) the effective Hamiltonian can be written as

$$H_{eff} = K + \sum_n T_n(1 + R\langle T_n \rangle)^{-1} \tag{20 II}$$

We see that CPA-method combines two ideas namely

— to calculate the average for a given quantity associated with a random medium by introducing a perriodic effective medium;

— to determine this effective medium by a self-consistency requirement i e. by demanding that the fluctuations of a given quantity due to local fluctuations around the effective medium average to be zero

2 *Single — Band Model.* The systems with strong correlations are generally described in the tight-binding approximations for the electrons We start with a single atomic orbital $|n\rangle$ which is considered to be associated with each site n

For a pure crystal in this simple case will result a *"single band"*. In the binary alloys there are two sub-bands which can be treated in what is known to be the single band model. The one-electron Hamiltonian which describes such systems has the form

$$H = \sum_n |n\rangle \varepsilon_n \langle n| + \sum_{m \neq n} |n\rangle t_{nm} \langle m| \qquad (21\,\mathrm{II})$$

$$= D + W$$

The second line defines the decomposition of the Hamiltonian in a diagonal part D and an off-diagonal part W in the Wannier representation for the electronic system The model is valid in the following assumptions, which are physically correctly (and realizable) when the orbitals are sufficiently localized and the atomic potentials are not too different These assumptions are.

a) In the diagonal elements ε_n, the crystal field terms are assumed to be independent of the composition x and the atomic configuration. These elements may be regarded as atomic levels which assume one of the two possible values ε^A and ε^B depending on whether an atom A or B occupies n

b) The hopping integrals $t_{n,m}$ are asumed to be completely independent of the alloy composition The operator W way be interpreted as the Hamiltonian for pure crystal with $\varepsilon^A = \varepsilon^B = 0$ and $\varepsilon^A + W$ and $\varepsilon^B + W$, respectively, are the Hamiltonians for pure A and B crystals.

We may conclude that in (20 II) D is diagonal but a random quantity, and W off-diagonal but translationally invariant

The operator W is diagonal in the Bloch representation and

$\langle \vec{k}|W|\vec{k}'\rangle$ is

$$\langle \vec{k}|W|\vec{k}'\rangle = \delta_{\vec{k}\vec{k}'} \sum_n t_{0n} |\vec{k}\rangle e^{i\vec{k}\vec{a}_n} = \delta_{\vec{k}\vec{k}'} W s(\vec{k})$$

where

$$|\vec{k}\rangle = \frac{1}{\sqrt{N}} \sum_n e^{i\vec{k}\vec{a}_n} |n\rangle$$

The quantity $s(\vec{k})$, which describes the k-dependence of the band energy, is dimensionless.

In order to describe the band spliting it is convenient to introduce

$$\varepsilon^A = \frac{1}{2} D\delta\,; \quad \varepsilon^B = -\frac{1}{2} D\delta\,, \quad \delta = \frac{\varepsilon^A - \varepsilon^B}{D} \qquad (23\,\mathrm{II})$$

Usually, because D scales the entire Hamiltonian, we take $D = 1$ The effective Hamiltonian $H_{eff}(z)$ has the full crystal symmetry and in this case H_{eff} is diagonal in the k — representation

$$\langle \vec{k}|H_{eff}|\vec{k}'\rangle = [s(\vec{k}) + \Sigma(\vec{k}, z)]\delta_{\vec{k}\vec{k}'} \qquad (24.\mathrm{II})$$

and

$$\langle G(z)\rangle = (z - H_{eff})^{-1} \qquad (25.\mathrm{II})$$

is also diagonal in this representation In (24 II) Σ is the self-energy with respect to the perfect crystal having Hamiltonian W We define

$$G(k, z) \equiv \langle\langle k|G(z)|k\rangle\rangle = [z - s(k) - \Sigma(k, z)]^{-1} \tag{26 II}$$

which is defined by the spectral density

$$A(\vec{k}, E) = -\frac{1}{\pi} ImG(\vec{k}, E + i0) \tag{27 II}$$

or

$$G(\vec{k}, z) = \int_{-\infty}^{\infty} \frac{dE}{z - E} A(\vec{k}, E) \tag{28 II}$$

The density of states per atom

$$\rho(E) = \frac{1}{N} Tr\langle\delta(E - H)\rangle \tag{29 II}$$

may be expressed in terms of the Green function as

$$\rho(E) = -\frac{1}{\pi} Im\langle n = 0|G(E + i0\rangle|n = 0\rangle$$

$$= \frac{1}{N} \sum_{k} A(\vec{k}, E) \tag{30 II}$$

Now, let us introduce the auxiliary function, specific for the CPA approximation, and defined as

$$F(z) = \frac{1}{N} Tr\langle G(z)\rangle = \langle 0|G(z)|0\rangle \tag{31.II}$$

and the density of states (30.II) can be written as

$$\rho(E) = -\frac{1}{\pi} ImF(E + i0) \tag{32 II}$$

which is equivalent with the spectra representation

$$F(z) = \int_{-\infty}^{\infty} \frac{dE}{z - E} \rho(E) \tag{33 II}$$

3 *Single Band Model, Single Site Approximation* The single site approximation (SSA) can be used for the binary alloys which are described in the simple model of the single band The basic hypothesis of this approximation is to consider that the total scattered wave is composed of contributions from each atom, while the effective wave incident on a given atom excludes the contribution of that atom The contribution is obtained as product of the atomic t-matrix and the effective wave, which are both dependent on the configuration. The main point of SSA is that these quantities are not statisti-

cally correlated Using these approximations we can perform the calculation starting with the unperturbed Hamiltonian:

$$H = W + \sum_n |n\rangle U\langle n| = W + U(z)\hat{1} \tag{34 II}$$

where $U(z)$ is analytic every where except on the real axis The quantities which appear in the calculations are

$$G^0(z) = (z - W)^{-1}, \quad G(\vec{k}, z) = (z - s(\vec{k}))^{-1}$$
$$A(\vec{k}, E) = -\frac{1}{\pi} ImG^0(k, E + i0) = \delta(E - s(k)) \tag{35.II}$$

$$\rho^0(E) = \frac{1}{N}\sum_k A_0\left(\vec{k}, E\right) = \frac{1}{N}\sum_k \delta(E - s(\vec{k})) \tag{36 II}$$

and

$$F^0(z) = \int_{-\infty}^{\infty} \frac{dE}{z - E}\rho^0(E) = \frac{1}{N}\sum_k \frac{1}{z - s(k)} \tag{37.II}$$

For the Hamiltonian K we can define the Green function

$$R(z) = (z - k)^{-1} = (z - U(z) - W)^{-1} = G^0(z - U(z)) \tag{38 II}$$

This equation shows that $R(z)$ can be expressed simply in terms of G^0 Then we can define

$$\langle 0|R(z)|0\rangle = F^0(z - u(z)) \equiv \hat{F^0}(z) \tag{39.II}$$

a quantity which is specific for CPA method. From (21.II) and (34.II) we get

$$H - K = \sum_n |n\rangle[\varepsilon_n - u(z)]\langle n| \tag{40.II}$$

and using (9 II) we get

$$V_n = |n\rangle[\varepsilon_n - u(z)]\langle n| = |n\rangle\varepsilon_n\langle n| \tag{41.II}$$

From (13 II) we calculate

$$T_n(z) = |n\rangle \frac{V_n}{1 - V_n\hat{F}(z)}\langle n| \tag{42.II}$$

and this relation will be averaged on the configurations and we get:

$$\langle T_n\rangle = |n\rangle\left[\frac{x(\varepsilon^A - U)}{1 - (\varepsilon^A - U)\hat{F}} + \frac{y(\varepsilon^B - U)}{1 - (\varepsilon^B - U)\hat{F}}\right]\langle n| =$$
$$|n\rangle[x\tau^{\hat{A}} + y\tau^B]\langle n| \equiv |n\rangle\tau_n\langle n| \tag{3.II}$$

Using (20 II) we get

$$H_{\text{eff}} = W + \sum_n |n\rangle \left[U + \frac{\tau}{1 + \tau \widehat{F}} \right] \langle n| \tag{44.II}$$

and the self-energy is

$$\Sigma(\vec{k}, z) = u(z) + \frac{\tau(z)}{1 + \tau(z)\widehat{F}(z)} \tag{45.II}$$

and from the condition $\langle T_n \rangle = 0$ we get

$$\Sigma(z) = u(z) \tag{46.II}$$

From (43 II) and (46 II) we obtain the equation

$$(\varepsilon - u) - [(\varepsilon - u)^2 - (\varepsilon - u)(x - y)\delta - xy\delta^2]\widehat{F} = 0 \tag{47 II}$$

with

$$\varepsilon = \frac{1}{2}\,\delta(x - y)$$

The equation (47.II) gives

$$U = \varepsilon + xy\,\delta^2 \frac{\widehat{F}}{1 + (u + \varepsilon)\widehat{F}} \tag{48 II}$$

which can be written as

$$\Sigma(z) = \varepsilon + xy\delta^2 \frac{F^0(z, \Sigma)}{1 + (\Sigma + \varepsilon)F^0(z, \Sigma)} \tag{49.II}$$

where

$$F_0(z, \Sigma) = F_0(z - \Sigma(z))$$

Taking now the density of states as

$$\rho^0(E) = \begin{cases} \frac{2}{\pi D^2}\sqrt{D^2 - E^2}, & |E| < D \\ 0 \quad , & |E| > D \end{cases} \tag{50.II}$$

we can calculate $F^0(z)$ from (37 II) using (50 II)
Using now the relation

$$\int_{-a}^{a} \frac{\sqrt{a^2 - x^2}}{x - y}\,dx = \pi \operatorname{sign} y \sqrt{y^2 - a^2} - \pi y$$

we get

$$F^0(z) = \frac{2}{D^2}\,[z - \sqrt{z^2 - D^2}] \tag{51 II}$$

and using $F^0(z - \Sigma(z)) \equiv F(z)$ the self energy is

$$\Sigma(z) = z - \frac{1}{F(z)} - \frac{1}{4} F(z) \tag{52.II}$$

and 49. II—52.II) we get

$$\frac{1}{16} F^3 - \frac{1}{2} z F^2 - \left[z^2 - \frac{1}{4} (\delta^2 - 1) \right] F - (z + \varepsilon) = 0 \tag{53.II}$$

result which is quite general and can be used to calculate T_c for high-T_c superconductors

Before we start such a kind of calculation we present what is known as the "alloy analogy". Let us consider again the binary alloy, the A component being described by

$$G(\vec{k}, \omega) = [\omega - \varepsilon(\vec{k}) - \varepsilon_A - \Sigma(\varepsilon)]^{-1} \tag{54 II}$$

where the self-energy Σ is

$$\Sigma = \delta x [1 - (\delta - \Sigma) F]^{-1} \tag{55 II}$$

where $\delta = \varepsilon_A - \varepsilon_B$. The function F is defined by

$$F = \frac{1}{N} \sum_{\vec{k}} G(\vec{k}, i\omega) \tag{56.II}$$

or using (49 II) we get

$$F(z) = 2(z - \sqrt{z^2 - 1}) \tag{57 II}$$

where

$$z = \frac{i\omega - \varepsilon_A - \Sigma}{D} \tag{58 II}$$

In the limit $\varepsilon_A \to \infty$, the self-energy has a simple form

$$\Sigma = - \frac{x}{F} \tag{59.II}$$

where x is the concentration of the A component.
For a pure system we get for the self energy

$$\Sigma = - \frac{n}{F} \tag{60.II}$$

where n is the number of electrons. This result will be used in the calculation of T_c. With these results we can start the calculation of T_c for superconductors in CPA.

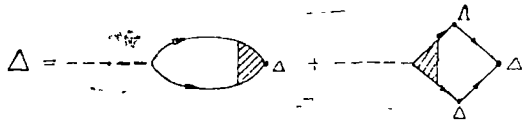

Fig 1

III **Critical temperature for high-T_c.**

1 General Method. In order to calculate the critical temperature of high-T_c we will present the general method which implies the CPA method

The equation for the order parameter gives the critical temperature as the solution of the equation

$$1 = \Pi(T_c) \tag{1 III}$$

where

$$\Pi(T_c) = \frac{1}{N}\sum_{\omega,k} G(\vec{k},\ i\omega)G(-\vec{k},\ -i\omega)\Lambda(\vec{k},\ -\vec{k};\ i\omega,\ -i\omega) \tag{2 III}$$

Λ being the vertex correction and $\omega = \pi T\left(n + \frac{1}{2}\right)$ The equation for the vertex correction has the form

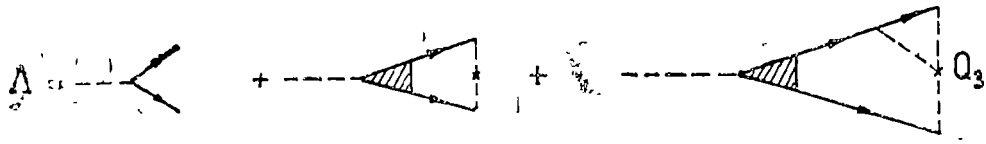

Fig. 2

which can be written analitically as

$$\Lambda = U + \Lambda A \sum_{s=2} Q_s U^s [F^{s-2} + F^{s-3}F_- + \ .\ .\ + F_-^{s-2}] \tag{3 III}$$

and we denoted by A and F the quantities

$$A(i\omega) = \frac{1}{N}\sum_k G(\vec{k},\ i\omega)G(-\vec{k},\ -i\omega) \tag{4.III}$$

$$F = \frac{1}{N}\sum_k G(\vec{k}, i\omega)\,,\quad F_- = \frac{1}{N}\sum_k G(-\vec{k},\ -i\omega) \tag{5 III}$$

and by Q_s a factor which is function of x and y.

The dotted line from Fig 1 and Fig 2 represents the "interaction" line which will be specified for each model The Green function G is

$$G(\vec{k}, i\omega) = [i\omega - \varepsilon(\vec{k}) - \varepsilon_i - \Sigma]^{-1} \tag{6.III}$$

where the self-energy is represented as

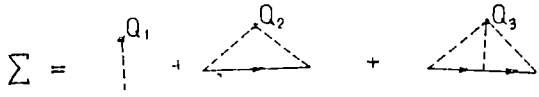

Fig 3.

and is given by

$$\Sigma = U \sum_{s=1} Q_s(UF) \tag{7.III}$$

The equation (3 III) gives for the vertex function the solution

$$\Lambda = \frac{U}{1 - A \dfrac{\Sigma - \Sigma_-}{F - F_-}} \tag{8.III}$$

where A has been calculated as

$$A = \frac{F - F}{-2i\omega + \Sigma - \Sigma_-} \tag{9 III}$$

The equation (8 III) has the form

$$\Lambda = U\left[1 + \frac{2i\omega - \Sigma + \Sigma_-}{2i\omega} \cdot \frac{\Sigma - \Sigma_-}{F - F_-} \cdot \frac{1}{N} \sum_{\vec{p}} G(\vec{p},\ i\omega) G(-\vec{p},\ -i\omega)\right] \tag{10.III}$$

and from (1 III), (2 III) and (10 III) the equation for the critical temperature is:

$$1 = U\left[\frac{1}{N} \sum_{\omega} \sum_{\vec{k}} \vec{G}(k,\ i\omega) G(-\vec{k},\ -i\omega) f^2(\vec{k}) + \right.$$

$$\left. + \sum_{\omega} \frac{2i\omega - \Sigma + \Sigma_-}{2i\omega} \cdot \frac{\Sigma - \Sigma_-}{F - F_-} \cdot \left(\frac{1}{N} \sum_{\vec{p}} f(\vec{p}) G(\vec{p},\ i\omega) G(-\vec{p},\ -i\omega)\right)^2\right] \tag{11.III}.$$

where $f(k)$, the symmetry factor of the pairing, is indicated by the model. Such an equation has been used first by Yoshioka and Fukuyama [3] in order to explain the superconductor-semiconductor transition in $BaPb_{1-x}Bi_xO_3$ or $Li_{1+x}Ti_{2-x}O_4$ compounds

The model proposed in [3] consist in taking this materials as a binary alloy system $A_{1-x}B_x$, the PbO_3 being assigned to the A atom and BiO_3 to the B atom Using the CPA method the calculation of T_c suposed the solving of an equation of the type (53 II) for the non — magnetic Hubbard Hamiltonian reduced to the form (21 II) As such an equation has no simple analytical solution, the authors used the numerical method and calculated T_c as function of x for different parameters U and D, where U is the one-site repulsion from Hubbard Hamiltonian and D is the band-width

As the CPA method goes beyond the mean field, it was reconsidered for the high-T_c superconductors by Fukuyama and Yoshida [4].

2 *The Model* Strong Coulomb correlations are considered at the present time to play a very important role in the pairing mechanism of high-T_c oxides. Indeed, Anderson [5] proposed a new mechanism for superconductivity based on the result obtained by Hirch [6] who showed that for a Hubard Hamiltonian with strong correlations an attraction can appear which gives rise to aniso-

tropic singlet superconductivity Later many authors [6—11] considered the standard Hubbard Hamiltonian

$$H = \sum_{i,j,\sigma} t_{ij} c^+_{i\sigma} c_{j\sigma} + \sum_{i\sigma} \varepsilon_i c^+_{i\sigma} c_{i\sigma} - U \sum_{i\sigma} a^+_{i\sigma} a^+_{i-\sigma} a_{i-\sigma} a_{i\sigma} \tag{12.III}$$

which can be transformed in an effective Hamiltonian

$$H_{eff} = t \sum_{i,j,\sigma} (1 - n_{i-\sigma}) c^+_{i\sigma} c_{j\sigma} (1 - n_{j-\sigma}) + J \sum_{i,j} \left(s_i s_j - \frac{1}{4} n_i n_j \right) \tag{13 III}$$

where the band energy is now

$$\varepsilon(\vec{k}) = -2t f(\vec{k}) \tag{14.III}$$

with

$$f(\vec{k}) = \begin{cases} \cos k_x a + \cos k_y a & \text{for } d = 2 \\ \cos k\, a & \text{for } d = 1 \end{cases} \tag{15 III}$$

d, being the dimensionality of the system
This Hamiltonian has been obtained by $U \gg t$ and the coupling constant from (12.III) is $J = 4t^2/U$. If we take the space where the double occupancy of the same site is excluded, the Hamiltonian (13.III) is reduced to

$$H_{eff} = K - \frac{1}{2} \sum_k (\Delta_{\uparrow\downarrow}(k) c^+_{k\downarrow} c^+_{-k\uparrow} + h.c.) \tag{16 III}$$

where the order parameter is defined by

$$\Delta_{\uparrow\downarrow}(\vec{k}) = 2J \sum_p f(\vec{k} - \vec{p}) \langle c_{p\uparrow} c_{-p\downarrow} \rangle \tag{17 III}$$

As these materials are a special cases of $3d$ superconductors, we will calculate T_c for $3d$, $2d$ and $1d$ cases Using these results we will give a general formula for T_c which will be analysed (for $d = 3, 2, 1$) as function of the concentration of electrons and of the position of the Fermi energy.

3 *The General Equation for* T_c. In order to calculate T_c we introduce the notations.

$$x = \frac{i\omega}{D}; \quad \nu = \frac{\mu}{D}; \quad U = DF; \quad V = DF_- \tag{18 III}$$

$$S = \frac{\Sigma}{D}; \quad S_- = \frac{\Sigma_-}{D}$$

and the quantities:

$$A_1 = \frac{1}{N} \sum_k f(\vec{k}) G(\vec{k}, i\omega) G(-\vec{k}, -i\omega) \tag{19 III}$$

$$A_2 = \frac{1}{N} \sum_k f^2(\vec{k}) G(\vec{k}, i\omega) G(-\vec{k}, -i\omega) \tag{20 III}$$

Using (15 III) and (18 III) we get

$$A_1 = \frac{d}{D^2} \frac{zU - z_- V}{z - z_-} \tag{21 III}$$

and

$$A_2 = \frac{d^2}{D^2} \left[1 - \frac{z^2 U - z_-^2 V}{z - z_-} \right] \tag{22 III}$$

where

$$z = \frac{i\omega + \mu - \Sigma}{D}; \quad z_- = \frac{-i\omega + \mu - \Sigma_-}{D} \tag{23 III}$$

With these results the equation (11 III) we get

$$1 = \frac{2y}{d} T_c \sum_{\omega} \left[A_2 + D^2 \frac{z - z_-}{2x} \frac{S - S_-}{U - V} A_1^2 \right] \tag{24.III}$$

which can be written as

$$1 = \frac{Jd}{D} \frac{1}{2\pi i} \int_{-\infty}^{\infty} dx \ \text{tangh} \frac{x}{2\tau_c} \left[A_2 + \frac{[(\nu + x)U - (\nu - x)V]^2}{4UV - n(U - V)} \right] \tag{25.III}$$

where $\tau_c = \frac{T_c}{D}$. This equation has been obtained using the approximation (60 II). This is a main point of the model which considers that the system consists from two levels separated by a large quantity This model is similar with the Anderson's [5] Resonanting Valence-Bond (RVB) but not identical The equation (25 III) will be simplified because the first term (proportional to A_2) is independent of T_c and we will take·

$$U(x, \nu, n) \simeq U(x = 0, \nu, n) \tag{26.III}$$

$$V(x, \nu, n) \simeq V(x = 0, \nu, n)$$

This approximation is justified if the band-width $D \gg \omega_c$ where is the maximum energy from the system

With this approximation (25.III), becomes

$$1 = \frac{J}{\pi t} \Phi(n, \nu) \int_{-\infty}^{\infty} \frac{dx}{2x} \ \text{tangh} \ \frac{x}{2\tau_c} \tag{27.III}$$

where

$$\Phi(n, \nu) = -\frac{\nu^2}{4t} (U - V) \tag{28.III}$$

these results will be applied for three dimensional ($3d$) superconductor as well as for the cases of superconductors of lower dimensionality $2d$ and $1d$.

4 *Three dimensional model for high-T superconductor.* If we take the density of states of the form

$$N_{3d}(\varepsilon)=\frac{1}{2\pi D}\sqrt{1-\left(\frac{\varepsilon}{D}\right)^2} \tag{29.III}$$

the functions F and F_- are given by

$$F=\frac{2}{D}\left[z+\imath\sqrt{1-z^2}\right] \tag{30a.III}$$

$$F_-=\frac{2}{D}\left(z_-+\imath\sqrt{1-z^2}\right) \tag{30b III}$$

where z and z_- are given by (23 III). Using again the approximation $\Sigma = -n/F$ we get

$$U=2\left[\nu+x-i\sqrt{1-\frac{n}{2}-(\nu+x)^2}\right] \tag{31a III}$$

$$V=2\left[\nu-x+i\sqrt{1-\frac{n}{2}-(\nu-x)^2}\right] \tag{31b.III}$$

which gives

$$z=\frac{U}{4}+\frac{1}{U},\quad z_-=\frac{V}{4}+\frac{1}{V} \tag{32.III}$$

Then we can write

$$U-V=4\sqrt{i\overline{1-\frac{u}{2}-\nu^2}} \tag{33 III}$$

and neglecting again the term in A_2 (27.III) becomes

$$1=\frac{J}{\pi t}\nu^2\sqrt{1-\frac{n}{2}-\nu^2}\int_{\infty}^{\infty}\frac{d\tau}{x}\ \text{taugh}\ \frac{x}{2\tau_c} \tag{34 III}$$

The critical temperature will be obtained as

$$T_c^{3d}=1.13\,\omega_c\exp\left[-\frac{1}{\lambda(n,\nu)}\right]. \tag{35 III}$$

where

$$\nu(n,\nu)=\frac{1}{\pi}\frac{J}{t}\Phi(n,\nu) \tag{36 III}$$

$$\Phi_{3d}(n,\nu)=\nu^2\sqrt{1-\frac{n}{2}-\nu^2}\,.$$

The next step is to eliminate the chemical potential contained in Φ by ν Using now the general equation for the number of electrons·

$$N(\varepsilon) = -\frac{1}{\pi} Im(F - F_{-}) = -\frac{2}{\pi} Im\, F \tag{37 III}$$

we get

$$n = -\frac{2}{\pi} Im \int_{-\infty}^{\nu} d\xi\, U(\xi) \tag{38 III}$$

where $\xi = x + \nu$. If we introduce now the notation

$$a^2 = 1 - \frac{n}{2} \tag{39 III}$$

the equation (38.III) becomes

$$2(1 - a^2) = \frac{4}{\pi} \int_{-a}^{\nu} d\xi \sqrt{a^2 - \xi^2} \tag{40 III}$$

which gives

$$2(1 - a^2) = \frac{4}{\pi} \frac{a^2}{2} \left[\frac{\nu}{a} \sqrt{1 - \frac{\nu^2}{a^2}} - \arccos \frac{\nu}{a} + \pi \right] \tag{41 III}$$

We write this equation as

$$\frac{\pi(1 - a^2)}{a^2} = f(\nu/a) \tag{42.III}$$

where

$$f(\nu/a) = \frac{\nu}{a} \sqrt{1 - \frac{\nu^2}{a^2}} - \arccos \tag{43 III}$$

If we plot the function $f(\nu/a)$ for $-1 < \nu/a < 1$ we see that (43.III) is well approximated by

$$f(\nu/a) = \frac{\pi}{2} \left(\frac{\nu}{a} - 1 \right) \tag{44 III}$$

From (42.III) and (44 III) we get

$$\nu = \frac{2 - 3a^2}{a} = \frac{\frac{3}{2} n - 1}{\sqrt{1 - \frac{n}{2}}} \tag{45 III}$$

and using this result in (36.III) $\Phi_{3d}(n)$ becomes

$$\Phi_{3d}(n) = \frac{(3n - 2)^2 \sqrt{2n(1 - n)}}{4 \left(1 - \frac{n}{2}\right)^{3/2}} \tag{46.III}$$

The critical temperature obtained from (35.III) is

$$T_c^{3d} = 1.13\omega_c \exp\left[-\frac{\pi t}{J}\frac{4\left(1-\frac{n}{2}\right)^{3/2}}{(3n-2)^2\sqrt{2n(1-n)}}\right] \tag{47.III}$$

or as function of ν

$$T_c^{3d} = 1{,}13\omega_c \exp\left[-\frac{\pi t}{J}\frac{\nu^2}{3\sqrt{2}}\sqrt{12-17\nu^2-\sqrt{\nu^4+24\nu^2}}\right] \tag{48 III}$$

From (47 III) we can see that T has a maximum for $n = 0{,}2$ and becomes zero for $n = 3/2$. This last result is not relevant because it is due to the average on the Fermi surface of the structure factor $f(\vec{k})$ and appears in all anisotropic models even if $d < 3$. The $T_c^{3d}(\nu)$ has a maximum for $\nu \simeq 0\,8$, result which show that the position of the Fermi surface is essential in the high-T_c behaviour

IV. **Critical temperature for lower dimensional superconductors.** The experimental investigations showed the importance of the CuO planes as well as the Cu—O chains in the properties of high-T_c superconductors Then it is important to consider the $3d$ behaviour as a superposition of the $2d$ behaviour from planes and $1d$ from chains.

1 *The two dimensional model for high-T_c superconductor* The density of states for a $2d$ electronic system is given by

$$N_{2d}(\varepsilon) = \frac{2}{\pi^2 D}\,\theta(D - |\varepsilon|)\mathbf{K}(\sqrt{1-(\varepsilon/D)^2}) \tag{1.IV}$$

where $K(x)$ is the complet eliptic integral of the first order and $\theta(x)$ is the step function Near the band edge (1 IV) can be approximated by

$$N_{2d}(\varepsilon) = \frac{4}{\pi^2 D}\,\theta\,(D - |\varepsilon|)\ln\frac{2D}{\varepsilon} \tag{2 IV}$$

which is in fact an approximation used by different authors [13, 14] Using (56.II), (60 II) and (18.III) we can calculate U_{2d} and V_{2d} for a density of states given by (2.IV). After a simple algebra we get the result

$$U_{2d} = \frac{2}{\pi}\left[\mathbf{K}(z)\,\mathrm{sign}\,z - i\,\mathbf{K}(\sqrt{1-z^2})\right] \tag{3.IV}$$

and

$$V_{2d} = \frac{2}{\pi}\left[\mathbf{K}(z^-)\,\mathrm{sign} z_- - i\,\mathbf{K}\sqrt{1-z^2}\right] \tag{4 IV}$$

an expanding the function $K(x)$ as in (2 IV) we get

$$U_{2d} \simeq \frac{2}{\pi}\left[\ln\frac{4}{\sqrt{1-z}} - i\ln\frac{4}{z}\right] \tag{5.IV}$$

$$V_{2d} \simeq \frac{2}{\pi}\left[\ln\frac{4}{\sqrt{1-z^2_-}} + i\ln\frac{4}{z_-}\right] \tag{6.IV}$$

In the calculation of T_c^{2d} we will neglect the real parts in (5.IV) and (6.IV) because these give no contribution near the band edge and only the imaginary part will be considered. Using the approximation

$$\ln|z| \simeq \frac{\operatorname{sign} z}{z} \tag{7.IV}$$

(5.IV) and (6.IV) can be written as

$$U_{2d} = -\frac{i \operatorname{sign} z}{z}; \qquad V_{2d} = \frac{i \operatorname{sign} z_-}{z_-} \tag{8.IV}$$

The equation for the number of electrons can be written as in the $3d$ case and we get

$$n = \frac{2}{\pi} \int_{-1}^{\nu} \frac{d\varepsilon}{\varepsilon} \operatorname{sgn} \varepsilon \tag{9.IV}$$

and the singularity introduced in fact by the approximation (8.IV) will be approximated as

$$\frac{\operatorname{sign} \varepsilon}{\varepsilon} \simeq p \frac{1 - \varepsilon^2}{1 + \varepsilon^2} \tag{10.IV}$$

the parameter p being a measure of the derivation from $2d$ character of the system. Using (10.IV) Φ_{2d} calculated from (28.III) has been obtained as

$$\Phi_{2d} = p\nu^2 \frac{1 - \nu^2}{1 + \nu^2} \tag{11.IV}$$

and from (9.IV)

$$n = \frac{4p}{\pi} \left[\frac{\pi}{2} + 2 \operatorname{arctg} \nu - \nu - 1 \right] \tag{12.IV}$$

these (10 IV) has been used. Following the same method (12 IV) can be approximated as

$$\nu = \frac{\pi}{2p(\pi - 2)} n - 1 \tag{13.IV}$$

and

$$\Phi_{2d} = pb \frac{n(2 - bn)(1 - bn)^2}{1 + (1 - bn)^2} \tag{14.IV}$$

where $pb = \pi/2(\pi - 2)$

The critical temperature T_c^{2d} will be obtained now as

$$T_c^{2d} = 1.13\omega \exp\left[-\frac{\pi t}{Jpb} \frac{1 + (1 - bn)^2}{n(2 - bn)(1 - bn)^2} \right] \tag{15.IV}$$

or as function of ν as

$$T_c^{2d} = 1\ 13\omega_c \exp\left[-\frac{\pi t}{J}\frac{1+\nu^2}{\nu^2(1-\nu^2)}\right] \tag{16.IV}$$

The maximum in T_c^{2d} given by (15 IV) appears at $n < 0\ 6$ but for the same parameters we can see that is very sensitive to p, (by the parameter b) which shows that the approximation of singularity near the band edge by the Lorentzian (10.IV) is the main point of the $2d$ density of states.

2. *The one-dimensional model for high-T superconductor.* The density of states for $1d$ electronic systems in the tight-binding approximation is given by

$$N_{1d}(\varepsilon) = \frac{\theta(D - |\varepsilon|)}{\pi\sqrt{D^2 - \varepsilon^2}} \tag{17.IV}$$

Using the general relation for F, we obtain U_{1d} and V_{1h} as

$$U_{1d} = -\frac{t}{\sqrt{1-z^2}}; \qquad V_{1d} = \frac{t}{\sqrt{1-z^2}} \tag{18 IV}$$

which gives

$$\Phi_{1d}(n, \nu) = \frac{1}{2}\frac{\nu^2}{1-\nu^2}\sqrt{1 - \frac{n^2}{4} - \nu^2} \tag{19 IV}$$

The chemical potential can be eliminated as for the $3d$ and $2d$ models

$$n = \frac{2}{\pi}\int_{-\infty}^{\nu} d\varepsilon\ \frac{\sqrt{1 - \frac{n^2}{4} - \varepsilon^2}}{1-\varepsilon^2} \tag{20.IV}$$

which gives

$$\nu \simeq \frac{3n-2}{2}\sqrt{\frac{2+n}{2-n}} \tag{21.IV}$$

and

$$\Phi_{1d} = \frac{(3n-2)^3}{16 - 6n - 9n^2}\sqrt{\frac{(1-n)(4-n)^2}{2n}} \tag{22.IV}$$

The critical temperature T_c^{1d} can be written as

$$T_c^{1d} = 1\ 13\omega\ \exp\left\{-\frac{\pi t}{J}\ \frac{16 - 6n - 9n^2}{(3n-2)^2}\sqrt{\frac{2n}{(1-n)(4-n^2)}}\right\} \tag{23.IV}$$

or as function on ν

$$T_c^{1d} = 1.13\omega_c \exp\left\{-\frac{\pi t}{J}\ \frac{1+\nu}{\nu^2}\left[\frac{(1-\nu)(9-6\nu)}{4+2\nu-3\nu^2}\right]^{1/2}\right. \tag{24.IV}$$

The equation (23.IV) show a rapid decreasing of T_c^{1d} with n and an increasing with ν.

This feature is very important for the study of the influence of the impurities on high-T_c which are considered to be localized in the chains.

V. **Discussions.** A detailed investigation of the possibility for high-T_c in strong correlated electronic systems showed that the CPA method is an appropriate aproach for the calculation of T_c in this systems. We have been able to show that in the strong correlated systems the critical temperature T_c^{3d}, T_c^{2d} and T_c^{1d} is very sensitive to the concentration of the electrons and to the position of the Fermi energy

REFERENCES

1 P. Soven, *Phys Rev*, **156.** 809 (1967)
2 B Velicky, S Kirkpatrick and H Ehrenreich, *Phys rev*, **175**, 747 (1968).
3 D Yoshioka and H Fukuyama, *J Phys Soc Jpn*, **54.** 2996 (1985)
4 H Fukuyama and K Yoshida, *Jpn J. Appl. Physics*, **26.** L 371 (1987)
5 P W. Anderson, *Science*, **235.** 1196 (1987)
6 J E Hirch, *Phys Rev Lett*, **54.** 1317 (1985)
7 V J Emery, *Phys Rev Lett*, **58.** 2794 (1987)
8 V J Emery and G Reiter, *Phys. Rev. B*, **38.** 4547 (1988)
9 S Trugman, *Phys Rev B*, **37.** 1595 (1988)
10 Y. Isawa, S Maekawa and H Ebisawa, *Physica*, **148** B. 391 (1987)
11 N. M Plakida, V Yu Yushankhai and I V Stasyuk (Preprint E17—1988—749 Dubna)
12 G. Baskaran, Z. Zou and P W. Anderson, *Solid St Comm*, **63.** 973 (1987)
13 J Labeé and J. Bok, *Europhys Lett*, **3.** 1255 (1987)
14. R Combescot and J. Labbe, *Phys Rev*, B **38.** 262 (1988)

STUDIA UNIV BABEŞ—BOLYAI, PHYSICA, XXXIV, 1 1989

STRESS MEASUREMENT IN ELECTRODEPOSITED NICKEL WITH (001) FIBER TEXTURE

D. CIURCHEA*, M. POPOVICI and M. SERGHIUŢĂ****

Received February 27, 1989

ABSTRACT. — The electrodeposited nickel has a (001) fiber texture which yields an anisotropic residual stress in the surface layer. The theory of the stress measurement by X-Ray diffraction is reconsidered to account for this texture. It is shown that $T_{23} = 0$ is a reasonable assumption allowing stress determinations from only two tilt measurements. Isotropic bulk moduli should be considered with caution.

1. **Introduction.** The stress measurement by X-Ray diffraction is an adequate means to control macroscopic residual stresses in thin layers. In nuclear technology, nickel electrodeposition is used to avoid corrosion.

The method of stress measurement [1, 2] in the assumption of an isotropic polycrystal implies that the residual macrostrains slightly distort the crystal. The distorsion measured by X-Ray diffraction is related to the isotropic residual stress T by:

$$\frac{d_\psi - d_0}{d_0} = \frac{1+\nu}{E} T \sin^2 \psi \tag{1}$$

where d_ψ is the lattice spacing measured at the ψ tilt angle, d_0 is the lattice spacing measured at $\psi = 0$, E is the Young modulus and ν is the Poisson ratio.

However, the assumptions made in deriving Eq. (1) may yield systematic errors in the case of textured materials since the stress normal to the specimen and the anisotropy of the elastic constants are ignored.

The aim of this paper is to check the sources of errors in the case of electrodeposited Nickel.

2 **Experimental.** The texture was measured as direct pole figures of the (002) reflection by using a Philips PW 1130/00 diffractometer with a PW 1050 vertical goniometer and a PW 1178 texture attachement. It was found that all specimens have a fiber texture with the (001) planes parallel with the specimen surface. The texture may be fairly well approximated to an unidimensional Gaussian with a fullwidth at half maximum of 15—20°. This is seen from the measurements of both the (200) and (420) reflections — the latter being the reflection convenient for stress determinations (Fig. 1 and Fig. 2).

* *University of Cluj-Napoca, Faculty of Physics, 3400 Cluj-Napoca, Romania*
** *Institute for Nuclear Power Reactors, 0300 Piteşti, Romania*

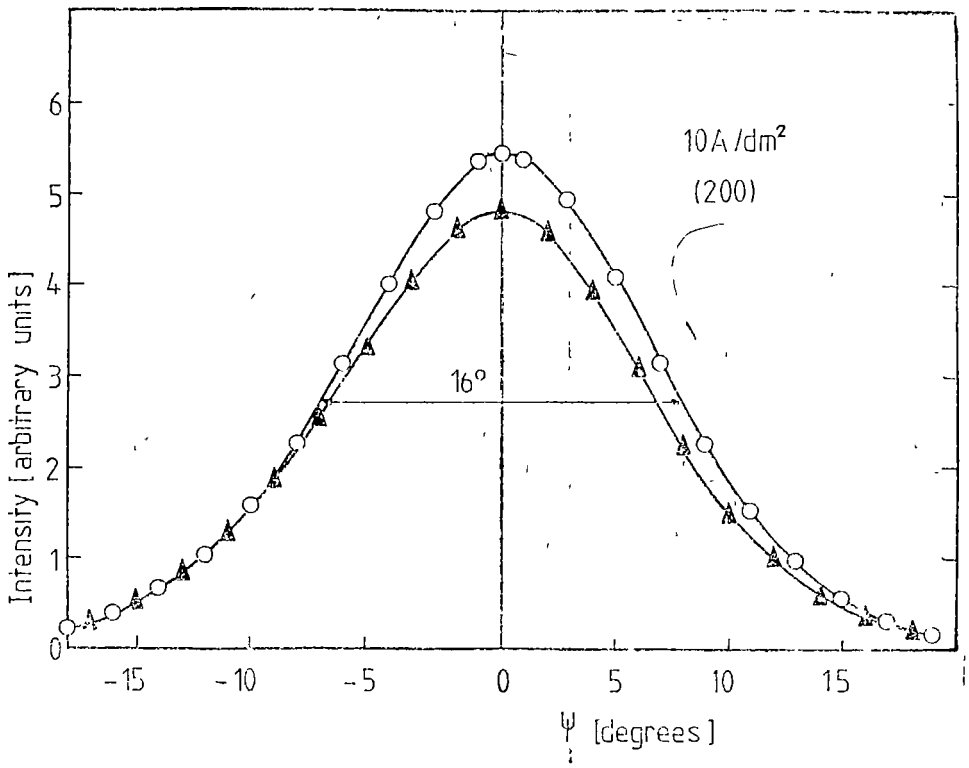

Fig. 1. Characterization of the gaussian texture in the (002) reflexion by using the ψ tilt in the DRON—2 equipment

3. **Theory.** By taking into account the very simple texture observed, the orientation distribution function may be written as [3]

$$f(g) = f(\psi) = \sum_{n=0}^{\infty} C_n \cos(n\psi) \tag{2}$$

where C_n are related to the Gaussian standard deviation σ in a simple manner.

For cubic crystals, such as Nickel, the elastic constants are of the form [4]:

$$s_{ijkl} = s^0_{ijkl} + N_{ijkl} r(\psi, \varphi) \tag{3}$$

where s^0_{ijkl} is a constant, N_{ijkl} are the nonor components and $r(\psi, \varphi)$ describes the direction in the crystal. Since our procedure always uses the (420) reflection, the φ dependence of $r(\psi, \varphi)$ may be ignored Therefore, $r(\psi)$ may be expanded in Fourier series also. The averaged elastic constants are then

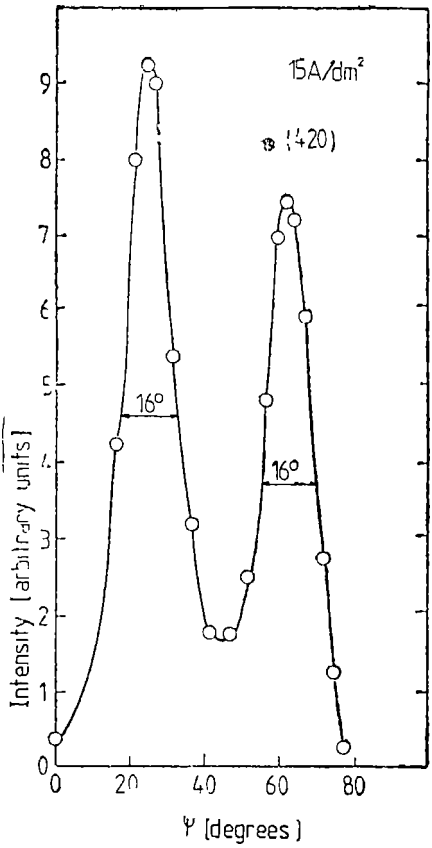

Fig 2 Characterization of the texture in the (420) reflexion by using the ψ tilt in the DRON—2 equipment

obtained by

$$\bar{s}_{ikl} = \int s_{ijkl}(\psi) f(\psi)\, d\psi \tag{4}$$

For the texture described we obtain finally

$$\frac{d_\psi - d_0}{d_0} = \tag{5}$$

$$= -(\bar{s}_{11}\bar{s}_{12})[(T_{22} - T_{33})\sin^2\psi + T_{23}\sin 2\psi]$$

where $T_{22} = T_{11}$ are the stress components in the specimen plane, T_{33} is the stress normal to the surface and T_{23} is a non-diagonal stress component $\bar{s}_{11}$ and $\bar{s}_{12}$ are given by:

$$\bar{s}_{11} = \frac{1}{8}(6s_{11} + 2s_{12} + s_{44}) + \frac{C_4}{8}(2s_{11} - 2s_{12} - s_{44})$$

$$\bar{s}_{12} = \frac{1}{16}(2s_{11} + 14s_{12} - s_{44}) - \frac{C_4}{16}(2s_{11} - 2s_{12} - s_{44}) \tag{6}$$

with $C_4 = \exp(-8\sigma^2)$, where σ is the standard deviation of the Gaussian

The comparison of Eq (5) and (1) shows that in the isotropic case, the dependence $\frac{d_\psi - d_0}{d_0}$ versus $\sin^2\psi$ is linear In the anisotropic case when $T_{23} = 0$ the $\sin 2\psi$ term implies a deviation from linearity Moreover, $\bar{s}_{11} - \bar{s}_{12}$ should be considered instead of $(1 + \nu)/E$

4. **Results and discussions.** The measurement of the residual stress was performed on a DRON—2 equipment by using the (420) reflection The reticular distance was measured as a function of the tilt angle ψ By using the single crystal elastic compliance [5,6]. $s_{11} = 7\,268\ 10^{-6}$ MPa^{-1}, $s_{12} = -2\,726\ 10^{-6}$ MPa^{-1} and $s_{44} = 8\,097\ 10^{-6}$ MPa^{-1} the following values for T_{ij} were obtained by a least squares procedure:

$$T_{22} - T_{33} = (-67\,6 \pm 5\,3)\text{MPa}$$

$$T_{23} = (-29.9 \pm 12.5)\text{MPa}$$

with a significance figure, $\chi^2/n = 0.8$.

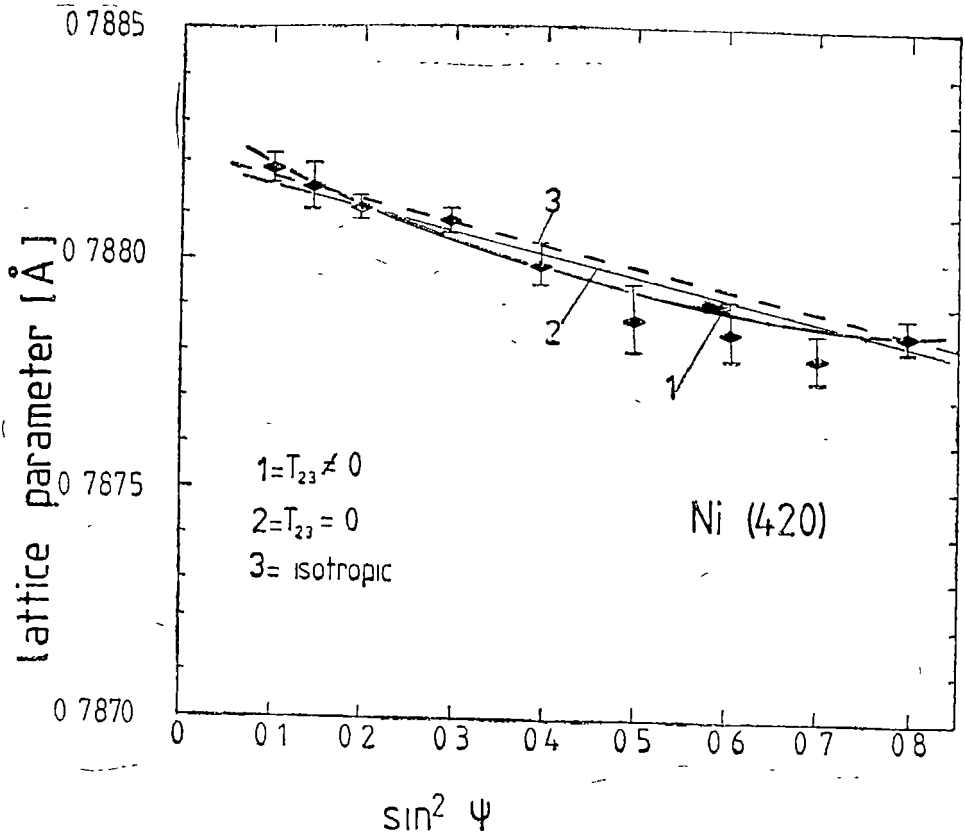

Fig 3 The plot d versus $\sin^2\psi$ showing the fit for various models discussed in the text. 1 refers to the case $T_{23} \neq 0$, 2 — refers to the case $T_{23} = 0$, 3 — refers to the isotropic case

Since the value of T_{23} is quite low, the assumption $T_{23} = 0$ was checked. We obtained $T_{22} - T_{33} = (-72\,1 \pm 5\,7)$ MPa with a significance figure, $\chi^2/n = 1\,06$.

The results of the fit are given in Fig. 3 The values of $T_{22} - T_{33}$ in the two cases analysed are very close However, by using macroscopic bulk moduli, the value of T is $T = (-97.5 \pm 10\,8)$ MPa, i.e an overestimate of about 20%, which may imply rejecting of good items during quality control.

As a conclusion, the linear dependence of $\frac{d_\psi - d_0}{d_0}$ versus $\sin^2\psi$ my be reliably assumed but single crystal compliances are compulsory The error in the measurement of the stress deviator is less than 10%. The X-Ray diffraction measurement, although expensive, is adequate for the nondestructive control of stresses Given the simple texture observed, the analysis of the stress anisotropy is greately simplified comparatively to the general case discussed by Dolle [7].

REFERENCES

1 H P Klug, L E Alexander, *X-Ray Diffraction Procedures*, Wiley and Sons, New York, 1974
2 C S Barett, T I Massalski, *Structure of Metals*, McGraw Hill, 1966
3 H J Bunge, *Mathematische Methoden der Texturanalyse*, Akademie Verlag, Berlin, 1969.
4 I I Sirotin, M P Saskolskaia, *Fizica cristalelor*, Ed Academiei, București, 1983
5 C Kittel, *Introducere în fizica corpului solid*, Ed Tehnică, București, 1974
6 Landolt-Bornstein, *Numerical Data and Functional Relationships in Science and Technology*, vol III/1, Springer Verlag, Wien, 1976
7 H Dolle, *J Appl Cryst*, **12**. 489 (1979)

STUDIA UNIV BABEŞ—BOLYAI, PHYSICA, XXXIV, 1 1989

TEMPERATURE DEPENDENCE ON THE MAGNETIC SUSCEPTIBILITY IN SOME THERNARY OXIDIC SEMICONDUCTING $\alpha-(Fe_2O_3-Al_2O_3-Cr_2O_3)$

L. POP* and M. CRISTEA**

Received March 15, 1989

ABSTRACT. — The temperature dependence of the magnetic susceptibility between 100 and 1 200 K has been investigated for some $\alpha-(Fe_2O_3-Al_2O_3-Cr_2O_3)$ solid solutions The investigated samples consist of a constant $\alpha-Fe_2O_3$ molar concentration of 50, 30 and 10 mol % and of variable concentration of $\alpha-Al_2O_3$ and $\alpha-Cr_2O_3$, respectively The system exhibits a second order phase transition from antiferromagnetic, ferromagnetic or a more complicated magnetic order state to paramagnetic state From the linear part of the temperature dependence of the reciprocal magnetic susceptibility was determined the effective magnetic moment per unit formula which has been found in good agreement with the calculated values using the formula $\mu_{eff} = [2(f_1 \cdot \mu^2_{Fe^{3+}} + f_2\mu^2_{Cr^{3+}})]^{1/2}$ where $\mu_{Fe^{3+}} = 5\ 92\ \mu_B$ and $\mu_{Cr^{3+}} = 3\ 87\ \mu_B$

Introduction. In the previous papers [1—4] we have already reported the interesting magnetic behaviour of some α-$(Fe_2O_3-Al_2O_3-Cr_2O_3)$ solid solutions in the antiferromagnetic ordered range, and corresponding in the paramagnetic range pointing out the magnetic phase diagram, the magnetic spin structure succesion of the second order phase transition and also the effective magnetic moment per unit formula.

Samples preparation and experimental technique. The starting materials for the preparation of the thernary oxidic system $\alpha-(Fe_2O_3-Al_2O_3-Cr_2O_3)$ were $AlCl_3 \cdot 6H_2O$; $FeCl_3 \cdot 6H_2O$ and $CrCl_3\ 6H_2O$ of p a purity.

The thernary oxidic samples were obtained by thermic decomposition of the aluminium, iron and chromium hydroxid coprecipitates The coprecipitates were calcined at 1 523 K and then slowly cooled down, and finally calcined for 7 hours in five cicles The homogenity of the solid solutions has been checked out through an X-ray analysis, using a TUR—M—61 diffractometer and a $Cu-K_\alpha$ radiation [2]

The thermal variation of the magnetic susceptibility has been determined using a Weiss and Forrer magnetic balance type, with 10^{-8} cm^3/g sensitivity in the temperature range 100—1 200 K and in a 9 200 Gs magnetic field intensity

Experimental results and discussions. As pointed out in previous papers [3, 4] the critical temperature of transition from the ordered state to the paramagnetic state decreases as the $\alpha-Fe_2O_3$ content in the thernary solid solutions of $\alpha-(Fe_2O_3-Al_2O_3-Cr_2O_3)$ decreases from 880 K for the samples with 90 mol% $\alpha-Fe_2O_3$ down to 700 K for the samples with 70 mol% $\alpha-$ $-Fe_2O_3$ Actually, if we represent these values as an $\alpha-Fe_2O_3$ concentration

* *Physics Department, Cluj-Napoca University, 3400 Cluj-Napoca, Romania*
** *Politehnical Institut „Traian Vuia", Timisoara—1900, Romania*

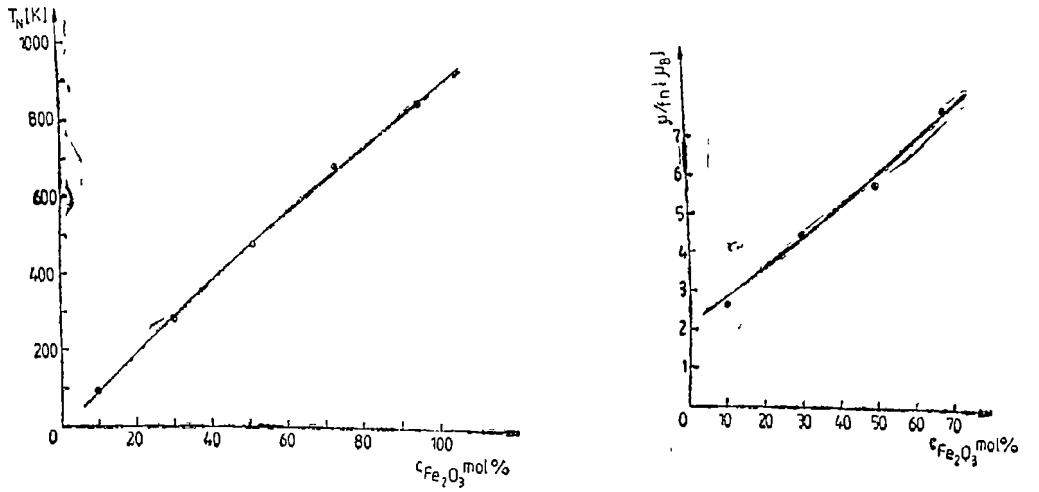

Fig 1. 2 Magnetic phase diagram $\alpha-Fe_2O_3$ concentration dependence of the effective magnetic moment per formula unit.

function together with the critical temperatures for the samples investigated in this paper, i e 50, 30; 10 mol% $\alpha-Fe_2O_3$, we obtain a linear dependence, as one can see from the magnetic phase diagram given in the Fig. 1. This means that the magnetic spin structure characteristic for the $\alpha-Fe_2O_3$ still persists superposed on the magnetic spin structure characteristic for the $\alpha-Cr_2O_3$ denoting a more complicated magnetic spin structure for the solid solutions $\alpha-(Fe_2O_3-Al_2O_3-Cr_2O_3)$ On the other hand the linear decrease of the critical temperature, T_N, with the $\alpha-Fe_2O_3$ content shows on the dilution effect of the $\alpha-Al_2O_3$ and $\alpha-Cr_2O_3$ content in the thernary solid solutions More than that, this means that the samples are homogeneous solid solutions, in good agreement with the X-ray results [2].

These conclusions are also confirmed by the $\alpha-Fe_2O_3$ concentration linear dependence of the effective magnetic moment per unit formula calculated from the slope of the temperature dependence of the reciprocal magnetic susceptibility, given in the Fig 2 The linearity of the effective magnetic moment per unit formula can be also observed when it is represented as an $\alpha-Cr_2O_3$ concentration function

The complicated magnetic spin structure is revealed by the temperature dependence of the reciprocal magnetic susceptibility below critical temperature, as one can see from Fig. 3, for the set of three samples containing 50 mol % of $\alpha-Fe_2O_3$ One observes that for the less $\alpha-Cr_2O_3$ concentrated sample, i.e. 25 mol% $\alpha-Cr_2O_3$, the temperature dependence is similar to that of the more concentrated $\alpha-Fe_2O_3$ samples [4], and when the $\alpha-Cr_2O_3$ concentration increases the shape of the curves is strongly modified, the temperature dependence, of the reciprocal magnetic susceptibility having a minimum which corresponds to the Néel temperature. For $T > T_N$ the temperature dependence of the reciprocal magnetic susceptibility is linear, obeing the Curie–Weiss law.

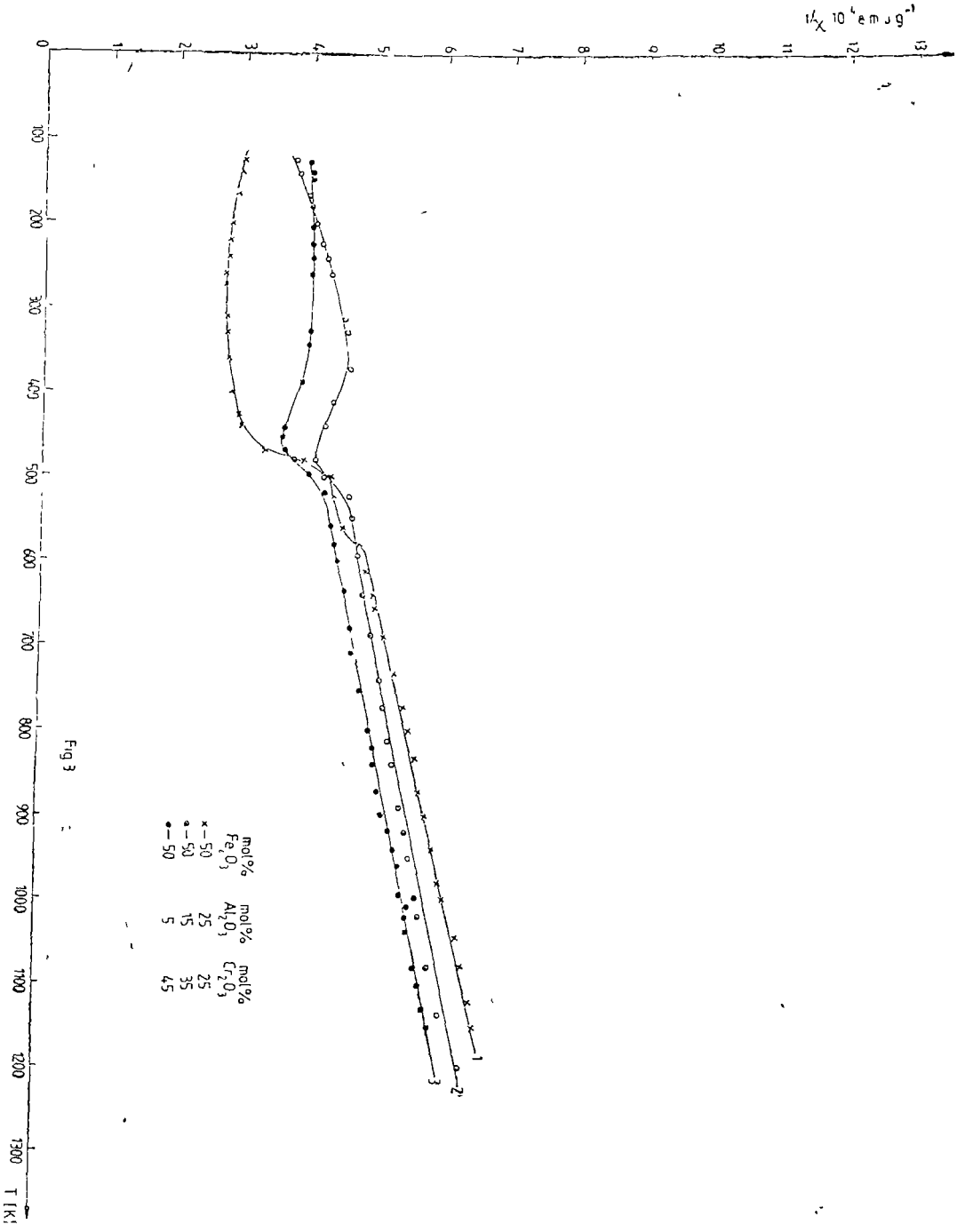

Fig 3. Temperature dependence of the reciprocal magnetic susceptibility for α—(Fe_2O_3—Al_2O_3—Cr_2O_3) samples with 50 mol % of α—Fe_2O_3

The magnetic spin structure picture is strongly changed when $\alpha-Fe_2O_3$ concentration decreases to 30 mol% in the $\alpha-(Fe_2O_3-Al_2O_3-Cr_2O_3)$ solid solutions, as one can see from Fig 4, where is given the temperature dependence of the reciprocal magnetic susceptibility for three samples with different $\alpha-Cr_2O_3$ concentration The shape of the thermal variation curves of the reciprocal magnetic susceptibility suggests some kind of ferromagnetic spin structure, colinear and noncolinear arrangement of the 3d spins, depending of the $\alpha-Cr_2O_3$ molar concentration In the paramagnetic region the temperature dependence of the reciprocal magnetic susceptibility is not linear.

The ferromagnetic ordering is better expressed when the $\alpha-Fe_2O_3$ concentrations is lowered down to 10 mol %, as one can see from the Fig 5, where is shown the temperature dependence of the reciprocal magnetic susceptibility for the set of samples with the constant 10 mol% $\alpha-Fe_2O_3$ and different concentration of $\alpha-Cr_2O_3$ and $\alpha-Al_2O_3$.

The thermal variation of the reciprocal magnetic susceptibility is not linear, obeing the Néel law in the paramagnetic region, as usual for the ferromagnetic ordered materials. One sample breaks the rule, namely the 81 mol% $\alpha-Cr_2O_3$ sample For this sample, at low temperature the reciprocal magnetic susceptibility does not change as the temperature increase towards the room temperature, but beyond this it obeys a Curie—Weiss law Such a behaviour is less usual, and we have reported it before for some binary solid solutions $\alpha-(Fe_2O_3-Al_2O_3)$ [5] and for $\alpha-Fe_2O_3$ [6]

From the slope of the linear part of the temperature dependence of the reciprocal magnetic susceptibility we have determined the Curie constant and afterwards we have calculated the effective moment per unit formula and per ion, using the relation

$$\mu_{eff} = [f_1\mu^2_{Cr^{3+}} + f_2\mu^2_{Fe^{3+}}]^{1/2}$$

where f_1 and f_2 are the molar fraction, and $\mu_{Cr^{3+}} = 3\,87\ \mu_B$, $\mu_{Fe^{3+}} = 5\,92\ \mu_B$ The obtained results as listed in the Table 1

Table 1

	Samples concentration mol %			Molar Curie—Weiss const C_M	$\mu_{eff}/f\mu$ μ_B	μ_{eff}/ion, μ_B determined	μ_{eff}/ion, μ_B calculated
	$\alpha-Fe_2O_3$	$\alpha-Al_2O_3$	$\alpha-Cr_2O_3$				
1	50	25	25	4 914	6 295	4 46	4 61
2	50	15	35	5 743	6 80	4 82	4 77
3	50	5	45	5 935	6'918	4 91	4 92
1	30	35	35	3 584	5 376	3 81	3 96
2	30	21	49	4 252	5 856	4 15	4 21
3	30	6	64	4 603	6 093	4 32	4 48
1	10	80	10	1 118	3 003	2 23	2 13
2	10	63	27	1 498	3 579	2 74	2 53
3	10	44	46	2 157	4,272	3 22	3 03
4	10	27	63	3 078	4 983	3 59	3 53
5	10	9	81	3 707	5 463	3 95	3 88

Fig. 4. Temperature dependence of the reciprocal magnetic susceptibility for $\alpha-(Fe_2O_3-Al_2O_3-Cr_2O_3)$ samples with 30 mol % of $\alpha-Fe_2O_3$

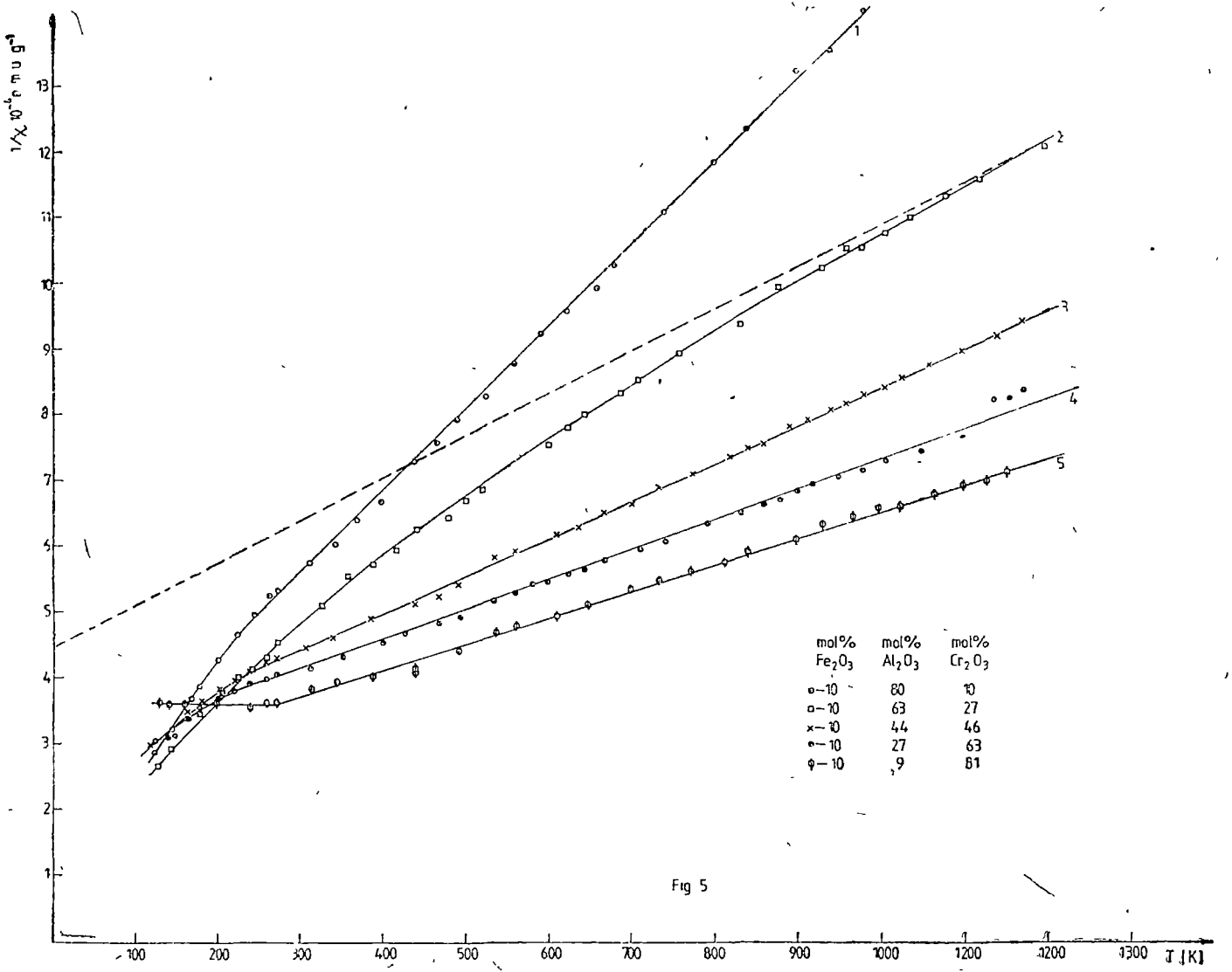

Fig 5

Fig. 5 Temperature dependence of the reciprocal magnetic susceptibility for $\alpha-(Fe_2O_3-Al_2O_3-Cr_2O_3)$ sample with 10 mol %

As one can see from the last two columns the determined and calculated effective magnetic moment values per ion are in very good agreement If the value of the effective magnetic moment per ion is multiplied by $\sqrt{2}$, then one obtains the effective magnetic moment value per unit formula determined from the molar Curie—Weiss constant value.

Conclusions. The investigated thernary system of the solid solutions α—$-(Fe_2O_3-Al_2O_3-Cr_2O_3)$ having the corundum crystalline structure presents interesting magnetic behaviour, depending of the molar concentrations of the two components, i e Fe_2O_3 and Cr_2O_3

The temperature dependence of the reciprocal magnetic susceptibility pointed out the existence of the magnetic order in the systems of the oxidic solid solutions of different type, i e antiferromagnetic order of the $\alpha-Fe_2O_3$ type for the high $\alpha-Fe_2O_3$ concentrated samples, antiferromagnetic order of the $\alpha-Cr_2O_3$ type for the high $\alpha-Cr_2O_3$ concentrated samples, superposed magnetic spin structure of these two types of magnetic structures and colinear, respectively noncolinear ferromagnetic spin structures in the less $\alpha-Fe_2O_3$ concentrated samples.

The concentration $\alpha-Fe_2O_3$, and $\alpha-Cr_2O_3$ dependences of the critical temperature, and of the effective magnetic moment per formula unit and per ion are linear.

The calculated and experimentally determined effective magnetic moment per unit formula and per ion are in good agreement.

REFERENCES

1 O Pop, L Stănescu, L Pop, *Studia Univ Babeş—Bolyai, Physica*, **XXX.** 30 (1985)
2 M Cristea, *Teză de doctorat*, Inst Politehnic Timişoara (1984)
3 L Pop, M Cristea, O Pop, I Pop, *Lucrările Conferinţei anuale de semiconductoare, C A S '87*, Ediţia a 10-a, 7—10 oct 1987, Sinaia, p 531
4 L Pop, M Cristea, O Pop, I Pop, *Studia Univ Babeş—Bolyai, Physica*, **XXXII 2.** 13—19 (1987)
5 L Pop, C Mărăloiu, L Stănescu, I Pop, *Studia Univ Babeş—Bolyai, Physica*, **XXXII.** (1). (1987).
6 L Pop, I Pop, *Studia Univ Babeş—Bolyai, Physica*, **XXXII** (2). 44 (1987).

STUDIA UNIV BABEŞ—BOLYAI, PHYSICA, XXXIV, 1, 1989

MAGNETIC INVESTIGATIONS AS FUNCTION OF HEAT TREATING IN THE Gd—Ba—Cu—O SYSTEM

AL. NICULA*, A. V. POP*, L. V. GIURGIU**, AL. DARABONT** and I. COSMA***

Received April 14, 1989

ABSTRACT. — Electron paramagnetic resonance and static susceptibility measurements on Gd^{3+} were performed in the system $GdBa_2Cu_3O_{7-\delta}$. The temperature dependence of g-value, linewidth for the Gd^{3+} signal function of temperature, atmosphere and time of heat treating samples were reported. The partial substitution of the nonmagnetic yttrium with gadolinium were investigated by EPR as a function of temperature.

Introduction. The discovery of high-T_c superconductivity [1] initiated the search for new compounds, the experimental analysis and the proposal of theoretical models.

There are numerous reports on the EPR measurements [2, 3] in high-T_c superconductors above 90 °K in the series of rare earth (Re)—Ba—Cu—O systems. A study of magnetism in related materials should serve for undersanding the superconductivity of the oxides. Practically, a Y—Ba—Cu—O system of poor quality exhibits a magnetic susceptibility of a Curie—Weiss type. Electron paramagnetic resonance is a useful means to identify the magnetic origin because it can specify the magnetic components through anisotropic g-values. The high sensitivity of EPR measurements also favors the detection of impurity phases. There are numerous reports on the EPR measurements in high-T_c superconducting Y—Ba—Cu—O system comparatively with Gd—Ba—CuO system. EPR will be a fruitful technique to reveal the electronic state of Gd and to probe the static and dynamic interactions with the superconducting system. However, all papers concerned with the Cu ions have failed to give any significant information on the underlying superconducting system. The single phase $YBa_2Cu_3O_7$ material, with the optimal oxygen composition, has no Curie moment [4] and it has been suggested that the observed Cu^{2+} EPR signal originates from an impurity phase. The Gd in $GdBa_2Cu_3O_7$ does have a large Curie moment and strong EPR signal [5, 6].

However, in common with its Y parent material, the EPR does not exhibit the characteristic signature expected for a local moment in a superconductor. It is therefore useful to compare these signals with those originating from the principal impurity phases. Intimately related to the "black phase" high $T_c \simeq$ $\simeq$ 90 K superconductors $YBa_2Cu_3O_7$ and $GdBa_2Cu_2O_7$ and the "green phase" insulators Y_2BaCuO_5 and Gd_2BaCuO_5 [7, 8], Gd^{+3} signal has in Gd_2BaCuO_5 an accurately Lorenzian shape and is temperature-indepedent at high tempera-

* *University of Cluj-Napoca, Faculty of Mathemtics and Physics 3400 Cluj-Napoca, Romania*
** *Institute of Isotopic and Molecular Technology, P O Box 700, R—3400 Cluj-Napoca, Romania*
*** *Politechnic Institute of Cluj-Napoca, Dept of Physics, R—3400 Cluj-Napoca, Romania*

ture In contrast, in $GdBa_2Cu_3O_7$ there is a slight asymmetry in the lineshape and a small temperature dependence in the linewidth above T_c [5, 7], Gd_2BaCuO_5 gives a Curie—Weiss $\theta \simeq -20$ K and for $GdBa_2Cu_3O_7$ a Curie Weiss law with $\theta \simeq -30$ K.

In this paper, we report the EPR and static susceptibility measurements in nonsuperconducting and super conducting $GdBa_2Cu_3O_{7-\delta}$ function of the temperature, atmosphere and time of heat treating samples The partial substitution of nonmagnetic yttrium with gadolinium have been investigated by analysing the EPR spectra in system $Y_{1-x}Gd_xBa_2Cu_3O_{7-\delta}$

Experimental procedure. The samples studied were prepared by the solid phase reaction method through reacting the mixture of $Gd_2O_3 \cdot CuO$ and $BaCO_3$ in cation ratio Gd Ba · Cu = 1 2 : 3 (samples 1, 2, 3) In sample 4, Y were substituted by 1% Gd The ceramic samples 1, 2 and 4 were obtained by calcination of oxides mixtures at 850° for 8 hours in air To obtain higher homogenity the powders were mixed with absolut alchool in an agate mortar and recalcinated at the same temperature for other 8 hours The samples were pressed into pellets and firing in air for 10 hours at 940°C, and then cooled down to 200°C in 8 hours Samples 2 and 4 were cooled in air atmosphere and sample 1 in oxigen Sample 3 were firing in oxygen for 12 hours at 900°C, cooled down to 200° in 16 hours, then regrinding the pellets and repeating the process

The electron paramagnetic resonance measurements were carried out by means of RADIOPAN spectrometer SE/X/2543 at room and liquid nitrogen temperature The samples were finely crushed and mixed by silicon fett Merck

The magnetic susceptibilities were measured using the standard Faraday balance

Results and discussions. The EPR spectra recorded from sample 3 at the room and liquid nitrogen temperature (LNT) are presented in Fig 1 and for samples 1, 2 in Fig 2 and 3

The EPR results in temperature dependence of the peak to peak linewidth of the first derivative of the absorption signal B_{pp} and the g factor are summarized in Table 1.

Table 1

Sample	Temperature	ΔB_{pp} (mT)	g	$(\Delta B_{pp})_{RT} - (\Delta B_{pp})_{NT}$	Δg
1	RT	146 1	2 013 ± 0 002	28 4	0 057
	LNT	117 7	1 956 ± 0 002		
	RT	105 5	1 982 ± 0 002		
2	LNT	90 0	1 966 ± 0 002	15 5	0 016
3	RT	113 3	1 974 ± 0 002	13 3	0 004
	LNT	100 0	1 970 ± 0 002		
4	RT	43 8	1 984 ± 0 002	1.1	0 006
	LNT	42 7	1 978 ± 0 002		

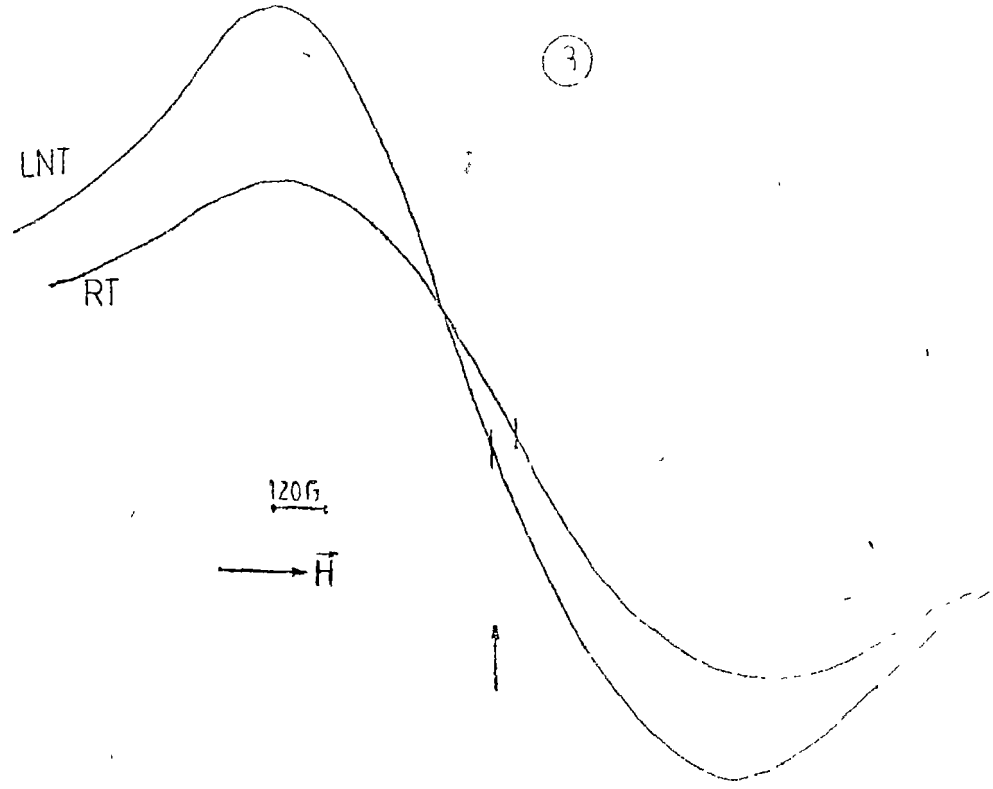

Fig. 1 The EPR spectra from sample 3 at the room (RT) and liquid nitrogen temperature (LNT)

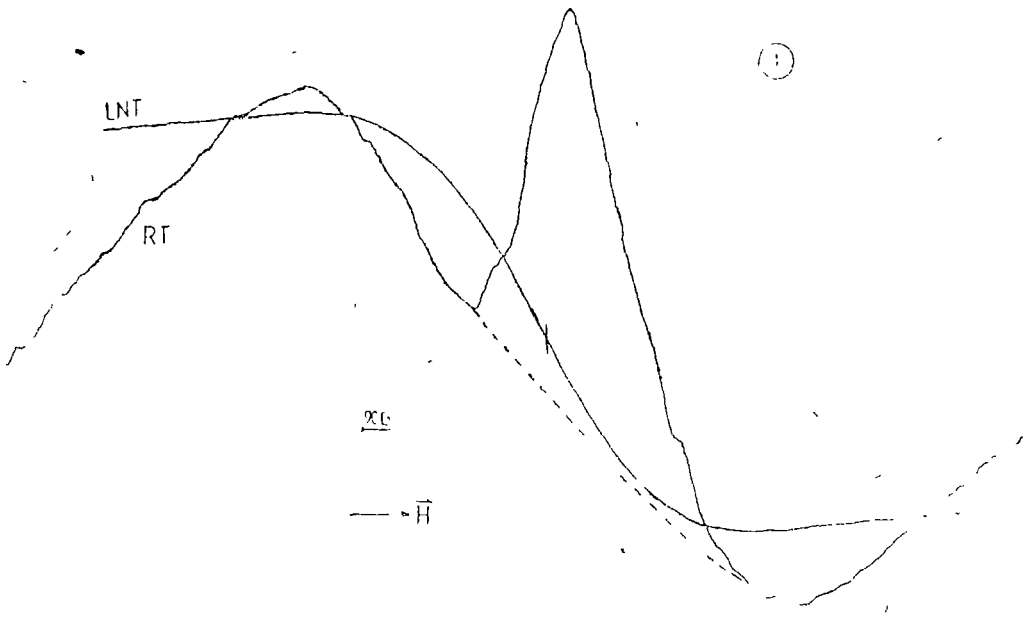

Fig. 2. The EPR spectra from sample 1 at the RT and LNT.

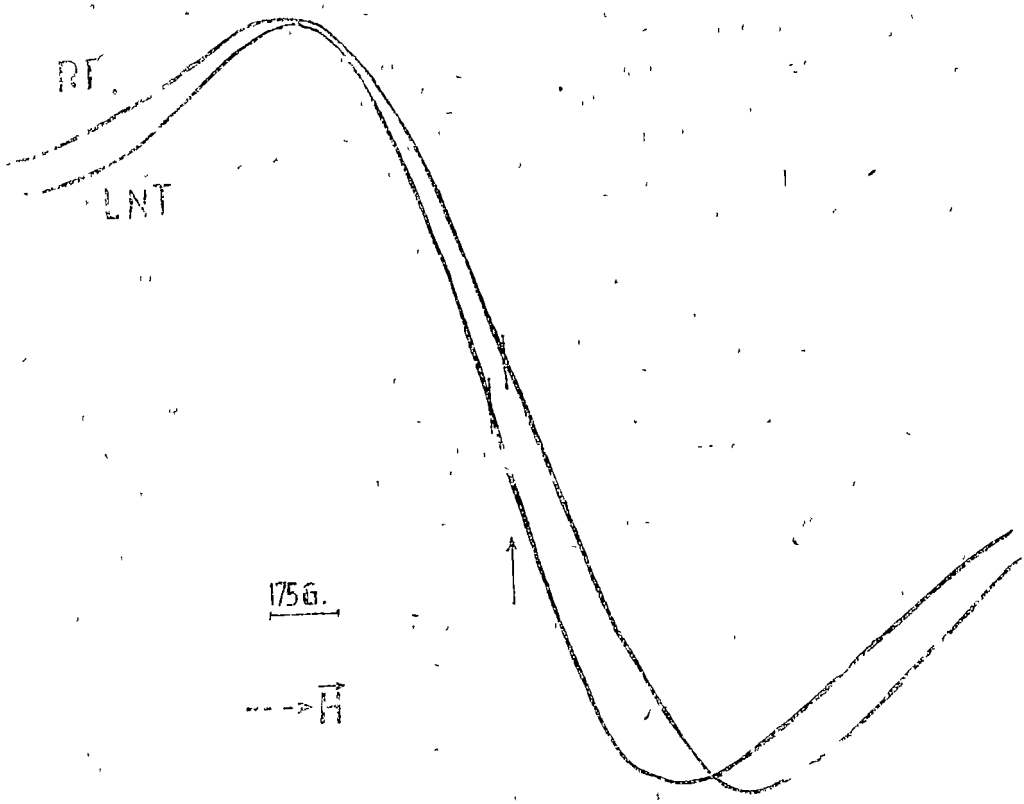

Fig 3 The EPR spectra from sample 2 at the RT and LNT

As shown in Fig 1, a clear resonance signal with strong intensity was observed in the sample 3 at the field corresponding to nearly $g \simeq 1{,}97$, which is typical of the Gd^{3+} ions [5, 8, 9] The crystal structures described by Michel and Raveau [10] are orthorhombic with Gd^{3+} in distorted monocapped trigonal prisms of GdO_7 with two neighboring GdO_7 prisms sharing one triangular face, forming Gd_2O_{11} blocks and the Cu^{2+} ions located in distorted tetragonal pyramids of CuO_5 The Gd^{3+} signal in sample 3 and their parameters are characteristic of "black phase" in $GdBa_2CuO_{7-\delta}$ supraconducting system The decrease of the g factor as function of temperature in samples 1 and 2 indicates the presence of "green phase" insulator Gd_2BaCuO_5 The g value for the sample 1 cooled in oxigen atmosphere evidenced greater amounts of "green phase" than in sample 2 colled in air The small decreases of linewidth above T_c is characteristic of a "black phase" superconductive [4], while in "green phase" the Gd^{3+} line sharphy broadens and shifts at lower temperatures, the linewidth beeing relatively constante for $T \simeq 90$ K [7] The temperature dependence of Gd^{3+} g factor and the linewidth in samples 1 and 2, indicated the presence of two phases "black" and "green" that influence specifically the EPR parameters.

The EPR spectrum for sample 1 indicates the overlapping over the characteristic Gd^{3+} line of a narrow line at room temperature The disappearance of this narrow line at liquid nitrogen temperrture is probably caused by the structural phase transformations in the microvicinity of Gd^{3+} that influences spin-spin relaxation The origin of this signal is not clear, and it is possibly to be due to the oxygen non-stoichiometry coupled with a structural transition

Sample 4 evidence a resonance signal typical of the Gd^{3+} ions in superconducting "black" phase This indicates that the substitution of the nonmagnetic yttrium with gadolinium also leads to the appearance of a superconducting phase

Gd ions are in the spin-only S-state and behave as paramagnetic local moments In this situation, one may expect the spin-lattice relaxation mechanism to have little effect on the linewidth. The shape of the resonance is determined by spin-spin relaxation [8] The line shape was found Lorentzian, indicating the presence of exhange narrowing According to the general theory of magnetic resonance, the exhange integral can be obtained from the Weiss temperature of the magnetic suspectibility

$$0 = 2zJ \cdot S(S+1)/3k_B \qquad (1)$$

where $z = 4$ is the number of nearest neighbors [11] and $S = \frac{7}{2}$ for Gd^{3+}.

The inverse of the static susceptibility as a function of temperature obtained by the Faraday balance method is presented in Fig 4 Susceptibility investigations performed in $GdBa_2Cu_3O_{7-\delta}$ does not follow a well defined Curie—Weiss law The susceptibility can be fitted by $\chi(T) = \chi_0 + \frac{C}{T-0}$ in limited range of temperature We obtained the paramagnetic Curie temperatures $0_p = -14$ K and $\theta_p = -24$ K for samples 1 and sample 3 respectively

These negative values of θ_p reflect antiferromagnetic interactions and suggest the presence of antiferromagnetism ordering in these materials at low temperatures and also the existence of the dipole-dipole interactions

By using the experimentally determined θ_p values we get the exhange integral $J = 3\,92 \cdot 10^{-17}$ (erg) and $J = 6\,72 \cdot 10^{-17}$ (erg) for sample 1 and sample 3, respectively

Conclusions. We have observed that the existance of the magnetic moments as shown by EPR and susceptibility measurements depends considerably on the treatment of samples The resonance of Gd^{3+} indicates the presence of two phases "black" and "green", that influence the EPR parameters. We evidenced at room temperature the presence of a narrowed line superimposed

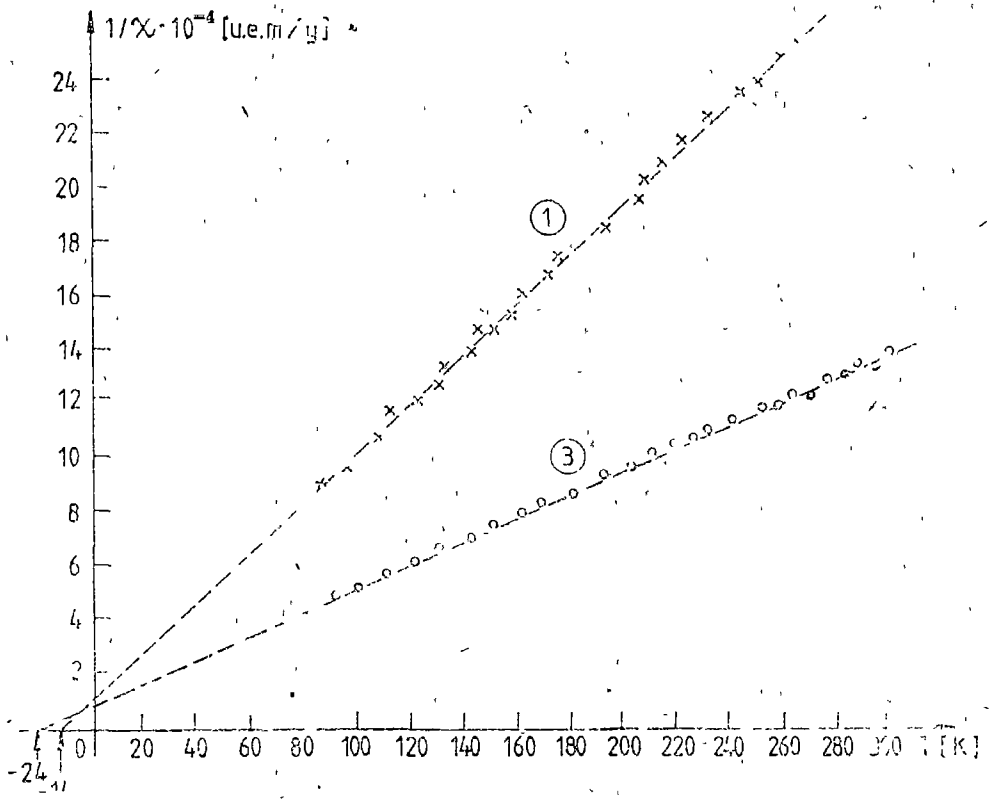

Fig. 4 The inverse of the static susceptibility ($1/\chi$) as a function of temperature (T) from sample 1 and sample 3.

over the characteristic Gd^{3+} line The origin of this signal is not clear Measuements of static susceptibility reflect the antiferromagnetic interactions and the fact that θ_p is function of heat treatment of samples The exchange integrals have been also derived for these samples

REFERENCES

1 J B Bednorz, K A Muller, *Z Phys B* **64.** (1986)
2 I Uisu, *La Resonance Paramagnetique Electronique*, Ed Dunod, Paris (1968)
3 *Proc Internat Conf on HTSC & M²S, Interlaken*, 1988 K Kanoda, T Takahashi, T Kawagoe, T Mizoguchi, *Proc Internat Conf on Science and Technology of Synthetic Metals*, June 26—July 2, 1988, Santa Fe USA
K Kanoda, T Takahashi, T Kawagoe, T Mizoguchi, M Hasumi, S Kagoshima, *Physica C*, **153—155** (1988)
D Shaltiel, J Genossar, A Gragevsky, Z H Kalman, B Fischer, N. Kaplan, *Solid St Commun*, **63.** 987 (1987)
S Simon, I Barbur, I Ardelean, *Studia, Physica*, **32(2).** 96 (1987)

4 T R McGuire, T R Dinger, P J P Freitas, W J Gallagher, T S Plaskett, R L Sandstrom, T M Shaw, *Phys Rev B*, **36.** 4052 (1987)
5 F Mehran, S E Barnes, C C Tsuei, T R McGuire, *Phys Rev B*, **36.** 7266 (1987)
6 R N Schwartz, A C Pastor, R C Pastor, K W Kirby, D Rytz, *Phys Rev B*, **36.** 8858 (1988)
7 F N Mehran, S E Barnes, E A Giess, T R McGuire, *Solid State Commun*, **67.** (1). 55 (1988)
8 H Kikuchi, Y Ajiro, Y Ueda, K Kosuge, M Takano, Y Takeda, M Sato, *Journal of Phys Soc of Jap*, **57.** 406 (1988)
9 Al Nicula, A V Pop, Al Darabont, L V Giurgiu, *Studia, Physica*, **32(2).** (1988)
10 C Michel, B Raveau, *L Solid State Chem*, **43.** 73 (1982)
11 Y Le Page, W R McKinnon, J M Tarascon, L H Greene, G W Hull, D M Hwang, *Phys Rev B*, **35.** 7115 (1987)

STUDIA UNIV BABEŞ—BOLYAI, PHYSICA, XXXIV, 1 1989

SPECTROSCOPIC STUDY AND DETECTION OF SOME HALOGENATED HYDROCARBONS BY *OA* LASER METHOD

ADRIANA BARBU* and I. BRATU*

Received April 17, 1989

ABSTRACT. — Laser optoacoustic spectroscopic study of some halogenated hydrocarbons, in the spectral range 9—11 μm, are reported The wavelenghts, for each molecular compound, at which the absorption cross sections are maximum in the investigated spectral range are chosen The trace detection in air for halogenated hydrocarbons was performed

I. **Introduction.** The monitoring of pollutants and toxic substances, both close and far from the emission source [1, 2, 3], represents a special interest. The irradiation of a sample with a laser tuned on one of their fundamental vibrational frequencies leads to their excitation Deexcitation, predominantly by collisions, of the molecules of the sample, produces a heat rising, respectively an increase of the gas pressure in the cell [4, 5] By modulating with a certain frequency the intensity of the laser beam, the pressure variations, ΔP, detected with a condenser microphone (or with electret) are converted into an electric signal, the optoacoustic (OA) signal [6, 7] The OA signal depends on the following parameters the incident radiation power, the modulation frequency, the concentration of the absorbing gas, in the cell (up to the saturation level), the nature of the absorbing gas through the absorption cross section, the nature and pressure of the buffer gas

The increase of the signal/noise ratio [8] is done by a convenient choice of the previously presented parameters

II **Experimental.** The experimental OA setup, Fig 1, used for obtaining the absorption spectra and the detection of the halogenated alkanes traces [9] is composed of CO_2CW frequency stabilized laser, mechanical chopper, with frequency range 4—4 000 Hz, LM2 powermeter, Car-Zeiss Jena, frequencymeter, absorption cell endowed with condenser microphone, lock-in nano voltmeter of 232B Unipan type, HeNe laser for the alignment of the OA device components1

The following halogenated hydrocarbons were analyzed halogenated alkanes — iodoform, dichlormethane and cloroform, halogenated alknenes — vinylchloride and trichlorethylene

The air at atmospheric pressure was used as a buffer gas

The incident radiation power was maintained at 0 2 W and the modulation frequency was 12 5 Hz.

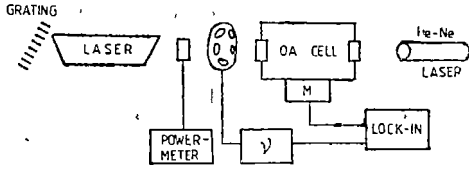

Fig 1. Experimental OA setup

III. **Results and discussions.** For the identification of a certain molecular compound from a multicomponent mixture is necessary to know its absorption

* *Institute of Isotopic and Molecular Technology, P O. Box 700, R—3400 Cluj-Napoca, Romania.*

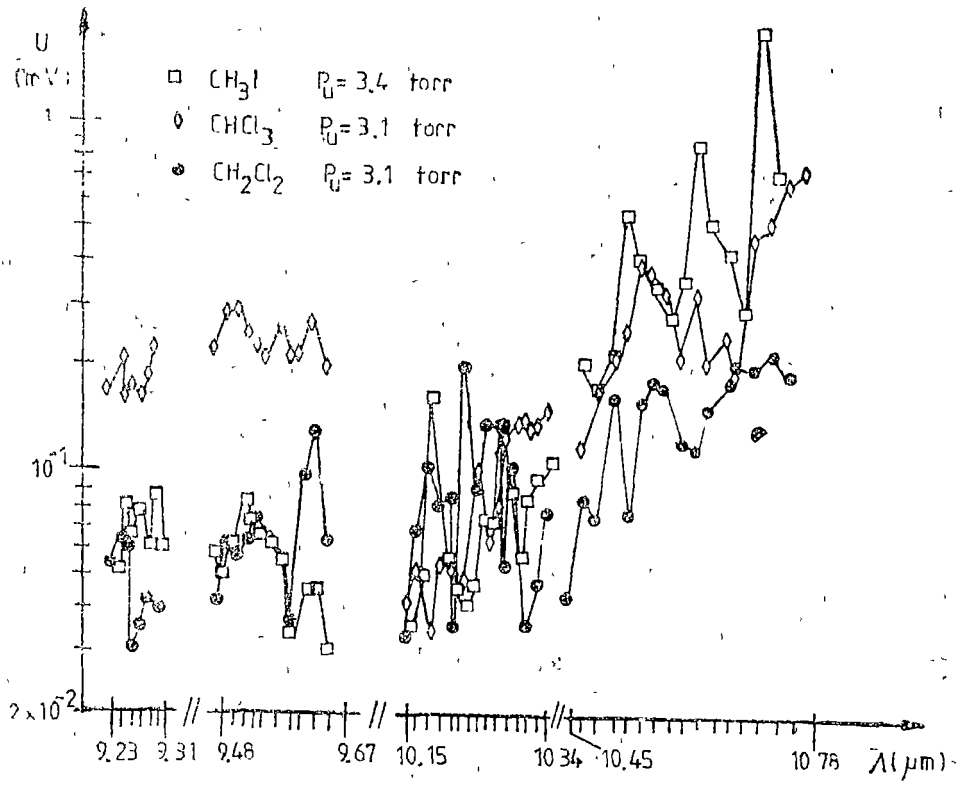

Fig 2. The OA absorption spectra for halogenated alkanes in the 9—11 μm spectral range

spectrum in a large spectral range The previously enumerated compounds were investigated in the emission range of the CO_2 laser, 9—11 μm, where these compounds have specific cross sections [10]

Fig 2 presents the absorption of halogenated alkanes, whereas in Fig 3 the absorption spectra of halogenated alkenes are showed.

From the absorption spectra presented in Fig 2 and 3 the wavelengths for each molecular compound at which the absorption cross sections are maximum in the investigated spectral range are chosen, Table 1.

Table 1

The wavelengths at which the analyzed molecular compounds present specific absorption cross sections

Substance	λ_i(μm)	λ(μm)
iodoform	10 72	10 65
dichlormethane	10 74	10 76
	10 22	
cloroform	10 78	10 78
vinylchloride	10 49	10 61
trichlorethylene	10 59	10 59
	10 69	

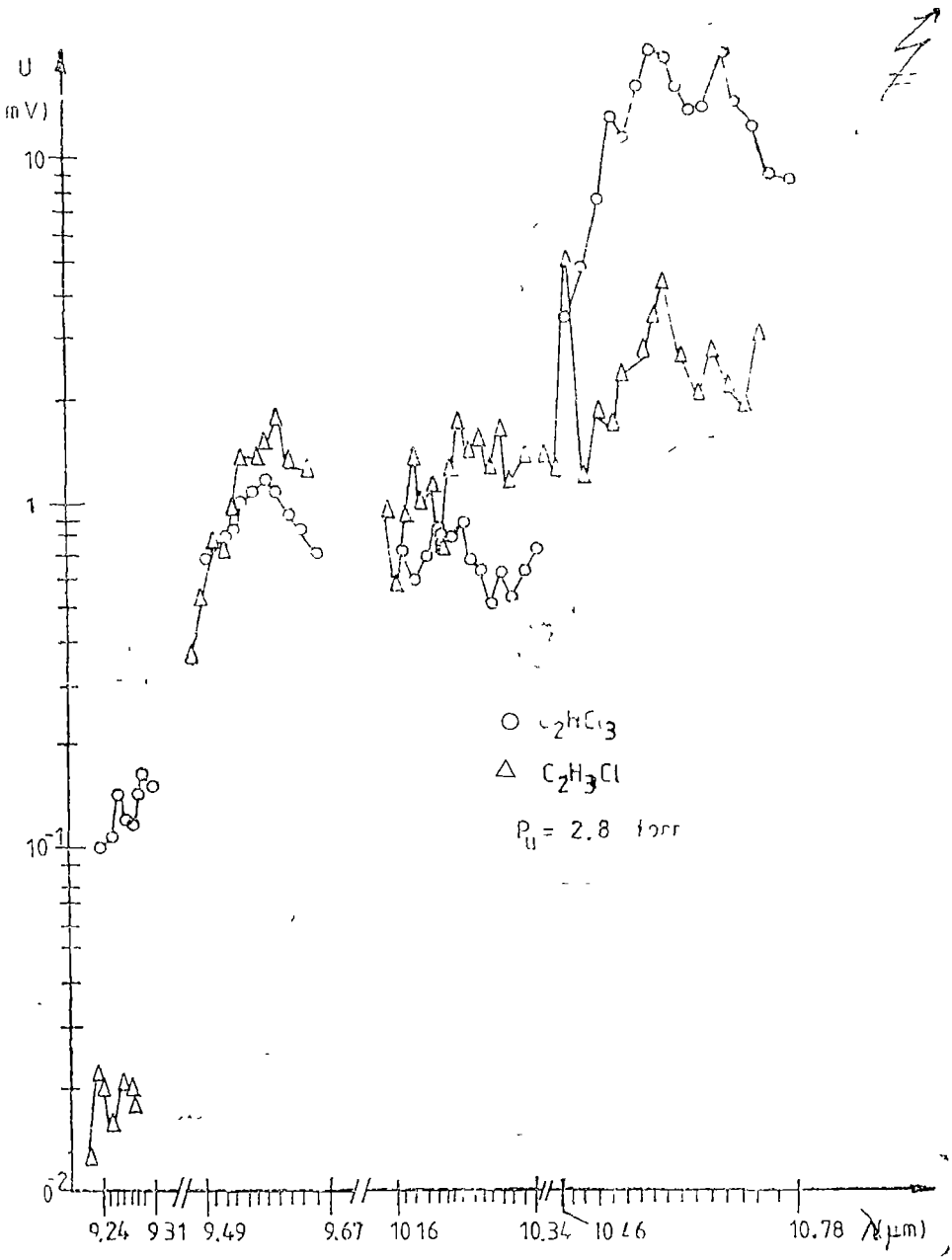

Fig 3 The OA absorption spectra for halogenated alkenes in the 9—11 μm spectral range.

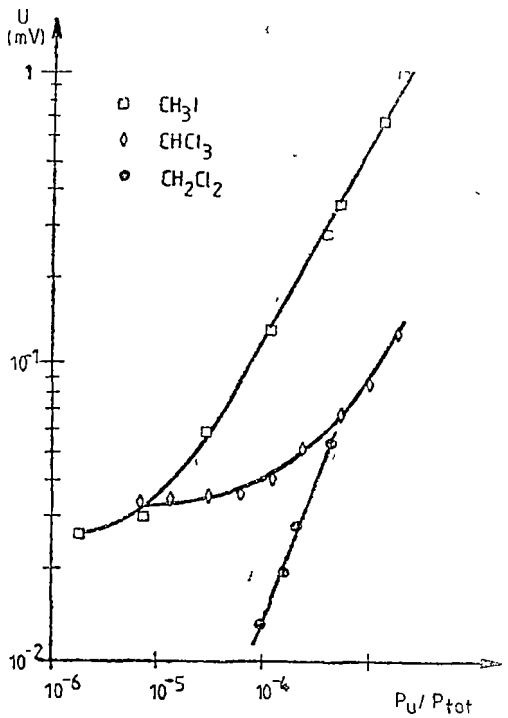

Fig 4 The detection of the halogenated alkanes in air

The trace detection in air for halogenated hydrocarbons was performed for each substance partly at the wavelengths, previously specified

In the spectral range 9—11 μm, at the wavelengths λ_i, the investigated molecular compounds present maximum values of the absorption cross sections For better trace gas detection of these compounds in air, the use of one of the λ_i values is recommended The wavelength for the sample irradiation, λ, used for their trace detection in these measurements, are specified in the Table 1, for each compound

Thus, *ppm* of halogenated alkanes in air were detected, exept dichlormethane

The trace detection for vinylchloride and trichlorethylene in air is presented in Fig 5.

In Fig. 4 and 5 the ratio of the absorbing gas pressure, P_u, and the total pressure in the cell, P_{tot}, that is the concentration of the absorbing gas, is represented on the abscissa whereas on the ordinate scale the OA signal is represented.

Due to the fact that the halogenated alkenes present absorption cross sections greater than that for alkanes, in the investigated spectral range, tenths of *ppm* of alkenes in air were detected

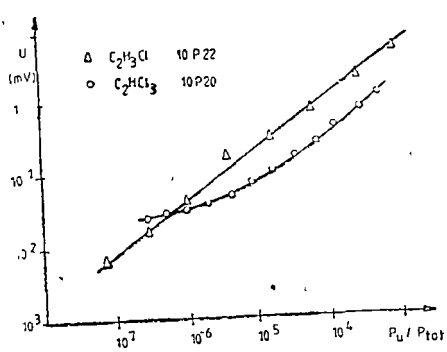

Fig 5 The trace detection for halogenated alkenes in air

Conclusions. The necessity of OA spectra registration for various molecular compounds results from the need of wavelengths determination at which, the absorption cross sections present maximum values in the investigated spectral range. These wavelengths are recommended to be used in the trace detection for each substance.

The lowering of the limit for trace detection can be done either by increasing the incident radiation power (up to the appearance of the saturation effects), or by extending the spectral range. The aim is to find eventually other wavelengths at

which the absorption cross sections are larger, or to increase the signal/noise ratio [11] (cell geometry, microphone sensitivity, cell walls manufacture, substance purity etc.).

REFERENCES

1. M W Sigrist, *Digest Symposium on Laser Photoacoustic*, Wageningen, NL, January, 13 (1986)
2. M M Thompson, R A Palmer, *Anal Chem*, **60.** 1027 (1988)
3. P D Goldan, K. Goto, *J Appl Phys*, **45(10).** 4350 (1974).
4. G West, J. J Barrett, D R Siebert, K. V. Reddy, *Rev. Sci. Instrum.*, **54(7).** 797 (1983)
5. M J. Colles, N R Geddes, E Mehdizadeh, *Contemp. Phys*, **20(1).** 11 (1979).
6. F. A McDonald, *Can J Phys*, **9.** 1023 (1986).
7. B K Bein, J Pelzl, *J. Phys C6*, **44(10).** 27 (1983).
8. T. Somasundaram, P. Ganguly, *J Phys. C6*, **44(10).** 239 (1983)
9. I Bratu, Adriana Barbu, *Studii şi cerc fiz.*, **40(5—7).** 461 (1988).
10. I Bratu, Adriana Barbu, *XXVI Colloquium Spectroscopicum Internationale*, Sofia, Bulgaria, 2—9 July, 1989
11. S. B Tilden, M B. Denton, *Appl. Spectr.*, **39(6).** 1022 (1985).

STUDIA UNIV. BABEŞ—BOLYAI, PHYSICA, XXXIV, 1, 1989

METHOD AND INSTRUMENTATION FOR THE STUDY OF FERROELECTRICAL PROPERTIES OF CERAMIC MATERIALS

AL. NICULA* and LIANA ŞANDRU**

Received: April 18, 1989

ABSTRACT. — The experimental methods, the installations designed by the authors to visualize the hysteresis loop are presented and then, by means of experimental data, the variation curves of static susceptibility, differential dielectrical constant and differential susceptibility depending on the electric field are traced

Introduction. Ferroelectrical substances based on $BaTiO_3$ keep being studied and investigated in technical literature to modify composition, structure, even distribution of different additives in the ferroelectrical mass and size reduction below 1 μm of grains making up ferroelectrical ceramic materials [1—9].

Experimental methods. Technical literature presents a number of methods and installations to measure ferroelectrical properties [6, 8].

For hysteresis loop study of ferroelectrical ceramic materials an installation was designed and manufactured, and its block diagram is shown in Fig 1 This installation consists of transformer 1, amplifier 2, supply apparatus 3 of ±30 V d c for amplifier current supply, transformer TIT and block 4 to visualize the hysteresis loop on oscilloscope 5

In Fig. 2, the supply apparatus and the amplified consist of transformer 1 providing a voltage of 4—5 V a.c.

The signal obtained in its secondary winding is introduced into amplifier 2 made up of an integrated circuit BA 741. This amplifier end stage consists of 2 complementary transistors of BD 273 and BD 238 type, obtaining a mean power amplifier It feeds the voltage step-up transformer TIT (220 V/9,000 V — 50 Hz). The block 3 represents the supply apparatus 2 consisting of transformer TR which produces, in the secondary winding, alternating voltages resulting, by rectification and stabilization, in direct voltages of ±30 V feeding the amplifier.

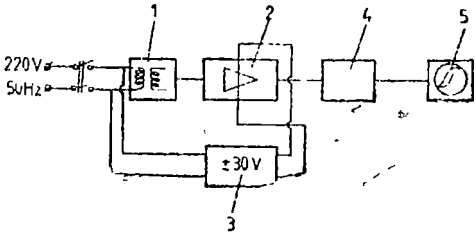

Fig. 1.

Fig. 3. shows the simplified diagram in which the supply apparatus and the supply apparatus in Fig. 2 are replaced by the audio generator. The installation, presented and manufactured, was used, after calibration, for vizualizing the hysteresis loop for Ba TiO_3 and rutile ceramic samples The polarization calculating relation is

$$P = \frac{C_0 U_0}{S} = \frac{Q}{S} = \frac{4C_0 U_0}{\pi d^2} \qquad (1)$$

The relation (1) shows that polarization measurement consists in determining the condenser area S and voltage U_0 Voltage U_x is applied to the horizontal inlet X of the oscilloscope, being

* *University of Cluj-Napoca, Department of Physics, Romania.*
** *IPG — Ploieşti, Department of FEA, 2000 Ploieşti, Romania*

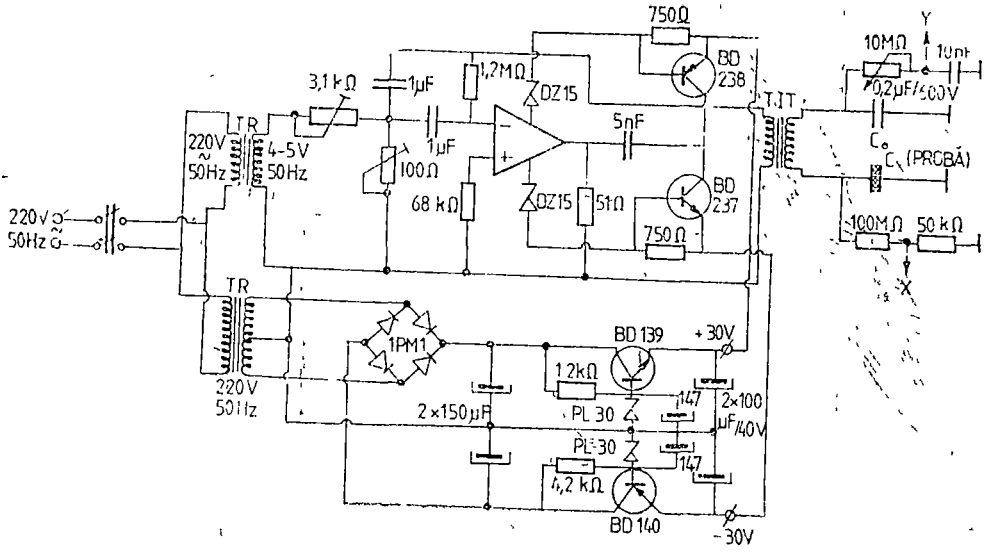

Fig. 2.

proportional to field E, which polarizes the electrical sample and voltage U_0 on the standard condenser C_0 is applied on plates Y which provide vertical deviation.

For the diagram in Fig. 3, it was set for $C_0 = 0{;}47 \cdot 10^{-6}/2$ in F. Voltage U_0 on the standard condenser is $U_y = U_0 = Q_0/C_0$, where Q_0 is the load on the condenser plate. Voltage $U_y = C_0 Q = C_0 S P \Rightarrow P = U_y/C_0 S$, $U_y = n_{\text{div}}\ 2\ V/\text{div} = 2n_{\text{div}}$V.. The horizontal and vertical axes of the oscilloscope were calibrated in polarization units $[C/m^2]$ and electric field units $[V/m]$, i.e. $U_y \sim P$ and $U_x \sim E$.

To calibrate the installation in Fig. 3 for setting out the cycle $P = P(E)$, the factors of proportionality α and β between the values P and E are determined, i.e.

$$P[C/m^2] = \alpha P[\text{div}], \text{ where } \alpha = \frac{8}{102}\,\frac{1}{C_0 S} = 1\ 68088 \cdot 10^9\ [C/m^2]$$

$$E[V/m] = \beta E[\text{div}], \text{ where } \beta = \frac{141\ 40}{h\ 102} = 24\ 04092 \cdot 10^3 \left[\frac{V/m}{\text{div.}}\right]$$

where $h = 2 \cdot 3 \cdot 10^{-3}$ represented sample thickness, m; 141 — divisor (140 + 1) characteristic to the diagram in the measuring installation

Experimental Results Interpretation. Using the wiring diagram of the installation in Fig. 3, the hysteresis loop in Fig. 4 were visualized on the oscilloscope. Each loop in the figure was photographed on the electronic oscilloscope screen and corresponds to a certain value of field E,

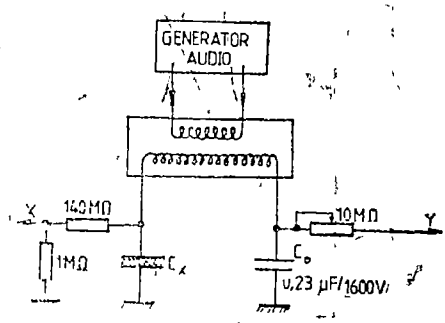

Fig. 3.

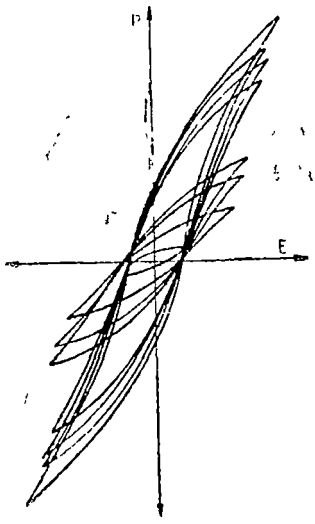

Fig 4

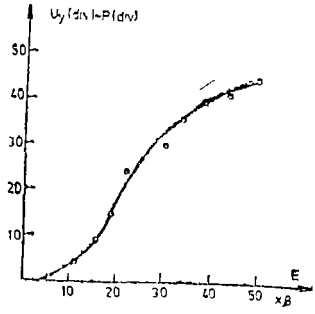

Fig 5

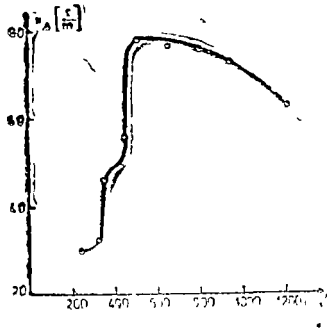

Fig 6

Using data resulted from Fig 4, the calibration curve in Fig 5 is represented. This curve ($P = P(E)$) serves to determine the static susceptibility χ_s, the differential dielectric constant ε_d and the differential susceptibility

In Fig. 6, using the data determined by ratio $P/E = \chi_s$, the variation $\chi_s = \chi(E)$ is represented The differential dielectric constant $\varepsilon_d = \chi_s + 1$ allows to analyse the ferroelectrical material behaviour in dynamic condition.

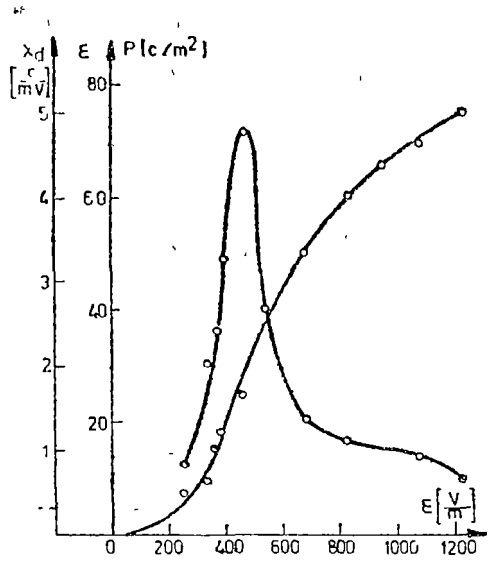

Fig. 7

In Fig 7, the variation curve 1($P = P(E)$) and the variation curve 2($\chi_d = \chi_d(E)$) obtained from graphical derivation of curve 1 are represented.

Conclusions. It results from the technical literature that the ferroelectrical materials keep being studied to improve ferroelectrical properties by elaborating new technologyes of preparing ferroelectrical layer materials, increasing material density, decreasing grain sizes below 1 μm and reducing energy consumption when preparing different materials based on ceramic materials

The installation for visualizing the hysteresis loop of ferroelectrical ceramic materials was designed and manufactured. Using experimental data, the curves were traced and the static susceptibility, the diferential dielectric constant and the differential susceptibility were studied.

REFERENCES

1. Duss L.A., Dehman V, Yamamoto T. R, *ISAF'86; Proc 6-th IEEE Int Symp Appl Ferroelec*, Bethlehem Pa June, 1986, New York
2 Huebner W, Jang F. C, Anderson H V, *Proc 21 St Univ Conf. Ceram Sci*, University Park, Pa 1985, New York.
3 Ito H, Uîda H, Nippon F, *Zaiavka*, 61—291458, Japonia, 1987
4 Kuloshov V V, Fesenk G G, Dudkevich V P, *Cryst Res and Technol*, **5.** 1983, 18
5. Lepkova P, Pavlova P, Iaucev A, *Electroprom i priborastr*, **4.** 1987, 22
6 Nicula Al, Puşcaş F, *Dielectrici si feroelectrici*, Ed Scrisul românesc, Craiova, 1982
7. Odajima A, Noto N, Yamane S, Iguchi M, *Repts Progr Polym Phys. Jap*, **23.** 205—208, 1980
8 Schuebring N. W, Molta J P, Dark R A, *The Review of scientific instruments*, XI, vol. 35, nr 11 1964
9. Uîda H., Ito H., *Zaiavka*, 61—291453, Japonia, 1987.

STUDIA UNIV BABEŞ—BOLYAI, PHYSICA, XXXIV, 1 1989

ON THE THERMAL CONDUCTIVITY OF SODIUM VAPOUR

CEZAR DOCA*, and MELITA PĂNESCU*

Received May 4, 1989

ABSTRACT. — This paper offers a calculation formula for thermal conductivity of sodium vapour in the range of 600—1250 °C at 0 01, 0 05, 0 1, 0 5 and 1 atm, obtained by fitting the experimental data of Stefanov et al This formula was obtained by applying Gauss criterion to a family of functions with numerical coefficients, given by the least squares approximation method at each of the considered pressures

1 **Introduction.** Processing and interpretation of the information obtained by experiments with alkaline metals in liquid or vapour state requires — among others — knowledge referring to the transport properties of the working medium This paper gives the values of the thermal conductivity for sodium vapour in the range of 600—1250 °C, at pressures of 0 01, 0 05, 0.1, 0 5 and 1 atm, obtained by fitting the experimental data of Stefanov et al [1]

2. **The fitting function.** The experimental data of Stefanov et al. reffering to the thermal conductivity of sodium vapour are presented in Table 1, they

Tabel 1

Thermal conductivity of sodium vapour $k \cdot 10^4$ (kcal/mh °C), experimental data of Stefanov et al [1]

t(°C)	p(atm)				
	0 01	0.05	0 1	0 5	1 0
627	308				
727	293	375	427		
827	310	339	370	524	
927	336	348	363	455	526
1027	363	369	377	429	478
1127	391	395	399	429	469
1227	421	423	426	444	465

were obtained with an average error of 20% [1] Sodium vapour can be considered according to the transport processes theory in alkaline metal vapour as an ideal reactive mixture with an atomic component and a molecular one The ideal behaviour deviation — in the real vapour case — does not modify the state parameters in the above mentioned range, more than 1% [2]. Meeting some experimental necessities of their own, the authors intended to evaluate the thermal conductivity of Na vapour at some other values of temperature

* *Institute for Nuclear Power Reactors Piteşti, PO BOX 78, 25930 Piteşti, Romania*

too excepting the ones presented in Table 1, using in this respect, fitting methods. Applying Gauss criterion [3] to a family of several functions, finaly we chose the formula:

$$k(t) = ae^{bt} + ct + d \tag{1}$$

where thermal conductivity, k, of sodium vapour is expressed in kcal/m · h°C and the temperature t in degrees Celsius, mentioning that the values of the numerical coefficients a, b, c, d are established by the least squares approximation for each isobar separately In other words, five systems of nonliniar equation of the type

$$\begin{cases} a\sum_i e^{2bt_i} + c\sum_i t_i e^{bt_i} + d\sum_i e^{bt_i} = \sum_i k_i e^{bt_i} \\ a\sum_i t_i e^{2bt_i} + c\sum_i t_i^2 e^{bt} + d\sum_i t_i e = \sum_i k_i t_i e^{bt_i} \\ a\sum_i t_i e^{bt_i} + c\sum_i t_i^2 + d\sum_i t_i = \sum_i k_i t_i \\ a\sum e^{bt_i} + c\sum t_i + d\,\mathrm{N} = \sum k_b \end{cases} \tag{2}$$

have been solved, where **N** is the number of the pairs (t_i, k_i), corresponding to each isobar.

The numerical results obtained by this method are presented in Table 2, while in Fig 1 the corresponding diagrams are traced, this noticing a good concordance with the data reported by Stefanov et al.

3. **Discussion.** Taking into consideration that function (1) approximates — — as one can see — the data of Stefanov et al very well, we consider that it can be successfully used in processing and interpreting the results obtained

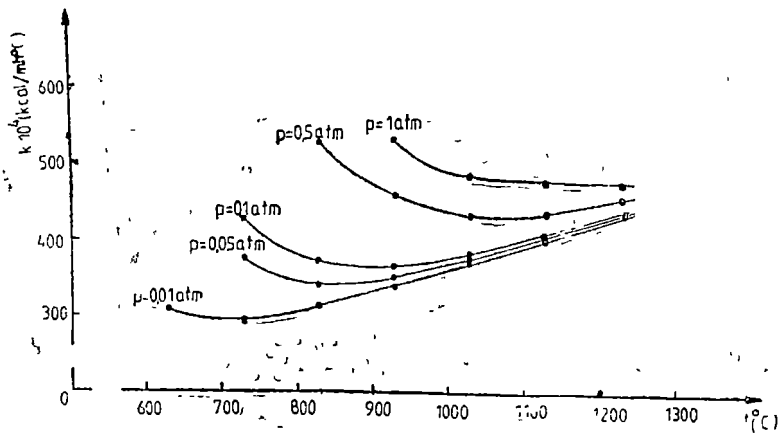

Fig 1 Thermal conductivity of sodium vapour, $k \cdot 10^4$(kcal/mh°C) as a function of temperature, (°C); · data enclosed in Table 1, — data enclosed in Table 2.

Tabel 2

Thermal conductivity of sodium vapour k 10 (kcal mh C), numerical results obtained with form. (1)

t(°C)	p(atm)				
	0 01	0 05	0 1	0 5	1
01	02	03	04	05	06
627	308				
630	307				
640	302				
650	299				
660	297				
670	295				
680	293				
690	293				
700	292				
710	292				
720	293				
727	293	375	427		
730	293	373	424		
740	294	366	415		
750	295	360	407		
760	297	355	400		
770	298	350	393		
780	300	347	388		
790	302	344	383		
800	304	342	379		
810	306	341	375		
820	308	340	372		
827	310	339	370	524	
830	311	339	369	521	
840	313	339	367	512	
850	315	339	365	503	
860	318	339	364	495	
870	320	340	363	487	
880	323	341	362	481	
890	326	342	362	474	
900	328	343	362	468	
910	331	345	362	463	
920	334	346	363	458	
927	335	347	363	455	526
930	336	348	363	454	523
940	339	350	364	450	514
950	342	352	365	446	506
960	345	354	366	443	500
970	347	356	367	440	494
980	350	358	369	437	490
990	353	360	370	435	487
1000	356	363	372	433	484
1010	358	365	374	431	481
1020	361	368	375	430	479
1027	363	369	377	429	478
1030	364	370	377	429	478
1040	367	373	379	428	476
1050	370	375	381	427	475
1060	373	378	384	427	474
1070	376	380	386	427	473

cntd.

01	02	03	04	05	06
1080	378	383	388	427	472
1090	381	385	390	427	471
1100	384	388	393	427	471
1110	387	391	395	428	470
1120	390	393	398	428	469
1127	392	395	399	429	469
1130	393	396	400	429	469
1140	395	399	403	430	468
1150	398	402	405	431	468
1160	401	404	408	433	468
1170	404	407	410	434	467
1180	407	410	413	435	467
1190	410	413	416	437	466
1200	413	415	418	439	466
1210	416	418	421	440	466
1220	418	421	424	443	465
1227	420	423	426	444	465
1230	421	424	427	445	465
1240	424	426	429	447	465
1250	427	429	432	449	464

within the vaporization and/or boiling sodium tests Using formula (1) one can calculate the thermal conductivity of sodium vapour at temperatures higher than the max limit considered by the experiments of Stefanov et al. However, it must be underlined that, for 1 atm isobar the experimental values we disposed of were relatively insufficient, which implies caution in using the calculated values of k for the above mentioned case.

REFERENCES

1 G H Golden, J V Tokar, "Thermophysical Properties of Sodium", *A N L.* 7323, Argonne National Laboratory (1967)
2 N. B Vargoftic, J K Vinogradov, K J Iachimovici, *Injenerno fiziceskii jurnal*, **55.** 970 (1980)
3. I. Constantinescu, D Golumbovici, C Militaru, *Prelucrarea datelor experimentale cu calculatoare numerice*, Ed Tehnică, Bucureşti, 1980

STUDIA UNIV BABEŞ—BOLYAI, PHYSICA, XXXIV, 1 1989

ON A NONLINEAR DIFFERENTIAL EQUATION FOR THE FAST DYNAMIC PHENOMENA

CONSTANTIN TUDOSIE*

Received March 15, 1989

ABSTRACT. — Accelerations existent in the third order nonlinear differential equation of some fast dynamic phenomena are determined A new mathematical method is used to calculate them, which I called "the method of successive groups"

1 **Introduction.** In this paper the accelerations existent in the third order nonlinear differential equation of some fast dynamic phenomena are determined

To calculate them a new mathematical methods used, which I called "the method of successive groups".

In view that the order of acceleration be given by the order of the derivative, space x was called zero order acceleration, velocity $\dot{x}$ was called first order acceleration, and derivative $\ddot{x}$ was called second order acceleration.

2 **Description of the method.** Let us have

$$a_3(t)\dddot{x} + a_2(t)\ddot{x} + a_1(t)(\dot{x})^3 + a_0(t)x = A(t), \tag{1}$$

the differential equation of a fast dynamic phenomenon, with the given initial conditions $\overset{(i)}{x}(0) = \overset{(i)}{x}_0$, $(i = 0, 1, 2)$.

The coefficients $a_i(t)$, $(i = 0, 1, 2, 3)$ and $A(t)$ are continuous functions on an interval $[0, a]$, $a > 0$, $a_i(t) \neq 0$ when $t \in [0, a]$

By introducing "the grouping functions" $F(t)$, $G(t)$ and $H(t)$, equation (1) is converted into the system of differential equations

$$\dddot{x} = G(t)\,[a_3(t)\,]^{-1} \tag{2}$$

$$\ddot{x} = [F(t) - G(t)\,]\,[a_2(t)\,]^{-1} \tag{3}$$

$$(\dot{x})^3 = H(t)\,[a_1(t)\,]^{-1} \tag{4}$$

$$x = [A(t) - F(t) - H(t)\,]\,[a_0(t)\,]^{-1} \tag{5}$$

* *Polytechnical Institute of Cluj-Napoca, 3400 Cluj-Napoca, Romania.*

By integrating (2) and (3) it follows

$$\ddot{x}(t) = \ddot{x}_0 + \int_0^t G(s)\,[a_3(s)]^{-1}\,ds, \tag{6}$$

$$\dot{x}(t) = \dot{x}_0 + \int_0^t [F(s) - G(s)]\,[a_2(s)]^{-1}\,ds. \tag{7}$$

From (3) and (6) one obtains

$$[F(t) - G(t)]\,[a_2(t)]^{-1} = \ddot{x}_0 + \int_0^t G(s)\,[a_3(s)]^{-1}\,ds. \tag{8}$$

From (4) and (7) it follows

$$\{H(t)\,[a_1(t)]^{-1}\}^{\frac{1}{3}} = \dot{x}_0 + \int_0^t [F(s) - G(s)]\,[a_2(s)]^{-1}\,ds. \tag{9}$$

By integrating (4) we have

$$x(t) = x_0 + \int_0^t \{H(s)\,[a_1(s)]^{-1}\}^{\frac{1}{3}}\,ds \tag{10}$$

From (5) and (10) one obtains

$$[A(t) - F(t) - H(t)]\,[a_0(t)]^{-1} = x_0 + \int_0^t \{H(s)\,[a_1(s)]^{-1}\}^{\frac{1}{3}}\,ds. \tag{11}$$

Expressions (2), (3), (4), (5), (8), (9) and (11) make up a system (S) of 7 equations with 7 unknown quantities

$$x^{(i)}(t),\ (i = 0,\ 1,\ 2,\ 3),\ F(t),\ G(t),\ H(t)$$

3. **Determination of system (S) solution.** The approximate solution of system (S) is determined by a method of numerical integration On the interval $[0, a]$, $a > 0$, 0 we apply a method analogous to that of polygonal lines. We divide the interval $[0, a]$ through the points $t_k = k\,\frac{a}{m}$, $k = \overline{1, m}$, and we consider the quadrature formula

$$\int_0^{k\frac{a}{m}} f(s)ds \approx \frac{a}{m} \sum_{\nu=1}^{k} f\left(\nu\,\frac{a}{m}\right), \qquad (k = 1, 2, \ldots, m). \tag{12}$$

By writing that system (S) is verified for $t_k = k\frac{a}{m}$, and by using formula (12) for the approximate calculation of the integrals, we obtain a system of $7m$ algebraic equations with $7m$ unknown quantities

$$
\begin{cases}
\dddot{x}\left(k\frac{a}{m}\right) - G\left(k\frac{a}{m}\right)\left[a_3\left(k\frac{a}{m}\right)\right]^{-1} = 0, \\
\ddot{x}\left(k\frac{a}{m}\right) - \left[F\left(k\frac{a}{m}\right) - G\left(k\frac{a}{m}\right)\right]\left[a_2\left(k\frac{a}{m}\right)\right]^{-1} = 0, \\
\left[\dot{x}\left(k\frac{a}{m}\right)\right]^3 - H\left(k\frac{a}{m}\right)\left[a_1\left(k\frac{a}{m}\right)\right]^{-1} = 0, \\
x\left(k\frac{a}{m}\right) - \left[A\left(k\frac{a}{m}\right) - F\left(k\frac{a}{m}\right) - H\left(k\frac{a}{m}\right)\right]\left[a_0\left(k\frac{a}{m}\right)\right]^{-1} = 0, \\
\left[F\left(k\frac{a}{m}\right) - G\left(k\frac{a}{m}\right)\right]\left[a_2\left(k\frac{a}{m}\right)\right]^{-1} - \frac{a}{m}\sum_{\nu=1}^{k} G\left(\nu\frac{a}{m}\right)\left[a_3\left(\nu\frac{a}{m}\right)\right]^{-1} - \ddot{x}_0 = 0, \\
\left\{H\left(k\frac{a}{m}\right)\left[a_1\left(k\frac{a}{m}\right)\right]^{-1}\right\}^{\frac{1}{3}} - \\
- \frac{a}{m}\sum_{\nu=1}^{k}\left[F\left(\nu\frac{a}{m}\right) - G\left(\nu\frac{a}{m}\right)\right]\left[a_2\left(\nu\frac{a}{m}\right)\right]^{-1} - \dot{x}_0 = 0, \\
\left[A\left(k\frac{a}{m}\right) - F\left(k\frac{a}{m}\right) - H\left(k\frac{a}{m}\right)\right]\left[a_0\left(k\frac{a}{m}\right)\right]^{-1} - \\
- \frac{a}{m}\sum_{\nu=1}^{k}\left\{H\left(\nu\frac{a}{m}\right)\left[a_1\left(\nu\frac{a}{m}\right)\right]^{-1}\right\}^{\frac{1}{3}} - x_0 = 0, \\
\qquad\qquad (k = 1, 2, \ldots, m)
\end{cases}
\tag{13}
$$

The unknown quantities of system (13) are

$$
\overset{(i)}{x}\left(k\frac{a}{m}\right),\ F\left(k\frac{a}{m}\right),\ G\left(k\frac{a}{m}\right),\ H\left(k\frac{a}{m}\right),
$$

$$
(i = 0, 1, 2, 3),\ (k = 1, 2, \ldots, m)
$$

The constant $\dddot{x}_0$ results from (1), for $t = 0$.

The value of constants $F(0)$, $G(0)$, $H(0)$ are given by the relations

$$
F(0) = \dddot{x}_0\ a_3(0) + \ddot{x}_0\ a_2(0),
$$

$$
G(0) = \dddot{x}_0\ a_3(0),\ H(0) = (\dot{x}_0)^3\ a_1(0)
$$

In numerical values, the solution of system(13) is obtained by the known methods [1].

The variation diagrams of accelerations $\overset{(i)}{x}(t)$, $(i = 0, 1, 2, 3)$ and of the "grouping functions" $F(t)$, $G(t)$ and $H(t)$, on the interval $[0, a]$, $a > 0$, are constructed through points

The given method is valid for the linear or nonlinear differential equations of any order.

REFERENCES

1 Démidovitch, B., Maron, I., *Éléments de calcul numérique*, Éditions Mir, Moscou, 1973
2 Tudosie, C., "Deduction of higher order accelerations by the method of associated angular velocity", *Strojnícky Časopis*, **34**, č 3, pp 337—341, 1983
3 Tudosie, C., "Determination of higher order accelerations by a functional method", *Acta Technica, ČSAV*, **2**, pp 218—224, 1983
4 Tudosie, C., "A method for calculating the higher order accelerations", *Mathematica*, Tome 25 (48), No 1, pp 69—74, 1983

STUDIA UNIV BABEŞ—BOLYAI, PHYSICA, XXXIV. 1, 1939

ESR, IR AND MAGNETIC SUSCEPTIBILITY STUDIES ON $xV_2O_5(1-x)[2B_2O_3 \cdot Li_2O]$ GLASSES

O. COZAR*, I. ARDELEAN*, I. BRATU, GH. ILONCA* and S. SIMON***

ABSTRACT — ESR investigations of $xV_2O_5(1-x)$ $[2B_2O_3\ Li_2O]$ glasses with $0.5 \leqslant x \leqslant 50$ mol % have shown that the geometry of VO^{2+} complex is distorted from Oh toward C_{4v} with the increase of V_2O_5 content. This fact and IR data suggest that the V_2O_5 oxide is a former network at high concentration Also, the magnetic susceptibility investigation show that only a small fraction of vanadium ions are in the V^{4+} valence state and the N_{V4+}/N_{V5+} ratio decreases when the V_2O_5 content increases

1. **Introduction.** Vanadyl ion (VO^{2+}) incorporated in glasses as a spectroscopic probe has been measured by several researches [1—10] in order to characterise glass structure. This involves many particular aspects as the geometry of structural units of the glass network, the character of chemical bonds in glasses as well as the coordination polyhedra (local symmetry) of transition metallic ions and its change with the composition of glasses

Thus, Bogomolova et al. [5] and Hosono et al [7] have found two sets of hyperfine structure for vanadyl ions in some phosphate glasses containing Mg, Zn, Be, Cd as modifier cations

Toyuki and Akagi [3] pointed out that the ligand field absorption energy $\Delta E = B_2 - E_\pi^*$ of VO^{2+} sensitively reflected the electron-donating ability of ligand oxygens coordinating at equatorial positions (Oe) of VO^{2+} — complex However, Hosono et al [6] have shown that the response ΔE of VO^{2+} is associated not directly with Oe but with Oa (vanadyl oxygen) which is isolated from the glass network

Recently, we [11, 12] have shown by ESR method that in the $x(CuO \cdot nV_2O_5)(1-x)[2B_2O_3 \cdot K_2O]$ glass systems with $0 \leqslant x \leqslant 40$ mol % and $n = 2, 3$, the C_{4v} distortion of VO^{2+} complex tends to relax toward O_h symmetry because of the sixth oxygen atom coordinated in the transposition of the vanadyl oxygen

In the present work, the influence of the V_2O_5 content on the local symmetry and interaction between vanadium ions in lithium—borate glasses has been investigated by ESR, IR and magnetic susceptibility methods.

2 **Experimental.** In order to obtain further informations on the local symmetry and interaction between metallic ions in oxide glasses, we have studied the $xV_2O_5(1-x)$ $[2B_2O_3 \cdot Li_2O]$ glasses with $0.5 \leqslant x \leqslant 50$ mol %, maintaining the B_2O_3/Li_2O ratio constant Thus, initially, the glass matrix $2B_2O_3 \cdot Li_2O$ was prepared by mixing H_3BO_3 and Li_2CO_3, and melting then this admixture in a sintered corundum crucible After cooling, the host glass was crushed and the resulting powder mixed with V_2O_5 before final melting at $T_e = 1150$ °C for 1 h. The melting glasses was

* *Physics Department, Univ of Cluj-Napoca, 3400 Cluj-Napoca, Romania*
** *Institute of Isotopic and Molecular Technology, 3400 Cluj-Napoca Romania*

poured onto a stainless-steel plate The structure of glasses has been studied by X-ray diffraction analysis and did no reveal any crystalline phase up to $x = 50$ mol %

The ESR measurements were performed at 9 4 GHz (X—band) using a standard JEOL—JES —3B equipment, at the 295 K IR absorption spectra in the range 400 to 1700 cm^{-1} were recorded in KBr pellet form on a Carl Zeiss Jena spectrophotometer (UR 20 model) The magnetic data were obtained using a Faraday type balance in the temperature range 80 to 300 K.

3 **Results.** 3 1. *ESR spectra* ESR spectra obtained at room temperature for glasses with small content of V_2O_5 ($x \leqslant 5$ mol %) show a well resolved hyperfine structure typical for isolated vanadium ions in a ligand field of C_{4v} symmetry, presented as VO^{2+} species (Fig 1) These are similar with the spectra reported by previous workers [1—9] for vanadium ions in other oxide glasses and may be analysed by an axial spin Hamiltonian

$$\hat{\mathcal{H}} = \beta_0[g_{\parallel} H_z S_z + g_{\perp}(H_x S_x + H_y S_y)] + A_{\parallel} S_z I_z + A_{\perp}(S_x I_x + S_y I_y) \qquad (1)$$

Here β_0 is the Bohr magneton while $g_{\parallel}$, $g_{\perp}$ and $A_{\parallel}$, $A_{\perp}$ are the component of the $\tilde{g}$ — tensor and hyperfine structure tensor, respectively H_z, H_y,

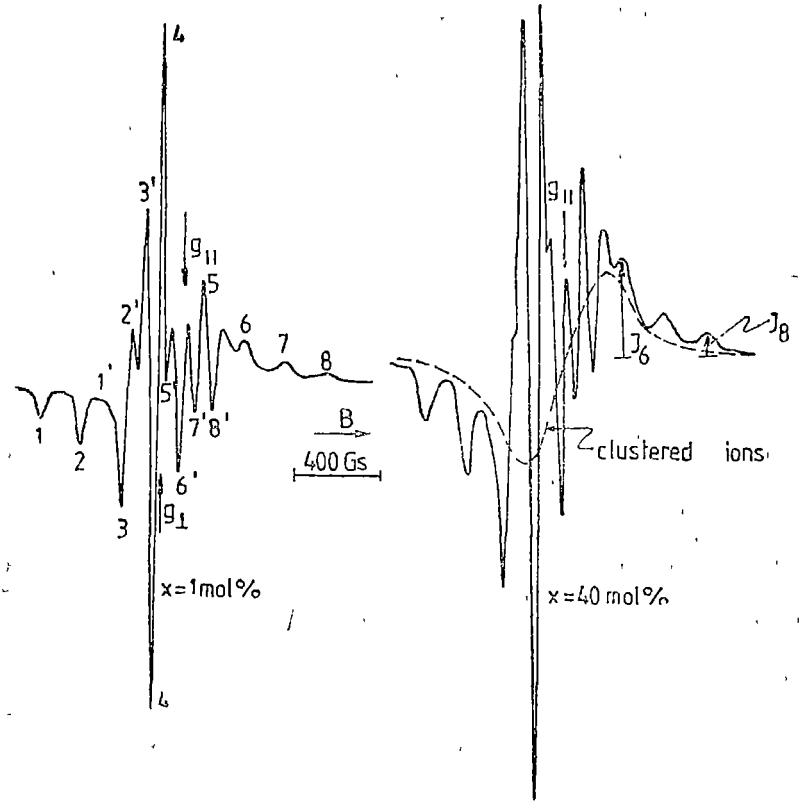

F i g 1 ESR spectra of $xV_2O_5(1-x)$ [$2B_2O_3$ Li_2O] glasses at 295 K.

H_z, are components of the magnetic field S_x, S_y, S_z and I_x, I_y, I_z are the component of the spin operators of the electron and the nucleus, respectively

The magnetic field positions of the parallel and perpendicular hyperfine peaks taking into account the second order perturbation terms, are given by [7, 9]

$$H_{\parallel}(m) = H_{\parallel}(o) - mA_{\parallel} - \frac{A_{\perp}^2}{2H_{\parallel}(0)}\left(\frac{63}{4} - m^2\right) \quad (2)$$

$$H_{\perp}(m) = H_{\perp}(o) - mA_{\perp} - \frac{(A_{\parallel}^2 + A_{\perp}^2)}{4H_{\perp}(0)}\left(\frac{63}{4} - m^2\right) \quad (3)$$

Here m is the nuclear spin magnetic quantum number taking the values $\pm 7/2$, $\pm 5/2$, $\pm 3/2$, $\pm 1/2$, $H_{\parallel}(o) = h\nu/g_{\parallel}\beta_o$ and $H_{\perp}(p) = h\nu/g_{\perp}\beta_o$ Other notations have the usual meaning

The ESR parameters obtained for the studied glasses are given in Table 1 The covalency degrees of the in-plane V—O σ bonds (β_1^2) and of π—bonding

Table 1

ESR Parameters, bonding coefficients and Fermi contact term values for studied glasses

x [mol %]	$g_{\parallel}$	$g_{\perp}$	$A_{\parallel}$ [10^{-4} cm^{-1}]	$A_{\perp}$ [10^{-4} cm^{-1}]	β_1^2	$(1 - \varepsilon_{\pi}^2)$	K
0.5	1 941	1 997	170 7	61 4	0 81	0 83	0 77
1	1 941	1 998	173 5	63 0	0 81	0 87	0,77
3	1 945	1 999	174 1	64 3	0 76	0 90	0 79
5	1.944	1.997	173 8	64 2	0 77	0 83	0 79
10	1.941	1 998	176 3	68 5	0 81	0 87	0 83
20	1 941	2 000	176 3	67.1	0 81	0 93	0 81
30	1.940	2 000	176 2	71 5	0 82	0 93	0 87
40	1.937	1 998	177 3	71 3	0 86	0 87	0.86

with the vanadyl oxygen (ε_{π}^2) were evaluated with the help of LCAO—MO scheme developed by Kivelson and Lee [13] We have taken the spin-orbit coupling constant $\lambda = 170$ cm^{-1} [13] and the energy transition $\Delta_{\parallel} = B_2 - B_1^*$ and $\Delta_{\perp} = B_2 - \varepsilon_{\pi}^*$ of 16800 cm^{-1}, and 10500 cm^{-1}, respectively [3] Also, having in view the results reported by Toyuki and Agaki [3] we have considered $\beta_2^2 = 0\,93$ for the studied glass system. The values obtained for β_1^2, $(1 - \varepsilon_{\pi}^2)$ and Fermi contact (K) parameters are given in Table 1, too.

The shape of ESR spectra is modified with the increasing of vanadium ions content (Fig 1). This consists from the partial disappearance of the vanadyl hyperfine structure and the appearance of a broad line at $g \simeq 1\,96$ value characteristic for the dipole-dipole coupled ions Thus the spectra obtained for $x > 20$ mol % may be considered as the result of the superposition of two ESR signals, one with resolved hyperfine structure typical for isolated VO^{2+} ions and one consisting from a broad line without structure typical for asso-

ciated ions [9]. Their number increases with the V_2O_5 content The concrete shape of the ESR spectra depends of the relative weight of the concentration of the two types of V^{4+} ions

The modification of the ESR spectra in function of the V_2O_5 content is illustrated by the ratios of the heights of some hyperfine peaks from the parallel band (Fig. 2) The I_6/I_8 ratio increases together with the V_2O_5 content because I_6 is situated close on the maximum of broad line due to the clustered ions (Fig 1) and thus its height increases with the number of clustered ions Their contribution at the I_8 peak is not significant The I_3/I_5 ratio practically remains constant, both peak being situated near to the extremum positions of the broad line Thus the contribution of clustered ions at these hyperfine peaks is the same

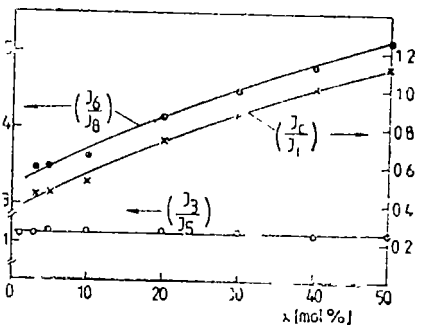

Fig 2 The composition dependence of the ratios between some hyperfine peaks from the paralell band and of the clustered/isolated ions (I_c/I_i).

As a measurement of the ratio between clustered and isolated ions (I_c/I_i) we have considered [9]·

$$\left(\frac{I_c}{I_i}\right)_x = \frac{I_{6x} - \alpha I_{8x}}{\alpha I_{8x}} \qquad (4)$$

where I_{6x} and I_{8x} are the heights of the 6 and 8 peaks from the parallel spectrum of the sample with x (mol % V_2O_5) content and α is the value of I_6/I_8 ratio sample with $x = 0.5$ mol % We have considered that in glasses with $x \leqslant 0.5$ mol % all V^{4+} ions are manifest as isolated species The variation of (I_c/I_i) ratio versus V_2O_5 content is shown in Fig. 2 It can be observed that for $x \geqslant 40$ mol % dominates the species of clustered ions

3.2. *IR Spectra.* Fig 3 shows the IR spectra of $xV_2O_5 \cdot (1-x)\,[2B_2O_3 \cdot Li_2O]$

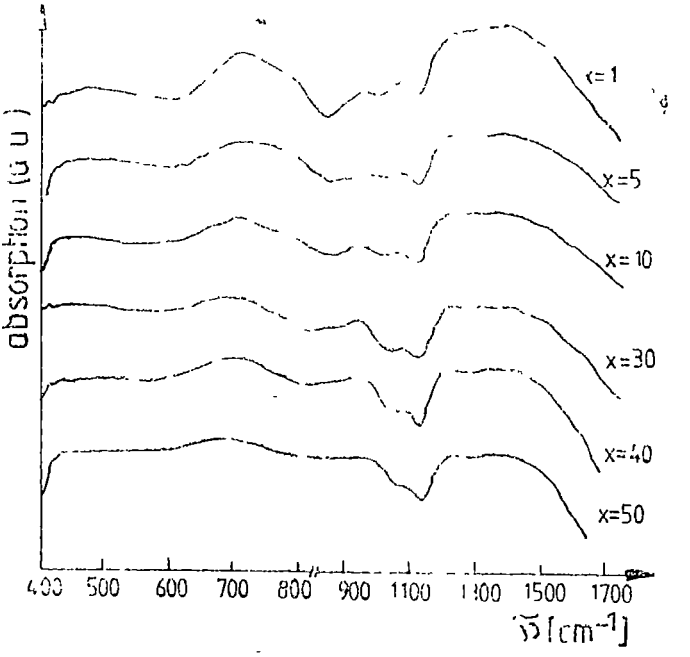

Fig 3. IR spectra of $xV_2O_5(1-x)\,[2B_2O_3 \cdot Li_2O]$ glasses

glasses These contain the absorption bands characteristic for $2B_2O_3 \cdot Li_2O$ glass matrix and also for the presence of V_2O_5 oxide

The band which appears at 720 cm^{-1} in the IR absorption spectra of vitreous B_2O_3 and which was attributed to the bond-bending vibration of the B—O—B groups [14] appears also in the IR spectra of studied glasses at about 700 cm^{-1}.

Another important band of vitreous B_2O_3 at 1265 cm^{-1} characteristic for B—O stretching frequency is also maintained in the spectra of our glasses as a broad feature around 1250 cm^{-1}. We note that these B—O bonds involve B^{3+} atoms The band which appears at 1070 cm^{-1} may be also attributed to stretching vibration of B—O bonds, but these bond involve B^{4+} atoms [14]

Another broad band is centered at around 1400 cm^{-1} As already reported, the characteristic B—O < stretching is assigned to a broad band from 1428 to 1333 cm^{-1} in $Na_2O—B_2O_3$ glasses [15] and to a broad band at 1450 cm^{-1} in crystalline B_2O_3 The fact that for our samples this band appears at lower wave number than in crystalline B_2O_3, confirms the amorphous nature of these samples [16]

The presence of Li_2O in the vitreous matrix leads to the appearance in the IR spectra of a little intensity band at 410—430 cm^{-1}. In our case this band occurs at 415 cm^{-1} indicating the existence of $2B_2O_3 \cdot Li_2O$ structural units in the studied glass system [17].

V_2O_5 oxide determines the appearance in the IR spectra of two absorption bands at 950 cm^{-1} and 1070 cm^{-1}. The 1070 cm^{-1} band is characteristic for vanadyl V = O bond and the 950 cm^{-1} band may be attributed to V—O bonds and also to the polyvanadate (clustered) ions formations [18].

The intensity of the 950 cm^{-1} band increases with the increase of V_2O_5 content, while the 1070 cm^{-1} band decreases.

The composition dependence of the ratio between the two absorption bands (A_{1070}/A_{950}) is presented in Fig 4 This suggests that the number of V — O bonds or polyvanadate ions formations increases more rapidly than the number of V—O bonds with the increase of the V_2O_5 content. Also the variation of the A_{950}/A_{700} ratio versus x(V_2O_5 mol %) shows (Fig. 4) that the number of V = O bonds is slowly modified with the change of the glass composition.

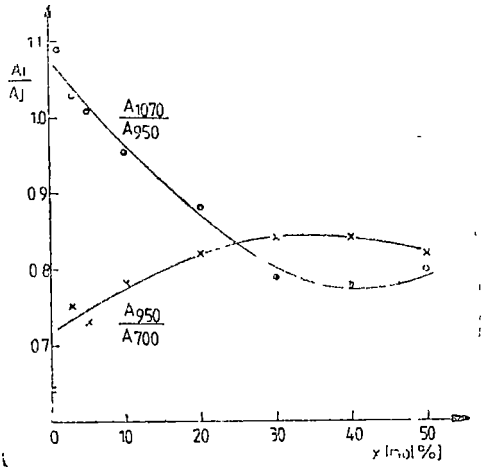

Fig 4 The composition dependence of the IR absorbtion bands.

3 3 *Magnetic susceptibility data.* The temperature dependence of the reciprocal magnetic susceptibility of the various glasses from this system is presented in Fig. 5 For these glasses, in all concentration range of vanadium ions, a Curie law is observed. This suggests that the predominant

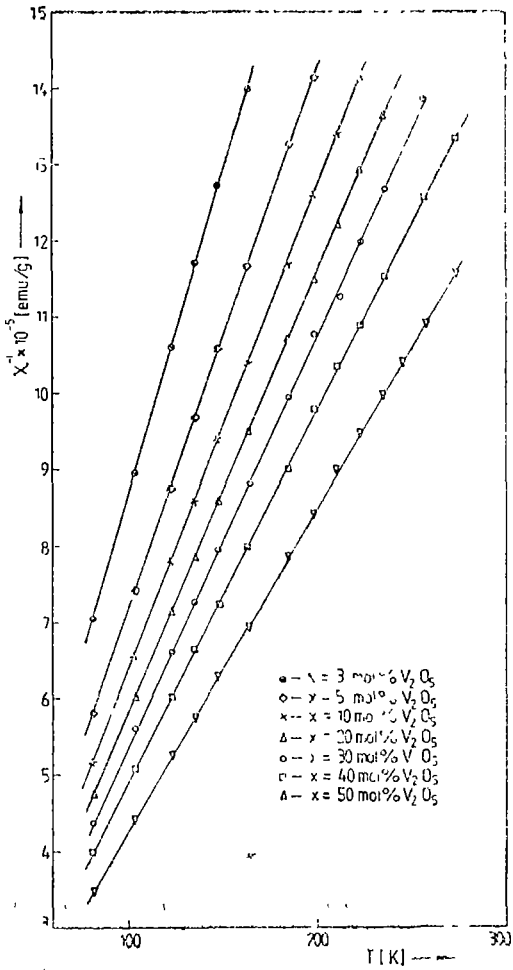

Fig 5 The temperature dependence of the reciprocal magnetic susceptibility.

part of vanadium ions are magnetically isolated and that no magnetic order is present This behaviour agrees with the ESR study conslusions.

To determine accurately the values of the Curie constants, C_M and atomic magnetic moments, μ_{at}, a correction due to the diamagnetism of the glass matrix and V_2O_5 was taken into account The composition dependence of the Curie constants, C_M is presented in Fig 6. The values of the Curie constant, which is proportional to the paramagnetic ions concentrations, increase with vanadium ions concentration Having in view that the Curie constant is

$$C = \frac{N \cdot \mu_{ef}^2}{3K} \tag{5}$$

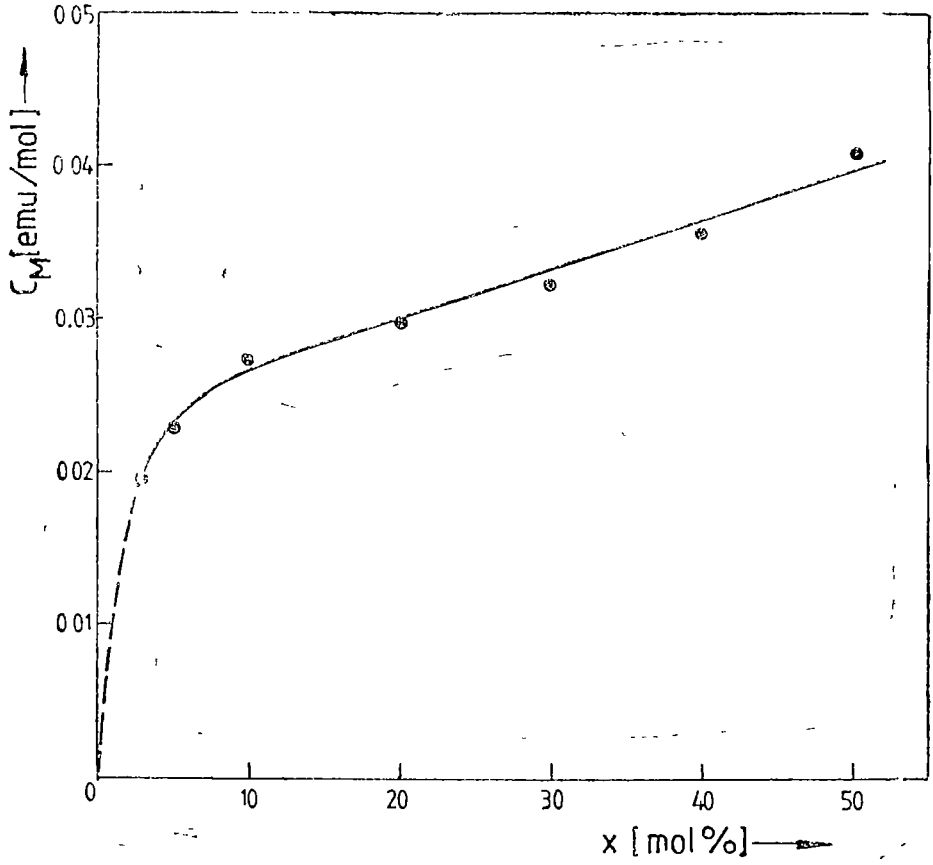

Fig. 6 The composition dependence of the Curie constant.

it results that this depends on the square of the effective magnetic moment. The experimental values of Curie constants and of the atomic magnetic moments obtained for these glasses are smaller than those which correspond to V_2O_5 content, considering that all vanadium ions are in V^{4+} valence states. In this way, we suppose that in these glasses are present both V^{4+} and V^{5+} ions, the last being diamagnetic The presence of V^{4+} ions and their increase with V_2O_5 content was evidenced by ESR measurements (Fig 1, 2). Other valence states of the vanadium ions in oxide borate glasses, up to now, have not been evidenced [1—9].

In this case, having in view that the atomic magnetic moment of free V^{4+} ions is $\mu_{V4+} = 1\,73\ \mu_B$, which was usually observed in paramagnetic salts [19], we have estimated the molar fraction of the vanadium ions which are in V^{4+} valence state (Table 2, notated by y). It results that only a small fraction of vanadium ions are in V^{4+} valence state and this fraction decreases when

the V_2O_5 content decreases. From these data we have estimated the N_{V4+}/N_{V5+} ratio (N_{V4+} and N_{V5+} are the molar fraction of V^{4+} and V^{5+} ions, respectively). These ratio decreases when the V_2O_5 content increases.

4 Discussion and Conclusions. The small values of the Fermi contact term ($K \leqslant 0.79$) for glasses with $x \leqslant 5$ mol % suggest a hexacoordinated geo-

Table 2.

Curie constants, amount of the vanadium ions in the V^{4+} valence state (y) and N_{V4+}/N_{V5+}

x [mol % V_2O_5]	C_M [emu/mol]	y [mol % V_2O_4]	N_{V4+}/N_{V5+}
3	0 0197	1.75	1.40
5	0.02279	2.00	0.67
10	0.02705	2.40	0 32
20	0.0296	2.65	0 15
30	0.03221	2.90	0.11
40	0.03556	3 20	0.09
50	0.0413	3.70	0.08

metry of the VO^{2+} complex near octahedral (Oh) symmetry because of the reduction of the V—O interaction in the vanadyl group caused by a strong axial perturbation arising from the sixth oxygen atom coordinated in the transposition to the vanadyl oxygen This geometry of the VO^{2+} complex is typical for high alkali (20—30 mol % R_2O = Li_2O, Na_2O, K_2O) borate glasses [3, 6].

The values of β_1^2 coefficient shown an appreaciable covalency degree of the in plane V—O σ-bonds This fact is also consistent with a reduced V—O interaction and an increased V—O bond lenght in the vanadyl group [20], both being related to an increase of the electron donability of the four oxygen atoms coordinated in xOy plane.

The K values increase (> 0.81) with the increase of V_2O_5 content ($x > 20$ mol %). This suggests [3] a strong V = O interaction which makes the bond leght in the vanadyl group (V^{4+}—Oa) to be shorter than others V—O bonds from complex. Thus the geometry of VO^{2+} complex is distorted from Oh toward C_{4v}, which is characteristic for low alkali (< 5 mol % R_2O) borate glasses [6]. The increase of the ligand field along the O_z axis is consistent with an weakness of the in plane V—Oe bonds. The increase of β_1^2 values for glasses with $x \geqslant 20$ mol % (Table 1) shown a decreasing covalency degree of the in plane V—O σ—bonds in agreement with a C_{4v} local symmetry of isolated vanadium ions

On the other hand the structural distortion of the VO^{2+} complex from Oh toward C_{4v} symmetry which is correlated with the change of borate glass composition from high alkali to low alkali suggests that in our glass system the V_2O_5 oxide is a former of the network at high concentration ($x > 20$ mol %) together with B_2O_3 oxide.

The same conclusion results from the variation mode of the 1070 cm^{-1} and 950 cm^{-1} band intensities with increase of V_2O_5 content

The magnetic susceptibility investigation show that only a small fraction of vanadium ions are the V^{4+} valence state and the N_{V4+}/N_{V5+} ratio decreases when the V_2O_5 content increases.

The experimental results obtained from EPR, IR and magnetic susceptibility studies suggest that the V_2O_5 is a former of the network at high concetration ($x > 20$ mol %) together with B_2O_3 Also, the V^{4+} ions seem to be randomly distributed in the glass matrix and experience dipole-dipole interactions

REFERENCES

1. G. Hochstrasser, *Phys. Chem. Glasses*, **7**, 178 (1966).
2 H. G Hecht, T. S. Johnston, *J. Chem Phys*, **46**, 23 (1967).
3. H. Toyuki, S Akagi, *Phys Chem. Glasses*, **13**, 15 (1972).
4. A. Paul, F. Assabghy, *J. Mater. Sci.*, **10**, 613 (1975).
5. L. D. Bogomolova, V, N. Jackin, V. N. Lazukin, T. K. Pavlushkina, V. A. Shmuckler, *J. Non-Crystalline Solids*, **28**, 375 (1978).
6. H. Hosono, H. Kawazoe, T. Kanazawa, *J. Non-Crystalline Solids*, **33**, 125 (1979).
7. H. Hosono, H. Kawazoe, T. Kanazava, *J. Non-Crystalline Solids*, **37**, 427 (1980).
8. J. M. Dance, J. P. Darnaudery, H. Bandry, M Monneraye, *Solid State Commun.*, **39**, 199 (1981).
9 O. Cozar, I. Ardelean, Gh. Ilonca, *Mater. Chemistry*, **7**, 155 (1982).
10. Al. Nicula, E Culea, *Phys. Stat. Sol. (b)*, **142**, 265 (1987)
11. I. Ardelean, O. Cozar, Gh. Ilonca, *J Non-Crystalline Solids*, **68**, 33 (1984)
12 O. Cozar, I Ardelean, Gh. Ilonca, Gh Cristea, *Rev. Roum. Phys*, **33**, 1125 (1988)
13 D. Kivelson, S. K. Lee, *J. Chem Phys.*, **41**, 1896 (1964).
14 I Bratu, P. Oană, M. Culea, *Phys. Stat Sol. (a)*, **100**, K195 (1987)
15 Y. T. Quan, C E. Adams, *J. Phys. Chem.*, **70**, 331 (1966).
16. B. K. Sharma, D C. Dube, A. Mansingh, *J. Non-Crystalline Solids*, **65**, 39 (1984)
17 J. Wong, C. A. Angell, *Glass Structure by Spectroscopy*, Marcel Dekker, Inc., New York and Bassel, 1976, p 435.
18. H. Miyata, K. Fujii, T. Ono, Y Kubokawa, T. Ohno, F. Hatayama, *J. Chem. Soc. Faraday Trans.* 1. **83**, 675 (1987)
19. E. Burzo, L. Stănescu, I. Ardelean, V. Teodorescu, *Revista de Chimie*, **29**, 305 (1978).
20. O. Cozai, R. Semeniuc, V. Znamirovschi, I. Haiduc, *Rev. Roum. Phys*, **33**, 1131 (1988).

STUDIA UNIV BABEŞ—BOLYAI, PHYSICA, XXXIV, 1 1989

RECENZII

The Spectroscopy of Molecular Ions. (A Discussion organized and edited by A Carrington, F R.S , and B. A Thrus, F R S) in *Philosophical Transaction of the Royal Society of London A. Mathematical and Physical Science,* Vol 324, pp 73—294, No. 1578, 26 January, 1988, Published by Royal Society, 6 Carlton House Terrace, London SW1Y 5AG

Molecular ions are now recognized as major chemical reagents in extraterrestrial and terrestrial environments where ionization occurs Spectroscopic analyses offer the most comprehensive means to understand their structure and to pursue their behaviour

The herereviewed volume consits of 18 papers, all in the field of molecular ions spectroscopy The collection opens with an account on some major topics partaining to the spectroscopy of molecular ions, compiled by Wtt. Wing from the Department of Physics, University of Arizona The papers following provide discussion on the use of various techniques to obtain information at the level of different molecular ions.

Thus, infrared spectroscopy of carbo-ions (T. Oka), infrared laser spectroscopy of cations (P B Davies), infrared diode laser and microwaves spectroscopy of molecular ions (E. Hirota), photoelectron spectroscopy of reactive intermediate ions (V. Butcher et al), fluorescent excitation spectroscopy of ionic cluster containing the $C_6F_6^+$ cromophore (C Y Kung et al) are but a few of the papers gathered in the volume

Many of the papes are accompanied by interesting discussion meant to better understand the issues treated.

The Spectroscopy of Molecular Ions is an easy to read book. the style of the papers is clear, concise and straight-forward, and also just the right amount of prerequisite is provided for a synthetic presentation of the aspects discussed The concepts and techniques specific to the spectroscopy of molecular ions are harmoniously presented so as researchers may avail thamselves of the experience of previous contributors to this field of science The collection also stands out in that up-to-date techniques employed in molecular ions spectroscopy investigations are approached and described. It is intended for student environment, as well as for the research milieu — students and the teaching-staff and researches may find that the nature of the problems to be solved necessitates rapid acquisition of some knowledge of that subject.

TRAIAN ILIESCU

ÎNTREPRINDEREA POLIGRAFICĂ CLUJ, Municipiul Cluj-Napoca, Cd nr. 424

În cel de al XXXIV-lea an (1989), *Studia Universitatis Babeş—Bolyai* apare în specialităţile:

matematică
fizică
chimie
geologie-geografie
biologie
filosofie
ştiinţe economice
ştiinţe juridice
istorie
filologie

In the XXXIV-th year of its publication (1989), *Studia Universitatis Babeş—Bolyai* is issued as follows:

mathematics
physics
chemistry
geology-geography
biology
philosophy
economic sciences
juridical sciences
history
philology

Dans sa XXXIV-e année (1989), *Studia Universitatis Babeş—Bolyai* paraît dans les spécialités:

mathématiques
physique
chimie
géologie-géographie
biologie
philosophie
sciences économiques
sciences juridiques
histoire
philologie

43 904

Abonamentele se fac la oficiile poştale, prin factorii poştali şi prin difuzorii de presă, iar pentru străinătate prin „ROMPRESFILATELIA", sectorul export-import presă, P. O. Box 12—201, telex. 10876, prsfir, Bucureşti. Calea Griviţei nr. 64—66.

Lei 35